STRUCTURAL AND DYNAMIC PROPERTIES OF THE TRANSLOCASE MOTOR SecA

By Dimitra Keramisanou

A dissertation submitted to the

Graduate School-Newark

Rutgers, The State University of New Jersey

in partial fulfillment of requirements for the degree

Doctor of Philosophy

Graduate Program in Chemistry

Written under the direction of

Professor Charalampos G. Kalodimos

and approved by

_____

_____

_____

_____

Newark, New Jersey

May, 2009

ABSTRACT OF THE THESIS

Structural and dynamic properties of translocase motor SecA

By Dimitra Keramisanou

Thesis director: Professor Charalampos G. Kalodimos

SecA is a large, 204 kDa, homodimeric, helicase-like protein that is a key component of the bacteria protein secretion machinery. SecA, being a motor protein, couples the translocation of polypeptide segments across or into biological membranes with the expenditure of metabolic energy extracted from ATP hydrolysis. SecA adopts a compact conformation in the cytoplasm but switches to a relaxed one when is engaged to translocation at the membrane. Specific interaction of SecA with SecYEG induces large conformational changes to both partners that result in the stimulation of SecA's ATPase activity and trigger the opening of the channel.

We use a combination of NMR spectroscopy, Isothermal Titration Calorimetry (ITC) and biochemical techniques to characterize *E. coli* SecA along the protein secretion pathway. Recent advances in isotope labeling and NMR methodology (methyl-TROSY) enabled the NMR study of SecA.

We found that the nucleotide binding cleft of SecA exists in a metastable state that undergoes a disorder-order transition upon nucleotide binding. Our data show that

SecA uses a novel mechanism wherein conserved regions lining the cleft undergo cycles of disorder-order transitions while switching among functional catalytic states. The structural relation of SecA to helicases suggests that these proteins may utilize similar mechanisms to convert the ATP binding/hydrolysis energy to mechanical work.

Our data reveal that C domain undergoes cycles of detachment and rebinding to the motor that are linked with the ATPase activation of SecA. When the contacts with the C domain are loosened, SecA becomes activated and this process is probably facilitated by the membrane. Moreover, allosteric communication between the preprotein binding and the motor domain of SecA is regulated by nucleotide and signal peptide binding. Finally, we found that the extreme C terminus of SecY (C6 loop) contacts both the motor and the C domain of SecA and we identified important residues from the loop C6 that mediate this interaction.

In summary, our studies revealed the intimate relation between flexibility and catalytic efficiency in SecA as well the allosteric communication among the domains.

Acknowledgments

Thesis Advisor:

Prof. Charalambos G. Kalodimos

Committee Members:

Prof. Frank Jordan (Rutgers-Newark, The State University of New Jersey)

Prof. Phillip Huskey (Rutgers-Newark, The State University of New Jersey)

Prof. John Hunt (Columbia University, New York)

All the present and past members of Prof. Kalodimos Lab,

Dr. Ioannis Gelis, Nataliya Popovych, Paramita Sarkar, Li Chen, Tamjeed Saleh, Wojciech Jankowski, Pragati Sharma, Soma Mandal, Dr. Eve Tseng, Dr. Ming Tao Pai Anand Ramanathan, Ryan Walsh, Sulyman Barkho, Dr. Nikos Biris, Dr. Cungen Zhang, Dr. Mandar Naik, Dr. Jennifer Wulf, Shangjin Sun, Onyi Uchime.

Our Collaborators from Institute of Molecular Biology and Biotechnology, Greece

Prof. Tassos Economou, Dr. Giorgos Sianidis, Dr. Lily Karamanou, Sanny Papanikou

Rutgers-Newark, The State University of New Jersey

Dr. Lazaros Kakalis (NMR manager), All the Department of Chemistry Faculty and staff

My Friends in USA and Greece

Last but not least my Family in Greece

My father Panagiotis, My mother Maria, My sisters Popi, Eirini and my Brother Spyros

Contents

List of figures

List of tables

Chapter I. Introduction

I.1.1 Protein translocation

Proteins are synthesized at the ribosome in the cytosol, in mitochondria and in chloroplasts. In all domain of life, more than 30% of the synthesized proteins are transported to other membrane-limited compartment or regions, inside a membrane, or to the extracellular milieu [1-4]. A fundamental question in this process is how proteins reach their final destination. To manage protein trafficking, cells have evolved sophisticated systems that are dedicated to correctly differentiate proteins destined for translocation.

The translocation process is topologically equivalent in all three domains of life and shares the same general principle: (a) Sorting of proteins as secretory and non-secretory; (b) Maintenance of secretory proteins in a translocation competent state; (c) Targeting of secretory proteins to the membrane; (d) Completion of translocation across the membrane; and (e) Maintenance of the permeability barrier during the translocation process. The machineries involved in these tasks are assembled from the same conserved components that include cytosolic chaperones, membrane-bound receptors/motors, and the protein conducting channel (Figure 1.1) [1, 2].

In the general mode of translocation, newly synthesized secretory proteins or nascent polypeptide chains emerging from the ribosome have to be directed to the translocase or translocon with the aid of cytosolic chaperones. The translocase is composed of a peripheral membrane receptor, which may act as a motor, and a membrane-embedded protein complex that forms a channel. Binding of secretory

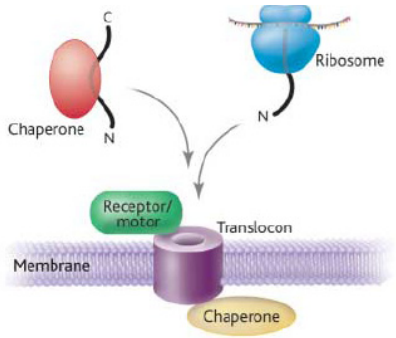

Figure 1.1: General mode of translocation. Schematic representation of the conserved components assembling the secretion machinery [2].

proteins to the membrane receptor and subsequent transfer to the channel facilitates the translocation across the membrane or the lateral release to the lipid bilayer with the assistance of motor proteins and chaperones in the cis and/or trans side of the membrane. Translocase couples protein translocation with the expenditure of metabolic energy provided by ATP hydrolysis and the Proton Motive Force (PMF) [5, 6].

The breakthrough in the field came in the 1970s when Günter Blobel discovered that proteins destined for translocation into the lumen of the endoplasmic reticulum (ER) are synthesized with an N-terminal extension, the so called signal sequence, that is proteollytically removed after translocation [7, 8]. Soon after, the ability to reconstitute in vitro the translocation system based on purified components opened a new era in the field [9]. Currently, biochemical and high-resolution structural studies provide us with a better understanding of protein secretion at the molecular level.

I.1.2 Bacterial Protein Secretion

Bacteria are simple organisms that lack a nucleus and can be classified as Gram-positive and Gram-negative depending upon their ability to retain crystal violet-iodine

dye, known as the Gram's stain. The fundamental difference in this classification is the composition of the cell envelope. In Gram-positive bacteria the cytoplasmic membrane is covered by many layers of peptidoglycans. Gram-negative bacteria have a double layered membrane: a cytoplasmic (inner) membrane followed by some layers of peptidoglycans (periplasm) and an outer membrane which contains phospholipids and lipopolysaccharides.

To facilitate protein secretion, bacteria have evolved a diverse set of pathways [3, 4, 6, 10] (Figure 1.2); to date, there have been reported 16 different translocation systems that can be subdivided to at least three classes, involving systems that are known to exist for secreting proteins into or across the cytoplasmic membrane. *Class 1* includes systems that translocate polypeptides across the cytoplasmic membrane, and they utilize different translocons for unfolded (SecYEG/YidC) and for folded (TAT/ABC transporter)

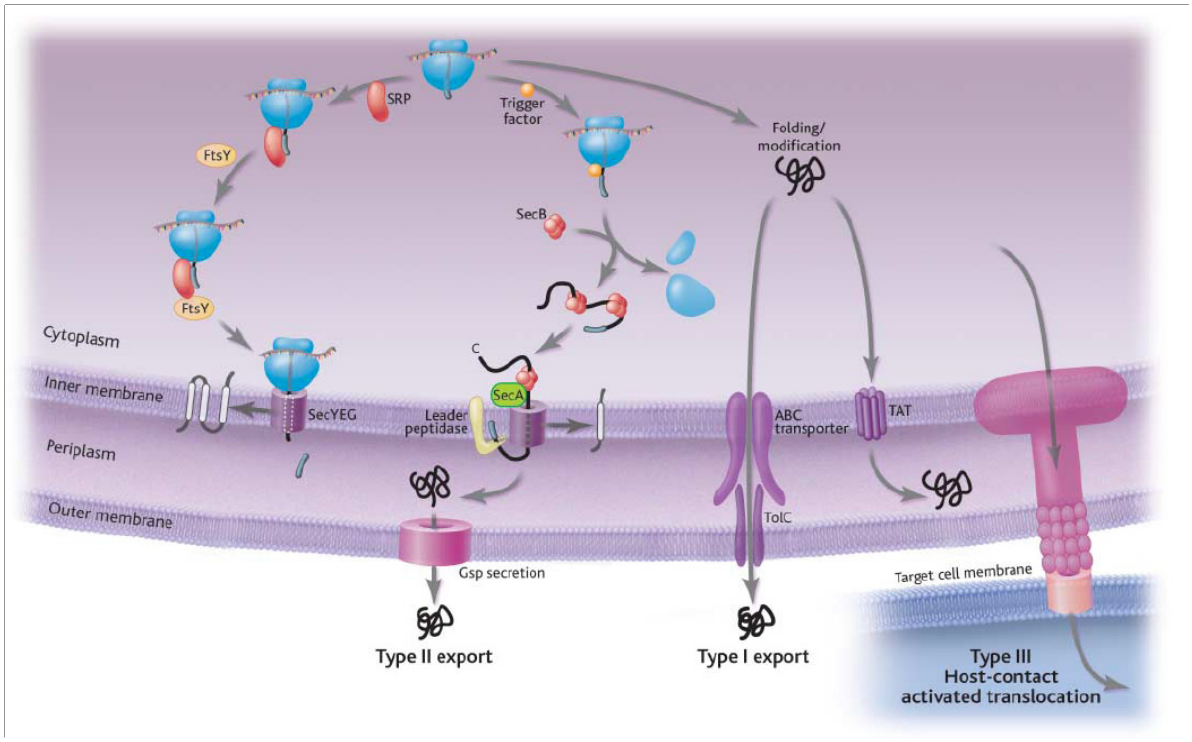

Figure 1.2: Diversity of bacterial translocation pathways [2].

proteins. *Class 2* consists of systems that facilitate the secretion of folded proteins from the periplasm to the outer membrane (Type II, IV). *Class 3* consists of systems that aid unfolded protein translocation from the cytoplasm to the extracytosolic milieu or into the cytoplasm of a host cell (Types I, III, flagella and the majority of Type IV).

The most essential and ubiquitous protein translocation pathway in all three domains of life is the Sec dependent pathway [3, 4]. This is the major route that bacteria use for protein translocation and acts as the entry point for many of the other protein export and sorting systems. The Sec pathway is responsible for membrane and cell wall biogenesis, secretion of hydrolytic enzymes, toxins, signaling molecules, attachments and mobility appendages (pilli and flagella).

Biochemical and genetic studies have identified all genes involved in the Sec pathway [11]. These include (i) cytosolic chaperones that assist with sorting, unfolding and targeting at the membrane and (ii) the membrane-embedded protein conducting channel SecYEG, which, together with the motor protein SecA, compose the translocase/translocon. An exciting aspect of studying the bacterial translocation is that it is very similar to the eukaryotic one. In eukaryotes, the internal ER membrane is analogous to the bacterial plasma membrane. In fact, the two organisms have positive and synergistic influence on each other and they even share the same systems, SRP (Signal recognition Particle) or the TAT (Twin Arginine Translocation) system in bacteria and chloroplasts.

I.1.3 Sec dependent protein translocation

I.1.3.1 The Signal Sequence

The entry of virtually all proteins to the export pathway, both in eukaryotes and prokaryotes, is controlled by a short signal sequence encoded at the N terminus end of the preprotein with a length of 15 to 30 residues [12-15]. In this small amino-acid stretch is encoded all of the information needed to correctly target secretory polypeptides to the translocon. In fact, the most decisive step in protein export pathways is the signal sequence recognition by its cognate receptors. This step controls the fate of the preprotein as it aids in the correct sorting of secretory proteins from non-secretory.

The importance of the signal sequence lies in its implication in many steps of the translocation process. The signal sequences may slow down the folding of the newly synthesized proteins and keep them in a translocation-competent state[16]. In addition, it determines the targeting route to the membrane [17, 18] and in a later step interacts with and activates the translocon [19]. Interestingly, the functionality of signal sequence in the case of integral membrane proteins is substituted by a Transmembrane Segment (TMS) of the protein which at the end functions as a permanent anchor.

The original signal sequence hypothesis was that signal sequences share sequence similarity, however, the absence of any strict consensus sequence soon became apparent. In fact, the primary sequences are highly degenerate and share only the same physical properties arising from the tripartite structure found in all signal sequences (Figure 1.3) [12, 15].

A positively charged region, encompassing one to five amino acid residues is located at the N-terminus (N domain), followed by a hydrophobic core consisting of ten

to fifteen residues (H domain). Finally, at the C-terminus a stretch of polar residues constitutes the signal peptidase cleavage site (C domain), which is the only conserved part in signal sequences [13].

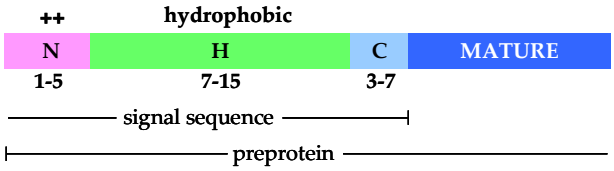

Figure 1. 3: The tripartite pattern of signal sequence

After translocation completion, the signal sequence is proteolitically removed by the signal peptidase, a membrane bound enzyme that utilizes a Lys-Ser catalytic sequence for peptide bond cleavage [20].

I.1.3.2 Co-translational vs. post-translational translocation

In bacteria there are two major routes that direct proteins to the translocation channel SecYEG, the co- and post- translational (Figure 1.2) [10, 21]. In co- translational translocation the main players are the ribosome and the ribonucleoprotein SRP [22]. This route is ubiquitous in all domains of life and mainly utilized for the integration of membrane proteins. The second route is the post-translational translocation, which involves the trigger factor (peptidyl-propyl cis-trans isomerase, TF), the molecular chaperone SecB and the peripheral motor ATPase SecA [4]. In this mode, preproteins are transported after completion of their synthesis. Post-translational translocation occurs by different mechanisms both in bacteria and in eukaryotes and is utilized mostly by soluble proteins that need to remain unfolded or loosely folded after their release from the ribosome. The two routes converge in the membrane protein conducting channel, SecYEG [23].

What features determine which pathway a preprotein enters to reach its final destination? Signal sequences determine at a very early stage of protein synthesis whether transport across biologic membrane will occur co-translational (SRP) or post-translational (SecB) (Figure 1.4) [17, 24]. SRP and TF compete for binding to the emerging nascent chain from the ribosome and what governs the fate of the preprotein are the length, the hydrophobicity [17] and the folding degree of the signal sequence [18]. SRP preferentially interacts with highly hydrophobic signal peptides at a very early stage of protein synthesis and is responsible mainly for the recognition and targeting of membrane proteins by binding directly to their hydrophobic TMSs [25]. The role of TF is

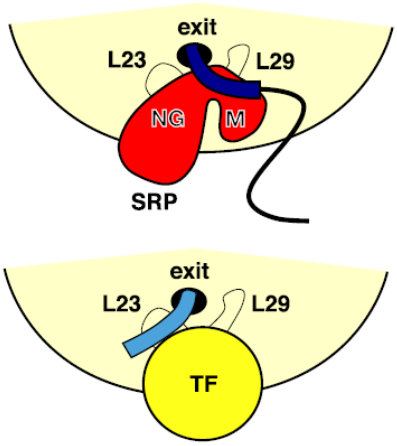

Figure 1.4: Schematic representation of interactions at the nascent chain exit site of the ribosome. SRP recognizes particularly hydrophobic targeting sequences (in dark blue) whereas TF interacts with less hydrophobic targeting sequences (in light blue) [22].

to block the interaction of SRP with the signal sequence and prevent the folding of the preprotein until the completion of synthesis [22]. Once synthesis of the emerging protein has reached a length of ~100 residues [26], or synthesis has been completed [27] then

SecB make contacts with the mature region of the preprotein and subsequently targets it to the membrane translocase post-translationally [22].

I.1.3.3 Signal Recognition Particle, Co-translational Targeting

The ubiquitous cytoplasmic SRP mediates targeting of nascent polypeptides to the translocation channel of the ER membrane of eukaryotes and the inner membrane of bacteria [28]. Bacterial SRP consists of 4.5S RNA (Ffs) and a 48 kDa single protein termed Fifty-four homolog (Ffh, homologous to the 54 kDa subunit of eukaryotic SRP). Ffh consists of three domains (Figure 1.5a) [29]: The N-domain is a four helix bundle structure responsible for the interaction with the ribosome. The "G-domain" is a conserved Ras-like GTPase domain responsible for the interaction with the SRP receptor. The C-terminal domain of Ffh, called the "M-domain" because of its high methionine content, comprises the RNA binding site and is implicated in signal sequence recognition.

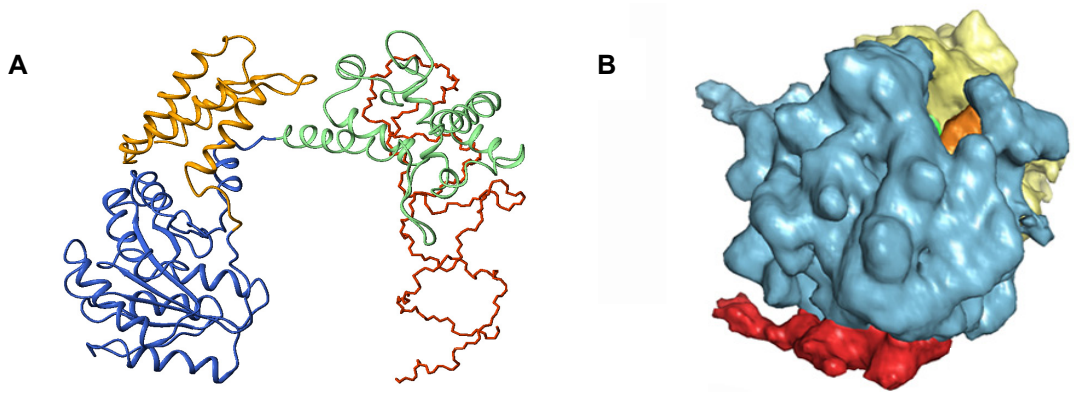

Figure 1.5: (a) Structural organization of *E. coli* SRP (PDB 1QZW). N-domain (yellow), G-domain (blue) and M-domain (green), RNA (brown) [29] (b) Cryo-EM structure of the *E. coli* SRP bound to a translating ribosome. Ribosomal subunits: yellow [30S] and blue [50S], tRNAs: green and orange, SRP: red [30].

SRP binds to a hydrophobic region of integral membrane protein (signal anchor sequence) as it emerges from the ribosome (RNC, Ribosome-Nascent Chain) and slows the chain growth [22, 30]. The resulting complex SRP-RNP is targeted to the membrane where it associates with the signal-particle receptor (FtsY) and the RNC is transferred to the protein conducting channel in a GTP-dependent manner [31]. Interestingly, *in vitro*, bacterial SRP and FtsY can efficiently replace their mammalian counterparts, indicating that these simpler components contain all of the essential features required for co-translational protein targeting [32, 33].

The signal-sequence-binding site of Ffh is located at the M domain. The structure of the M domain of *Thermus aquaticus* Ffh revealed a deep groove that is lined with conserved hydrophobic residues and includes all conserved methionines [34]. The dimensions and hydrophobic character of the groove suggest that it forms the signal sequence-binding pocket of the SRP [35]. The structure of mammalian SRP bound to an active 80S ribosome carrying a signal peptide has been solved to 12 Å resolution with cryo-EM [36] and together with the 16 Å cryo-EM structure from *E. coli* SRP bound to a translating ribosome (Figure 1.5b) [30] sheds some light on the structural arrangement of SRP and the recognition of the signal sequence. These structures indicate that the signal sequence is presented at the ribosomal tunnel exit in a spatial arrangement that allows it to slide directly into the proposed signal-sequence-binding site on the SRP. However, the available structural information regarding SRP dependent translocation is at very low resolution (10-20 Å). A better understanding of co-translational translocation requires higher resolution structures into all steps along the pathway.

I.1.3.4 SecB: a chaperone in post-translational targeting

SecB is a cytosolic chaperone that has so far only been found in prokaryotes and is involved in the post-translational export but is not essential for viability [37]. It maintains the newly synthesized preproteins in a translocation-competent state by keeping them in an unfolded or non-aggregated state [38]. Furthermore, SecB interacts specifically with either soluble or SecYEG-bound SecA to deliver the preprotein to the translocon [39].

SecB in solution forms a very stable tetramer of 69 kDa organized as a dimer of dimers (Figure 1.6a) [40, 41]. Two SecB dimers associate to form a tetramer by sandwiching four long α-helices between the eight stranded antiparellel β-sheets. The dimer-dimer interface is stabilized by polar interactions involving side-chains from the four α-helices.

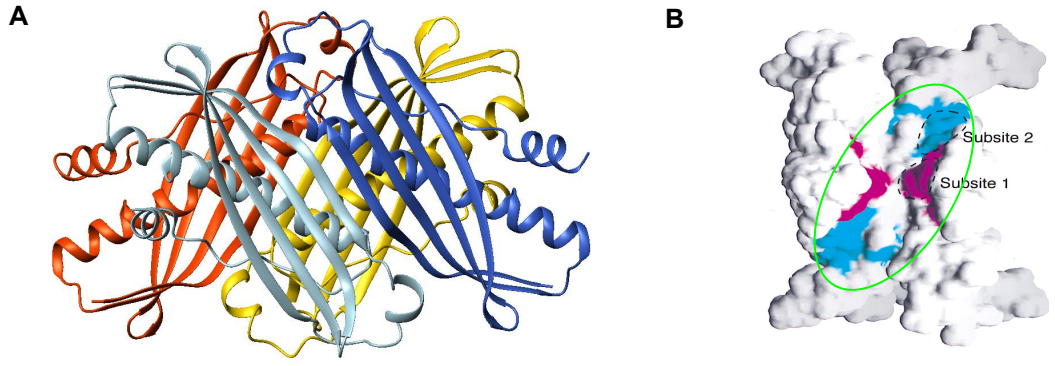

Figure 1.6: (a) SecB *H. influenza* (PBD 1OZB) tetramer structural organization. Front view showing the packing of the dimer of dimers. Each subunit in SecB tetramer is shown in different color. (b) Putative preprotein binding groove on SecB. Purple and blue surfaces indicate aromatic and hydrophobic aminoacids respectively [41].

The current view is that SecB interacts only with unfolded preproteins and specifically with exposed hydrophobic parts from the mature region (150-170 residues) that are normally buried in the folded state of the protein [42, 43]. SecB does not interact with signal sequence [44], although its presence is crucial for correct export. Based on crystal structures [40, 41] and in agreement with biochemical studies [45] there are two preprotein binding sites on SecB (subsite 1, 2) that together form the preprotein-binding groove (Figure 1.6b). One SecB tetramer contains two grooves that are solvent exposed and all together forms the preprotein binding channel ~70 Å long. Subsite-1 is a deep cleft formed from conserved aromatic amino acids and suitable for the binding of both aromatic and hydrophobic residues. Subsite-2 forms a shallow open groove with a hydrophobic surface that can accommodate mainly hydrophobic residues. The position of the binding groove suggests that the unfolded polypeptides are wrapped around the SecB tetramer.

I.1.3.5 The translocation channel

The translocation channel is universally conserved and formed by a heterotrimeric membrane embedded protein complex, known as the Sec61 complex (Sec61αβγ) in eukaryotes and SecY complex (SecYEG) in bacteria and archea [23, 46, 47]. The translocation channel has the unique ability not only to translocate proteins across biological membranes but also to integrate membrane proteins laterally into the lipid bilayer. SecY (α) and SecG (γ) show significant conservation and both are essential for the channel function as well as for cell viability, while SecG (β) subunit is not essential. The translocation channel is a passive pore and needs to associate with other proteins that

will provide the driving force for translocation. Biochemical and structural studies [9, 48, 49] have provided important insights and mechanistic details for the channel's function. The breakthrough in the field came with the crystal structure of an archaeal SecY complex (from *Methanococcus jannaschii*) at 3.2 Å resolution that revealed the architecture [49].

Architecture of the Channel: The channel is primarily formed by SecY, while the two small subunits SecG and SecE are located at the periphery of the complex (Figure 1.7a, b). SecY contains 10 TMS and can be divided into two halves, TMS 1-5 and TMS 6-10. The two halves share an inverted pseudosymmetry that resembles a clamshell with a central funnel-like pore and they are held together by SecE, which acts as a molecular clamp (Figure 1.7a). The crystal structure reveals a monomer of SecYEG complex that is

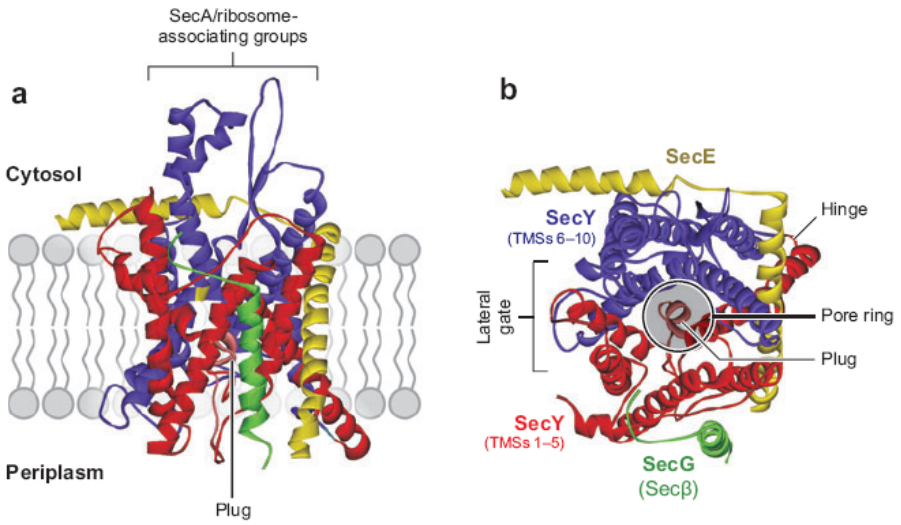

Figure 1.7: Architecture of the protein conducting channel (*a*) Membrane cross section and (*b*) a cytosolic view of the structure of the *M. jannaschii* SecYEβ (PDB 1RHZ). The protein-conducting channel consists of three subunits: the SecY (TMS1-5 red, TMS6-10 blue) that is embraced by the SecE (yellow) subunit and the peripheral bound SecG (green) protein [3].

probably representative for all species, as indicated by sequence similarity and comparison to a lower-resolution structure of *E. coli* SecYEG complex, determined by cryo-EM from two dimensional crystals within the membrane [50, 51].

At the cytosolic side, the channel is shaped as an inverted funnel with a diameter of ~ 20-25 Å at its widest point and ~ 4 Å at its narrowest point, forming the pore ring (Figure 1.7b). At the periplasmic side the structure shows a cavity, which is blocked by the first periplasmic loop of SecY that folds back as a distorted α-helix into the funnel like cavity. This structure is called the plug and is believed to be displaced from the periplasmic cavity upon initiation of protein translocation (Figure 1.7a, b) [52]. The plug domain is required to maintain the closed state of the channel and prevents the permeation of ions or other small molecules [53]. On the side of cytosol the channel has large loops extended out of the membrane plane, creating a docking site for the ribosome or other translocation ligands (Figure 1.7a) [21, 48, 54-58].

The pore ring consists of six hydrophobic residues that form a gasket-like seal around the translocating polypeptide, thereby restricting the passage of ions or other small molecules during protein translocation. The pore diameter, ~ 4 Å, is too small to accommodate an unfolded preprotein chain (width ~12 Å) or a disulfide bonded peptide loop or a preprotein with covalent attachments [59, 60]. Therefore, it is likely that the channel uses a mechanism to control the size of the pore which is based on its inherent flexibility that originates mainly from lateral shifts of the helices to which the pore residues are attached.

Opening of the channel might be achieved by a hinge movement of the loop region that connects TMS5 and TMS6 (Figure 1.7b) [49]. Signal sequence binding into

the channel walls could drive such a conformational change. The signal sequence intercalation site is located at a hydrophobic patch between TM2b and TM7 at the front of the cytoplasmic funnel and the residues forming the binding site are highly conserved [19].

The lateral gate of the channel is believed to facilitate the integration of nascent membrane proteins to the lipid phase [61] (Figure 1.7b). The TMSs moves from the aqueous interior of the channel to the lipid face one at a time. The lateral gate is located at the interface of the two halves of SecY, between TM2 and TM7 [49]. The arrangement of the two halves of SecY is such that there can be only one lateral opening of the complex in the front.

Oligomeric state of the channel: A functional export pore is formed by a single copy of SecYEG complex as shown from the *Methanococcus jannaschii* crystal structure and in contrast to previous reports suggesting that the pore is formed at the interface of SecYEG oligomers [49, 62]. Although the pore is formed by only one SecYEG copy, biochemical and structural data have indicated the formation of higher order SecYEG assemblies during translocation [63, 64]. Crosslinking studies demonstrated that the functional pore consists of two copies of SecYEG with only one being active during translocation [52, 65]. The second copy might facilitate the docking of other translocase subunits (SecA) and the ribosome. These dimers have a “front to front” orientation, with their lateral gates in contact and have different lipid accessibility (active state) (Figure 1.8). The “back to back” orientation was proposed by a previous study probably represents the inactive resting state of the channel (Figure 1.8) [50].

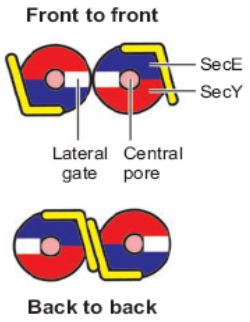

Figure 1.8: Schematic representation of possible SecYEG dimer configurations [3].

I.1.4.1 SecA ATPase

SecA is a highly conserved and essential component of the bacterial translocase machinery [4]. SecA is a motor protein and couples ATP hydrolysis to the translocation of preprotein across or into the bacterial plasma membrane [10, 23, 66, 67]. SecA is a central component of the translocase machinery because of its unique ability to interact with all of the partners involved in translocation [68, 69], including SecB, both the signal sequence and the mature domain of the preprotein, phospholipids, ATP, and SecYEG (Figure 1.9). Interestingly, SecA regulates its own expression by binding to its own mRNA [70].

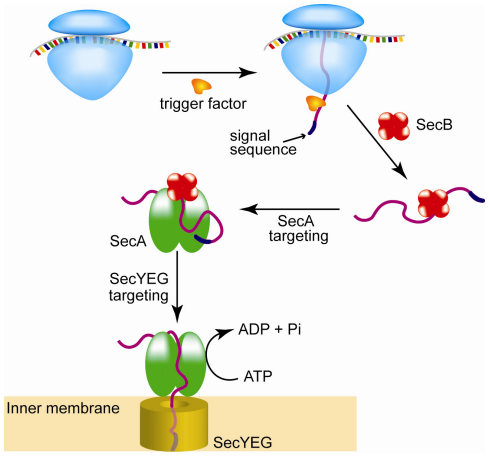

Figure 1.9: Schematic representation of the Sec dependent post translational translocation.

SecA partitions between a free cytosolic form and a membrane bound form [71]. SecA exhibits very low ATPase activity in the cytosol and is considered to be in the inactive, *closed state* [72, 73]. Binding of SecA to the membrane, especially in the presence of a preprotein, stimulates its ATPase activity and switches to its active *open state* [74-77]. In this state SecA drives efficiently translocation. Preprotein binding triggers ATP-driven cycles of conformational changes in SecA bound to SecYEG, described as insertion/de-insertion cycles [78, 79]. During this cycle 20–30 residue segments of preproteins are consecutively moved into the membrane through the SecYEG channel [80, 81].

SecA exists as a dimer (K_d = 1μM at 8 ^oC, 300 mM K^+ acetate [82]) and K_d of dimerization is modulated by temperature, salt concentration, and translocation ligands [76, 82]. The concentration of cytosolic SecA is 2-5 μM [82-84], thus it is expected to form a stable dimer in the cytoplasm. The functional oligomeric state of SecA at the translocon is a matter of controversy with some biochemical studies suggesting that SecA remains a dimer throughout translocation [85-89] and others arguing that SecA becomes monomeric when it interacts with SecY, lipids and signal peptides [57, 75, 76, 90-93].

The energy required for translocation is provided by ATP hydrolysis and the Proton Motive Force (PMF) (Figure 1.10). PMF is the sum of the membrane potential and the pH gradient. These energy forms are involved in different stages of translocation with ATP hydrolysis being essential for the initiation of translocation and PMF powering translocation in a later stage [59, 80]. The energy released from ATP hydrolysis is transformed to mechanical work that drives preprotein translocation across the membrane in a stepwise manner. When preprotein translocation is in progress, the PMF can further

drive the reaction and even complete it in the absence of ATP [79, 80]. In addition, PMF stimulates the release of ADP from SecA [94], promotes translocation–related conformational changes in SecA and has been suggested to be involved in the channel opening [95].

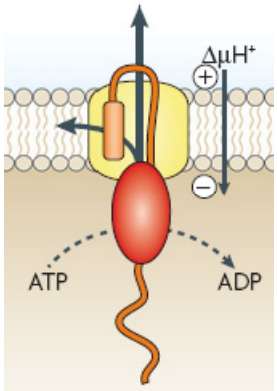

Figure 1.10: The energy for protein translocation comes from ATP and PMF [4].

I.1.4.2 Structural organization of SecA

SecA is a large (204 kDa) homodimeric protein consisting of 901 residues per protomer (Figure 1.11). The first crystal structure of SecA from *Bacillus subtilis* [73] provided a detailed insights into SecA structural organization and confirmed its structural homology to the superfamily 2 (SF2) DNA and RNA helicases [96-99]. Many crystal structures of SecA from various species have been subsequently reported [73, 74, 100-103] and in combination with available biochemical and biophysical data [97, 104-107] provide a better understanding of SecA at the level of structure and function.

While the protomer structural organization of SecA is very similar in all available SecA structures, the dimeric interface remains controversial the reason being that different crystal structures have shown different dimeric interfaces. In addition, SecA has

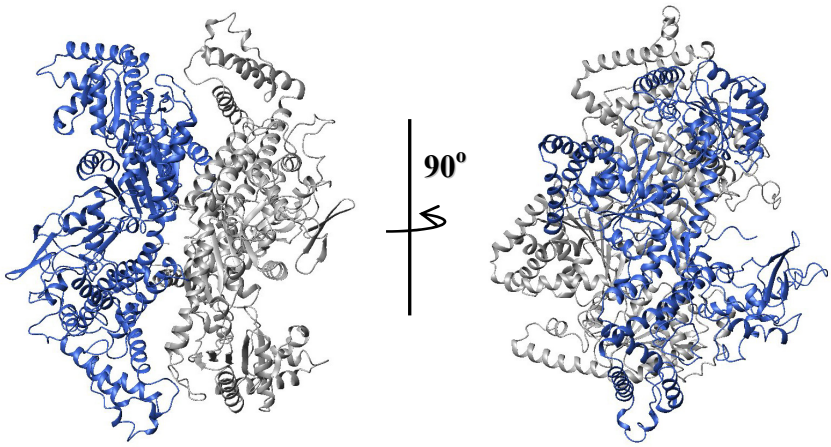

Figure 1.11: Structural model of *E. coli* SecA dimer, based on the most likely physiological dimer proposed for *B. subtilis* [67].

been crystallized both as a monomer and as a dimer. One explanation for different SecA dimeric organization may be that each one corresponds to a conformation dedicated for a distinct function along the intricate pathway of secretion. Another possibility is that extreme conditions employed for crystallization may induce non-physiological dimers.

The protomer of SecA can be subdivided into several structural domains and subdomains that are responsible for particular function (Figure 1.12). The motor domain of SecA is located at the N-terminus and is comprised of two domains, the Nucleotide Binding Domain (NBD or NBFI, Nucleotide Binding Fold I) and the Intramolecular Regulator of ATPase 2 (IRA2 or NBFII Nucleotide Binding Fold II). The crystallographic data revealed the structural homology of the SecA motor domain with the DEAD or DExH box RNA helicases [73, 97, 99, 102, 108].

The nucleotide binding cleft forms at the interface of NBD and IRA2. DEAD motors acquire specificity for diverse catalytic processes through additional non-homologous structural auxiliary domains that interact with different partners and

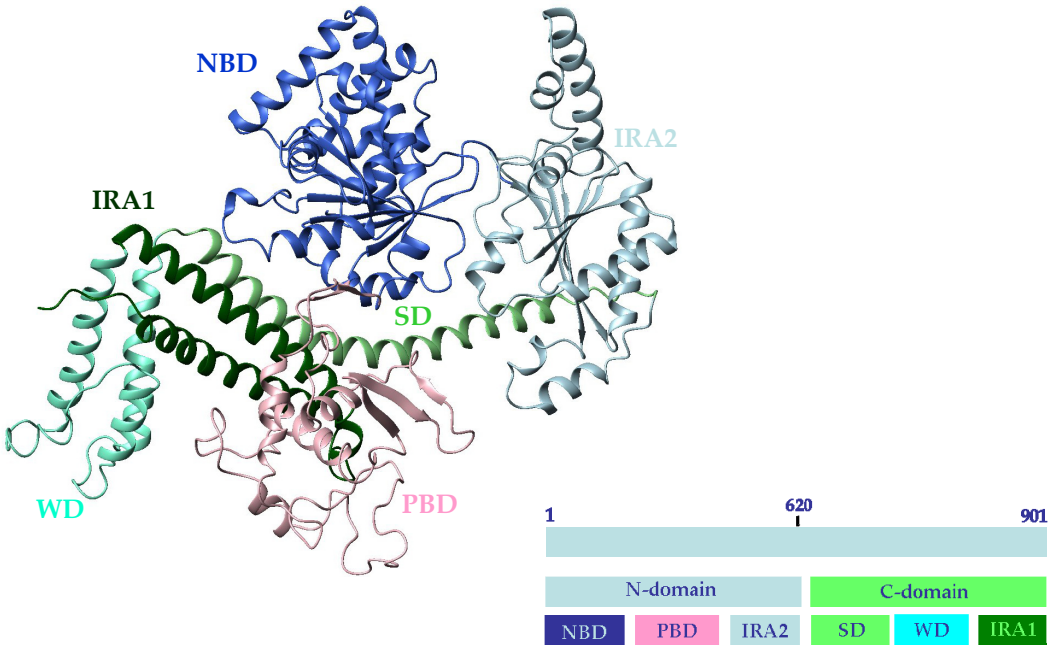

Figure 1.12: *E. coli* SecA protomer colored according to domain organization.

propagate the mechanical force generated by ATP hydrolysis. The specificity of SecA for the preprotein is conferred by an auxiliary domain, the Preprotein Binding Domain (PBD or PPXD, Pre-Protein Crosslinking Domain), which 'sprouts' out of the body of NBD through an antiparallel β-sheet.

A second appendage domain, termed the C-domain, is fused C-terminally to IRA2 domain and controls the mobility and the integrity of the N-terminal domain. The C domain is also divided into different substructures [97, 105, 109]. The Scaffold Domain (SD or HSD, α-Helical Scaffold Domain), a 46 residue long α-helix, acts as a molecular stapler that holds SecA's subdomains from moving apart and controls the opening and closing of the motor thus playing an important role in the catalytic cycle of SecA [105, 110, 111]. The Wing Domain (WD or HWD, α-Helical Wing Domain) is mainly α-

helical and its function is not well understood. The Intramolecular Regulator of ATP hydrolysis 1 (IRA1) is a conserved helix-loop-helix domain that prevents uncontrolled ATP hydrolysis in SecA.

The extreme C-terminal end of the C-domain is not highly conserved and is usually referred to as the C-Terminal Domain (CTD) or Carboxy-Terminal Linker CTL. CTD is not essential for catalysis and is very flexible therefore, mostly unresolved crystallographic [112]. The first half of the CTD has been resolved in only one SecA structure [73]. NMR [113-115] and biochemical data have shown the presence of a zinc finger of the last 25 residues of CTD which is involved in the interaction of SecA with SecB [116].

I.1.4.3 Structural homology of SecA with helicases

Helicases are motor proteins that catalyze the separation of oligonucleotides duplexes (DNA or RNA) to single strands in an ATP dependent manner [117, 118]. Helicases are using the extracted energy from ATP hydrolysis to bind and unwind nucleic acid substrates whereas SecA uses this energy to bind and move along polypeptide substrates while translocate them across or integrate them into the membrane.

The helicase/DEAD motor is highly conserved (Figure 1.13) and is assembled by two RecA- like domains first identified in RecA [119, 120], an *E .coli* recombination protein that catalyzes strand exchange within homologous segments of ssDNA and dsDNA. The two RecA domains can be in the same or different polypeptide chain in the various RecA-like motors.

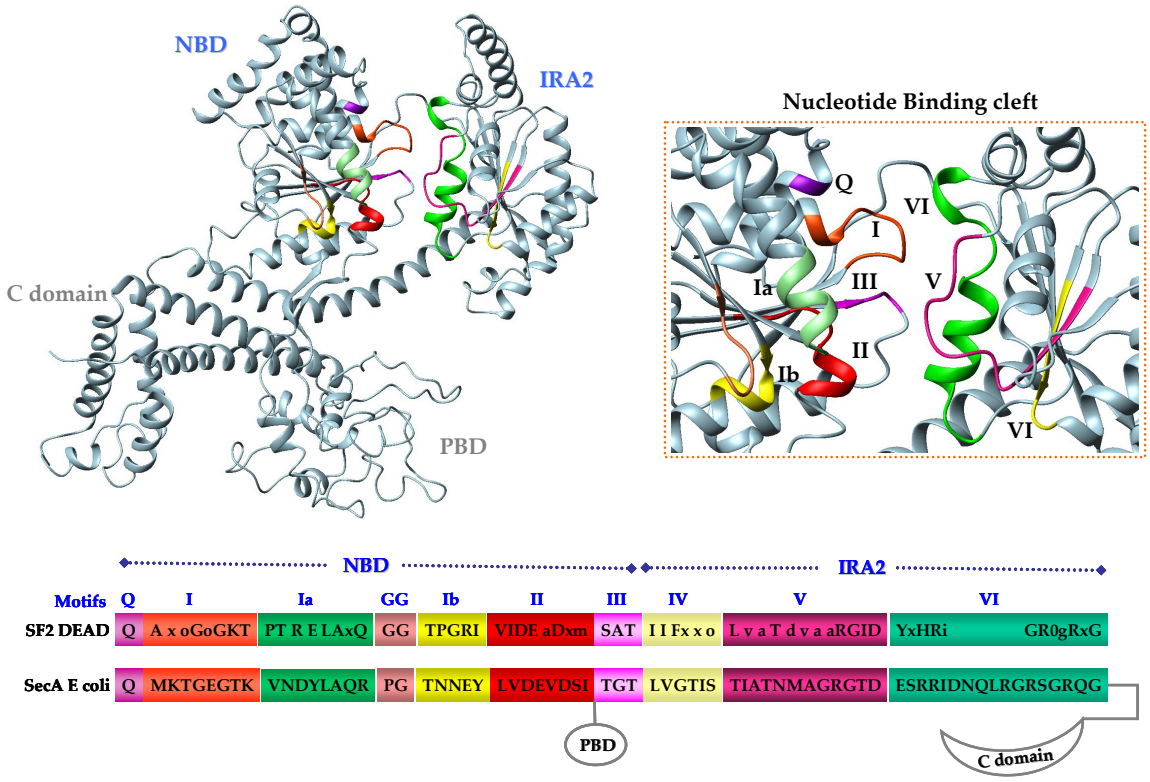

Figure 1.13: (a) The helicase DEAD motor of *E. coli* SecA. The helicase motifs are colored according to the lower panel. (b) Schematic representation of the nine conserved motifs of SF2 DEAD helicases aligned with those of the *E. coli* SecA. Capital letters indicate more than 80 % similarity; lower case letters indicate 50 – 79 % conservation. The 'o' represents threonine or serine. Figure adapted from [4].

Helicases share little sequence similarity with the exception of nine amino acid stretches, termed the 'helicase motifs' or 'helicase finger print', that are highly conserved (Figure 1.13) [121]. Most of the conserved motifs are located at the interface of the two RecA-like domains and are involved in ATP binding and hydrolysis [98, 99]. Some motifs are also are involved in the substrate binding. Furthermore, some of the helicase motifs are involved in the allosteric communication between the domains that result in

transducing the energy extracted from ATP hydrolysis to the displacement along or unwinding of the substrate. The most conserved motifs are the Walker A (phosphate binding P-loop) and Walker B (Mg^{+2} – binding aspartic acid) motifs named after J.E. Walker who first identified them (or motif I and II respectively) [122].

I.1.4.4 Interaction of SecA with the translocation partners

I.1.4.4.1 ATP hydrolysis in SecA

ATP hydrolysis is a simple and ingenious chemical reaction that is strictly controlled by regulatory factors so that the cell is protected from unnecessary consumption of energy. In case of motor proteins a series of events and a proper spatial arrangement of residues that line the nucleotide cleft should occur in order for ATP hydrolysis to take place [98].

ATP binds primarily in the RecA-like domain that contains the Walker A and B motifs (NBD in SecA). However, for hydrolysis, the presence of the second RecA-like domain (IRA2 in SecA) is required, which acts as a regulatory element. In the first step, a Lys at Walker A **(**A/GxxxGKT/S, MKTGEGKT in SecA) coordinates the γ-phosphate of ATP while the hydroxyl group of Thr or Ser ligates the Mg^{2+} ion. The Glu from Walker B **(**DExx, DEVD in SecA) polarizes the attacking water molecule whereas the carboxyl group of the aspartic acid coordinates the cofactor Mg^{2+} ion which is obligatory for ATP/ADP (Figure 1.14a). The most crucial step in ATP hydrolysis is the stabilization of the pentacovalent intermediate that is formed at the γ-phosphate after the nucleophilic attack of the water molecule [120].

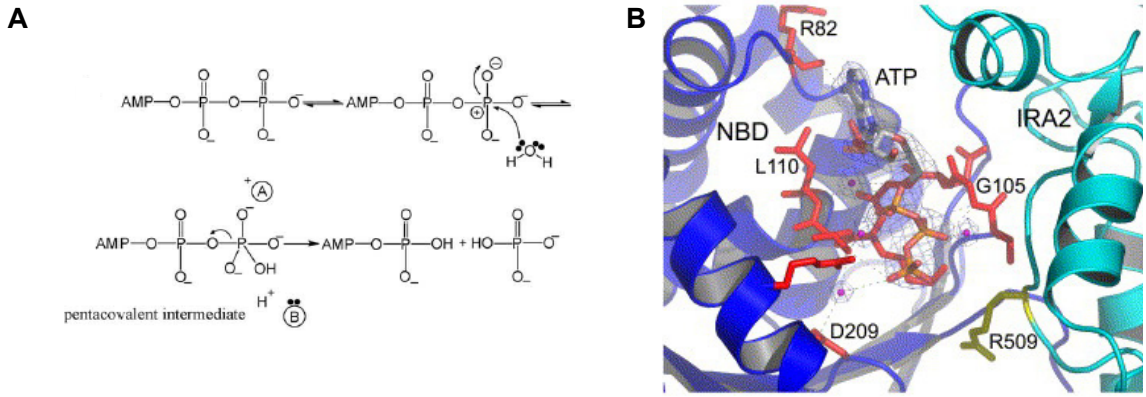

Figure 1.14: (a) ATP hydrolysis. The γ-phosphate is attacked by a water molecule, leading to a pentacovalent transition state that is stabilized by a general acid. (b) Atomic interactions in the nucleotide cleft of *E. coli* SecA:ATP [101].

A common mechanism of communication within RecA-like or GTP-binding domains is through an 'arginine finger' (motif V and VI in SecA), a conserved residue located in one of the domains (IRA2 in SecA) that inserts into the active site of the other domain (NBD in SecA) [123]. 'Arginine fingers' are ubiquitous in NTPases and they serve to neutralize developing charges in the transition state, thereby dramatically enhancing the catalytic activity of a protein [99, 124, 125]. The positively charged guanidinium group of the 'arginine finger' forms a salt bridge with the γ-phosphate of ATP and contributes to stabilization of the negatively charged pentacovalent transition state (Figure 1.14b). Release of the pyrophosphate would disengage the ‘arginine finger’ from the nucleotide and separate the second domain from the first, allowing an ATP regulated conformational change in the motor domain.

I.1.4.4.2 SecB interaction with SecA

Association of the SecB-preprotein complex with SecA results in the transfer of the SecB-bound preprotein to SecA for membrane translocation. The CTD region of SecA (25 residues) serves as a genuine binding site for SecB, although additional sites have also been suggested [126, 127]. The symmetry of SecB favors the binding of one SecA dimer per SecB tetramer, in consistence with the crystallographic data that revealed the ability of SecB to bind two C-terminal SecA peptides (Figure 1.15) [116].

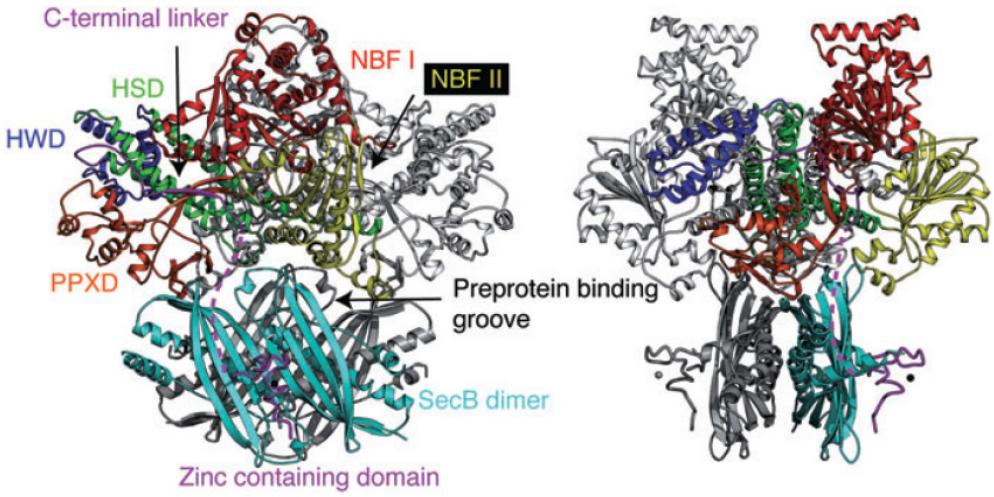

Figure 1.15: A hypothetical model of SecA-SecB complex. SecA dimer (*B. subtilis*) is on the top and SecB tetramer (*H. influenzae*) is on the bottom. C-terminal linker: magenta, dashed line: 15 residues that are missing between SecA crystalographycally resolved part and the zinc containing domain [116].

The CTD region of SecA is a highly flexible, positively charged region (rich in R and K) with three cysteines and a histidine residue that together coordinate a zinc finger needed for SecB binding. From the side of SecB, a negatively charged patch (rich in acidic residues and solvent exposed) present on both sides of the SecB tetramer serves as

the binding site for SecA. The SecA-SecB complex can be envisaged as a symmetric structure wherein the C termini of two SecA protomers embrace the tetrameric SecB with the postulated preprotein-binding grooves on SecB aligned with the preprotein–binding site on SecA (Figure 1.15) [128].

I.1.4.4.3 SecA interaction with the signal sequence

One of the most intriguing aspects of SecA is its capacity to recognize hundreds of different signal sequences. Specific interaction between a signal sequence and SecA is a decisive step incorrectly sorting secretory from non-secretory proteins. A recent NMR study reports the structure determination of the SecA-signal peptide complex demonstrating that the peptide forms an α-helix and binds by using both its hydrophobic and charged regions into a flexible and elongated groove in SecA [129] (Figure 1.16).

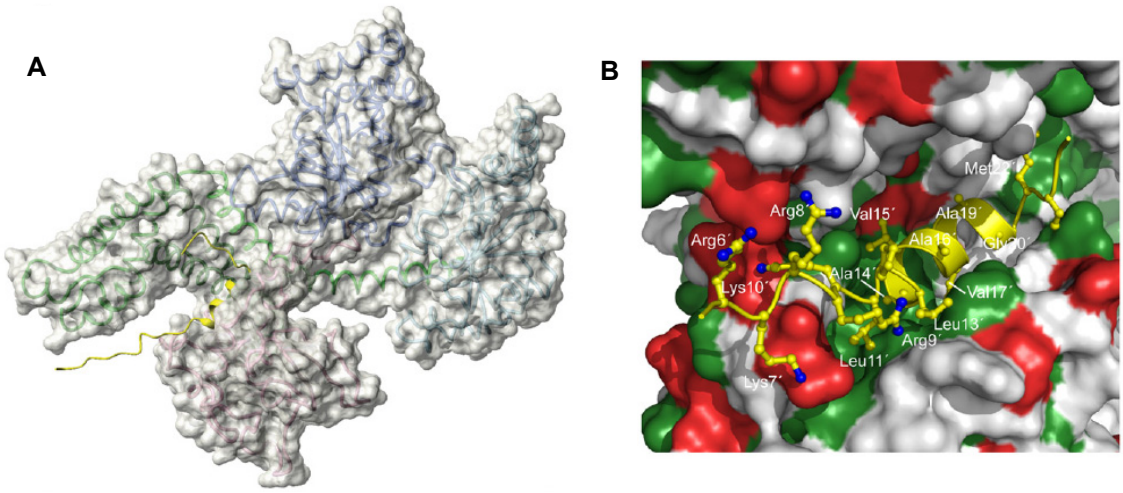

Figure 1.16: a) Structure of SecA bound to the KRR-LamB signal peptide, signal peptide is shown in yellow. b) Closer view of the groove bound to the signal peptide. Green and red surface indicates hydrophobic and acidic residues, respectively [129].

A central feature of the recognition process is the transition of the peptide hydrophobic region from a random coil conformation to an α-helix upon its interaction with SecA [130]. The binding groove has several distinct features (Figure 1.16b): (1) it is quite long (~28 A°), thus explaining how SecA can accommodate signal sequences with much longer α-helical hydrophobic regions; (2) it consists of hydrophobic residues and is surrounded by acidic ones, thereby permitting the signal peptide to bind in a dual mode; (3) it is relatively deep with many small pockets present at its sides, thereby accommodating signal sequences of varying length and bulkiness of side chains; (4) it is lined with several loosely packed methyl groups and Met residues, whose side chain is particularly flexible thereby providing a malleable hydrophobic surface that can adapt itself to the binding of signal sequences of varying dimensions and (5) it is formed at the interface of two domains, PBD and IRA1 which may render the groove flexible and expandable. Collectively, the structural plasticity of the binding groove might be crucial for SecA to recognize its diverse range of substrates.

I.1.4.4.4 Interaction of SecA with SecY

SecA interacts specifically with SecYEG and this interaction induces large conformational changes that results in the stimulation of SecA's ATPase activity [131, 132] and triggers the opening of the channel [57, 93]. The loops from the C-terminal half of SecY that protrude into the cytoplasm provide the main contacts for binding of cytosolic factors, such as SecA and the ribosome [21, 48-50, 54-58, 133] (Figure 1.17). These loops are extending ~20 Å above the membrane plane and amino-acid substitutions on these loops abolish ribosome and SecA binding [48, 54, 55].

Genetic and biochemical studies have shown that SecA binds with high affinity to SecYEG through C4, C5 and C6 [58, 133-135]. The C5 loop is one of the most conserved regions of SecY and contains R357 [136] that has been shown to be of special importance for a functional SecA-SecYEG interaction [137]. Residues in the vicinity of R357 in *E. coli* are also essential for SecA docking onto the channel and activation [133, 134, 136,

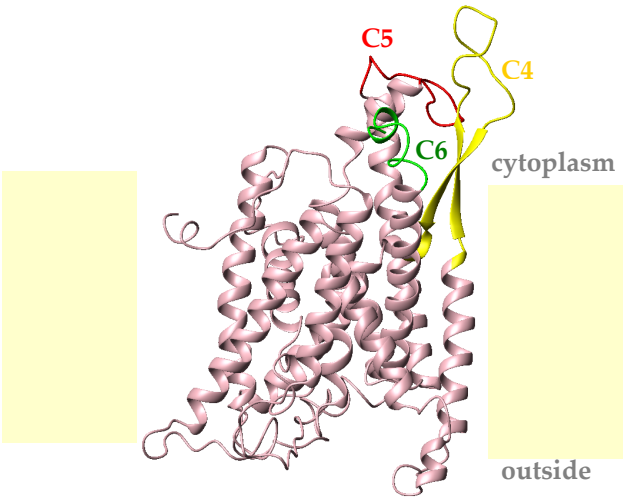

Figure 1.17: A model of *E. coli* SecY structure derived from the original structure of SecYEG from *M. jannaschii* (PDB 1HRZ). The cytoplasmic loops C4, C5 and C6 are colored to highlight the docking site for the cytoplasmic partners.

138]. *In vivo* photo-crosslinking studies suggested that C4 and C5 regions provide a relatively constitutive binding site for SecA and may be involved in its ATPase activation, while residues at C6 found to be approached by a working form of SecA as it is driving preprotein translocation [133].

In vivo sulfidryl labeling suggested that SecA associates with SecYEG primarily via PBD, IRA2, and CTL [139] whereas a crosslinking study showed that SecA interacts with SecY through its C domain and NBD [93]. Detailed peptide mapping showed that the cytoplasmic loops are in close contact with both SecA substructures (C and N

domain) [58]. Collectively, available data suggest that both the C and N domain of SecA are involved in the binding with SecY.

The SecY channel is formed from two SecYEG trimetric complexes with each copy having its own specific function. One copy is carrying out the actual translocation process while the second copy holds SecA in the correct place to carry out the translocation [65]. A disulfide bridge cross-linking study suggests that SecA docks onto the non-translocating SecYEG copy mainly through NBD, while SecA is translocating the preprotein through a neighboring copy of SecYEC [65]. The dimensions of SecA are consistent with one molecule interacting with two SecYEG complexes; however, the interaction sites for SecA are likely different for the two SecYEG copies.

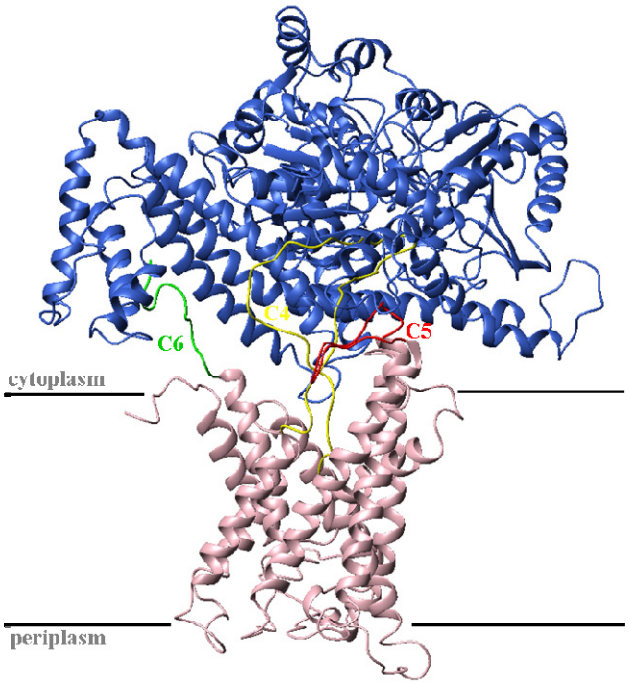

Figure 1.18: SecA-SecYEG complex (PDB 3DIN). SecA: blue, SecY: pink, C4: yellow, C5: red, C6: green. The black line indicates the membrane boundaries.

The crystal structure of SecA bound in an intermediate state of nucleotide hydrolysis (ADP–BeF_x) to the SecY complex from *Thermotoga maritime* solved at a resolution of 4.5 Å [57] (Figure 1.18) is in full agreement with the above observations. In this structure, the most crucial interactions occur between the PBD of SecA and the cytoplasmic loops C4 and C5 of SecY. The extreme C-terminal tail of SecY interacts with SD and IRA1 and amino acid substitution in this part of SecY abolish the translocation process [140, 141].

The crystal structure of SecA-SecY complex most likely represents the active copy of the SecY channel, the one through which polypeptide chains are translocated during secretion, while the supportive copy has been removed during the detergent solubilization.

I.2.1 Biomolecular NMR

NMR (Nuclear Magnetic Resonance) has been widely used in the field of structural biology to study biomolecular structure, dynamics and function [142-144]. Together with X-ray crystallography, NMR is the main tool to study biomacromolecules at atomic resolution [145]. The two techniques are complementary with NMR having the advantage of being capable to determine both structure and dynamics in semi-physiological conditions, in solution. The conditions used in NMR studies are much closer to the conditions found in the cell. Crystallization is not required and crystal packing effects may not influence the structure especially on the surface of a protein where interaction with other molecules may occur. Furthermore, partially folded proteins are not amenable to crystallization because they do not adopt one unique 3D structure in solution but fluctuate over an ensemble of conformations; therefore, these proteins can be ideally studied with NMR. Protein folding can be studied by monitoring folding (intermediates and even transition states) or denaturing of a protein in *real time* [146, 147]. Finally, the improvements in in-cell NMR-based methods allow the investigation of structural properties of a molecule and the interactions that underlie protein-protein complex formation *in vivo* [148, 149].

Recent advances in NMR equipment (higher magnetic fields, cryoprobes), in NMR methodologies and isotopic labeling schemes have enabled structural, dynamic and molecular interactions [150-152] in larger and more complex biological systems [153-157].

I.2.2 HSQC: The "fingerprint" of a protein

The Heteronuclear Single Quantum Coherence (HSQC) is a simple 2D NMR spectrum that generates cross peaks correlating ^{1}H and heteronuclei (^{15}N, ^{13}C) [158]. The "fingerprint" of a protein (Figure 1.19) is ^{1}H-^{15}N-HSQC that correlates the amide H-N pair and has a unique pattern for every protein that depends both on its primary sequence and its overall 3D structure (Figure 1.19). The exact resonance frequency of each amide pair depends on its chemical environment.

Because of the high sensitivity of the chemical shift (δ) to the chemical environment, the NMR spectrum of a protein will show NMR signals with slightly different frequencies depending on the amino acid composition and the folding of a protein. In the case of a folded protein, the peaks are usually well dispersed in the NH region (6-12 ppm) whereas in an unfolded protein resonance peaks are poorly dispersed.

Each ^{1}H-^{15}N cross peak in the HSQC spectrum represents a resonance peak from a single NH. Therefore, in an HSQC we expect to observe as many peaks as the number of residues of the protein with the exception of proline that lacks an NH-backbone

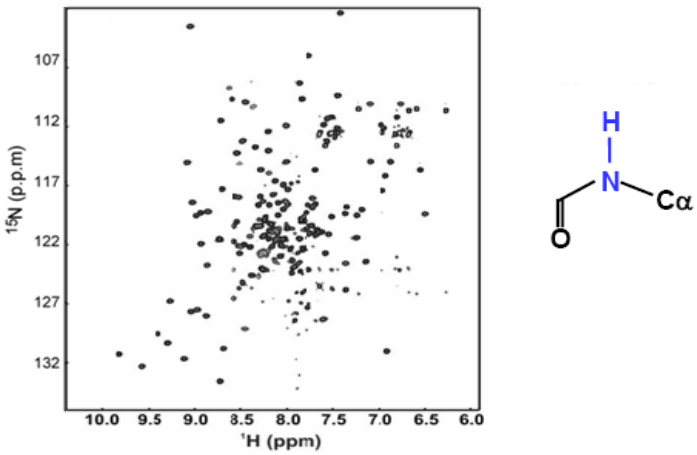

Figure 1.19: A typical 2D ^{1}H-^{15}N HSQC spectrum of a folded 20 kDa protein. The backbone NH of an aminoacid is highlited blue.

moiety. However, HSQC also contains signals from the NH_2 groups of the side chains of Asn and Gln because they also contain amide protons and of the aromatic HN protons of Trp and His.

The HSQC experiment is a very useful tool in detecting and studying interactions with ligands, such as other proteins or drugs [159]. In this case, we take advantage of the sensitivity of the chemical shift of an NMR-active nucleus to changes in its environment. An analogous experiment can be performed for ^{13}C and ^{1}H (^{13}C-HSQC).

I.2.3 Assignment of NMR resonance peaks

To use NMR to investigate the structure and dynamics of a macromolecule, it is necessary to assign the resonance peaks in the spectrum to specific atoms in the macromolecule. Multidimensional NMR experiments (3-4D) [160] and the availability of ^{13}C-, ^{15}N- labeled proteins provide excellent tools that have enabled straight forward resonance assignment of proton, nitrogen and carbon in proteins and protein complexes.

The most common strategy for resonance assignments is the use of triple-resonance experiments (^{1}H, ^{13}C, ^{15}N) [158, 161]. To record these experiments the protein or the nucleic acid of interest must be isotopically enriched by biosynthetic incorporation of ^{13}C glucose and ^{15}N ammonium. These experiments are based on the ability to transfer magnetization between NMR active nuclei through *J* couplings. Sequential assignment in a protein can be obtained by correlating the chemical shifts of the amide group (NH) of a spin system with both inter- and intra- residue chemical shifts of main chain (CO, Cα, N) or side chain atoms (Cβ, Cγ, etc) (Figure 1.20).

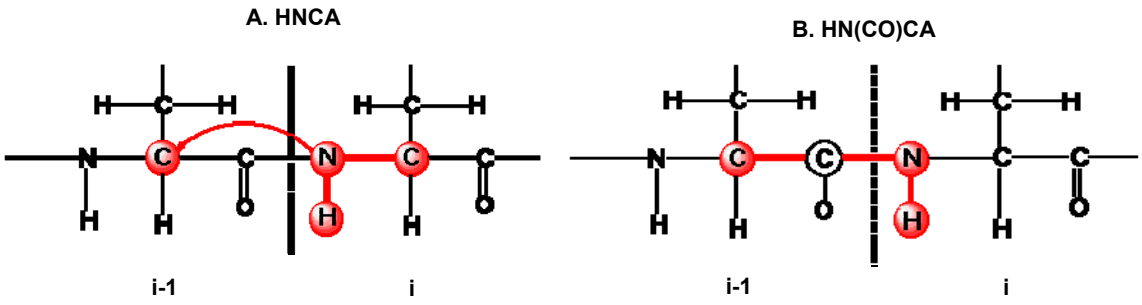

Figure 1.20: Magnetization transfer through bond in HNCA, HN(CO)CA triple resonance experiments. (a) HNCA, magnetization is transferred from ^{1}H to ^{15}N and then via the N-Cα J-coupling to the $^{13}C\alpha$ and then back again to ^{15}N and ^{1}H hydrogen for detection. (b) HN(CO)CA, magnetization is transferred from ^{1}H to ^{15}N and then to ^{13}CO. From here it is transferred to $^{13}C\alpha$ and the chemical shift is evolved. The magnetization is then transferred back via ^{13}CO to ^{15}N and ^{1}H for detection. Red circles indicate the recorded chemical shifts and white circled atoms mediate the transfer of magnetization but their chemical shift is not recorded [158].

The most common sets of 3D experiments for sequential assignment are: HNCACB with CBCA(CO)NH , HNCA with HN(CO)CA and HNCO with HN(CA)CO (atoms in brackets serve to transfer magnetization between atoms but their chemical shift is not recorded) [158]. The principles described in Figure 1.20 for HNCA/HN(CO)CA apply for these sets of experiments.

I.2.4 NMR of large proteins

The application of NMR in proteins and complexes with molecular weight larger than 30 kDa has been a challenge in the field and considerable effort has been devoted to overcome size limitations [162-164]. Systems of large molecular size give poor-quality

spectra (equation 1.1). This is because of the line broadening observed in the spectra due to fast transverse relaxation (T_2) associated with slower tumbling of the protein and the extensive spectral overlap from the sheer number of nuclei.

$$S/N \sim N\, \gamma_{exc}\, \gamma_{det}^{\ 3/2}\, B_0^{3/2}\, NS\, T_2^{1/2} \qquad (1.1)$$

S/N = signal-to-noise, N = number of spins

γ_{exc} = gyromagnetic ratio of excited spins

γ_{det} = gyromagnetic ratio of detected spins

B_0 = static magnetic field

NS = number of scans

T_2 = transverse relaxation ~$1/\Delta\nu$ (line width)

Transverse or spin-spin relaxation (T_2) is the mechanism by which loss of coherence in the transverse plane occurs due to spin-spin interactions. The line width in the spectrum is inversely proportional to T_2, which depends on the size of the molecule (Figures 1.21, 1.23a,b). The slow tumbling of larger macromolecules, which is represented by the rotational correlation time, τ_c, in solution leads to faster relaxation of transverse magnetization due to enhanced spin – spin interactions. The τ_c in ns of a molecule in solution at room temperature is about half its MW in kDa [158].

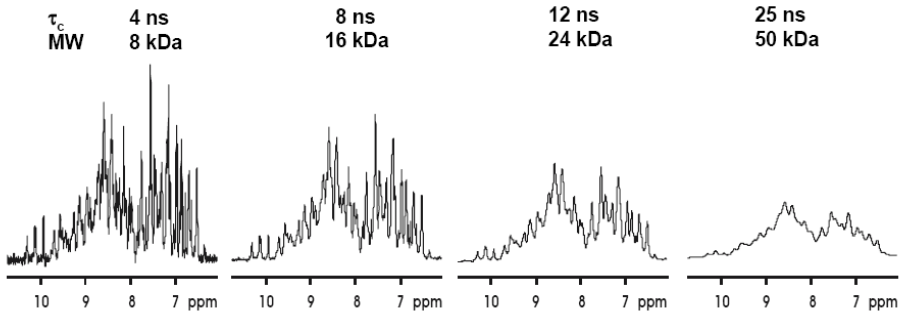

Figure 1.21: Effect of molecular weight in the linewidth of the NMR spectra. The linewidth is proportional to T_2 ($\Delta\nu = 1/\pi T_2$) [144].

Spins are sensitive to the presence of near-by magnetic fields e.g. dipole-dipole interactions with other spins (D-D, through space) or chemical shift anisotropy (CSA) due to non-spherical distribution of electrons around the nucleus. These magnetic fields lead to nuclear relaxation. In proteins, a major source of relaxation is the high density of protons present. A generally applicable approach to minimize spin-spin interactions that lead to fast T_2 relaxation is the replacement of protons with deuterons [165]. This strategy results in increased resolution and significant sensitivity gain because it eliminates the internal and external contribution to dipole-dipole relaxation. The gain in sensitivity after deuteration is related to the much smaller gyromagnetic ratio of the deuteron compared to the proton ($\gamma_D/\gamma_H \sim 1 / 6.5$, equation 1).

However, perdeuteration results in complete elimination of protons that are very important in protein NMR because they contribute considerably to the structural information, and produce the most sensitive NMR signal. To this end, a compromise can be made by using partial deuteration and alternative labeling protocols that allow the extraction of information from the protons. One very attractive approach is the use of metabolic precursors that allows the selective protonation of specific groups, e.g., methyls (Figure 1.22), allowing these to be monitored in concert with the backbone amides [165, 166]. With this methodology specific methyl labeling in an otherwise completely deuterated background can be achieved for Ala [167], Met [129], Val, Leu and Ile [168].

Methyl groups are excellent probes in protein NMR studies because they are distributed throughout the protein and are very frequently present in the hydrophobic cores of proteins, binding sites or at the interfaces of complexes. Furthermore, the

threefold degeneracy of methyl protons in $^{13}CH_3$ results in a higher effective concentration as compared to amide protons. Methyl groups rotate very rapidly about their axes of three-fold symmetry and thus giving rise to favorable relaxation properties [168-170].

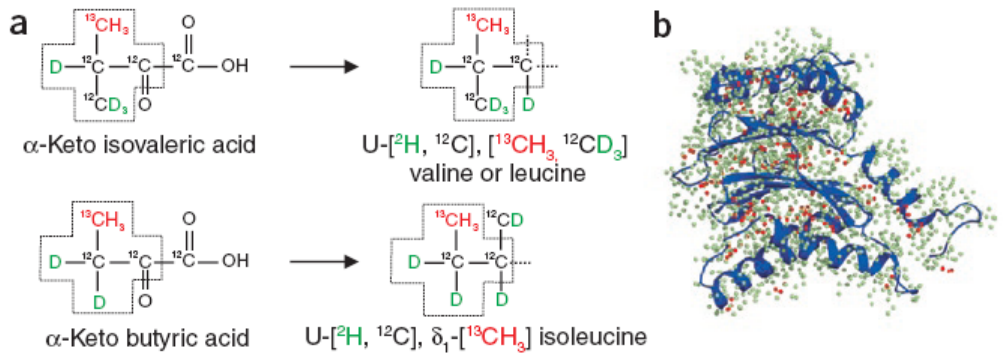

Figure 1.22: Methyl labeling strategy. (a) Precursors used to produce proteins with methyl labeling ($^{13}CH_3$) in isoleucine, leucine and valine (b) Ribbon diagram of the α subunit of *T. acidophilum* proteasome highlighting the labeling scheme used. Isoleucine (δ_1), leucine and valine methyl groups are indicated in red and deuterons in green [166].

Deuteration alone cannot extend the application of NMR above the size limit of 50 kDa. An important methodological advance has been the development of Transverse Relaxation-Optimized Spectroscopy (TROSY) [171, 172] which is based on manipulation of spin properties to overcome line broadening (Figure 1.23). TROSY uses spectroscopic means to reduce transverse relaxation based on the fact that the cross-correlated relaxation caused by DD and CSA interference gives rise to different relaxation rates of the individual multiplet components in a system of two coupled spins 1/2 [173]. By combining ^{2}H-labeling and TROSY, high-resolution ^{1}H-^{15}N-HSQC NMR spectra of macromolecules with molecular weights >100 kDa can be recorded. TROSY is

not limited to [^{15}N, ^{1}H]-correlation experiments. It has been successfully applied to methyl spin systems in [^{13}C^{Methyl}-^{1}H]-HMQC experiments. Remarkably, combination of deuteration with the methyl-TROSY methodology [174] has significantly extended the range of macromolecular systems that can be studied by NMR such as the molecular machinery of 20S proteosome core with molecular weight 670 kDa [169] and the 204 kDa translocase ATPase SecA [129].

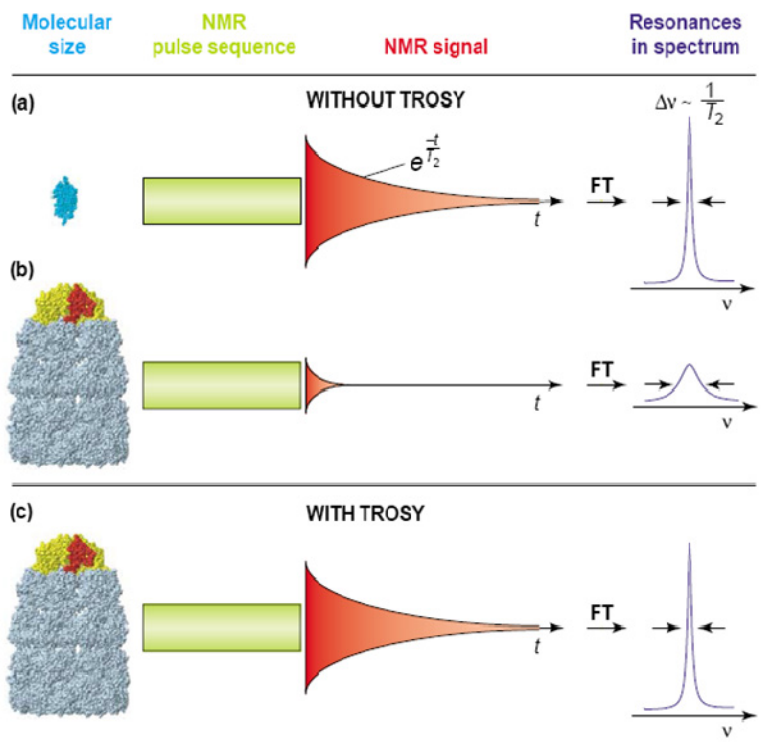

Figure 1.23: (a) The NMR signal obtained from small molecules in solution relaxes slowly. A large T_2 value results in narrow line widths ($\Delta\nu$) in the NMR spectrum. (b) For larger molecules, the decay of the NMR signal is faster (T_2 is smaller), producing a weaker and broader signal in the spectrum. (c) Using TROSY, the transverse relaxation can be substantially reduced, which results in improved resolution and sensitivity for large molecules [163].

I.2.5 Ligand binding and molecular interactions studied by NMR

Interactions of proteins with other macromolecules or small molecules play important roles in all biological processes. A powerful aspect of biomolecular NMR spectroscopy is its ability to characterize protein complexes under physiological conditions at atomic level even if the interactions are weak and transient [151, 152, 175].

NMR is an excellent tool for characterizing protein interactions e.g. protein/protein, protein/nucleic acid, protein/ligand or nucleic acid/ligand interactions without the need for high-resolution structure determination. The principle behind this approach, known as NMR mapping, is that titration of a ligand that interacts with a molecule induces changes in its NMR spectrum for signals of atoms near the binding site. A variety of experiments have been developed to study biomolecular interactions such as chemical shift perturbation mapping, saturation transfer difference spectroscopy (STD) [152], differential line broadening, the transferred cross-saturation experiment (TCS) [176], isotope labeling methods [177, 178] (isotope filtered NMR experiments) and residual dipolar coupling (RDCs) [175].

Chemical shift perturbation is the most widely used NMR method to map protein interfaces [151]. The technique is based mainly on analyzing ^{1}H-^{15}N-HSQC or ^{1}H-^{13}C-HMQC spectra. The chemical shift in both nitrogen and proton dimensions is sensitive to the chemical environment of the two nuclei. The ^{15}N-^{1}H HSQC spectrum of one protein is monitored when the unlabeled interaction partner is titrated in, and the perturbations of the chemical shifts are recorded [179]. Generally, one cannot use chemical shift changes to predict what exactly happens at the interface (e.g. structural changes). Chemical shift

perturbation measurements solely provide information about the interacting surfaces of the binding partners.

I.2.6 Protein dynamics by NMR

Structural flexibility plays an important role in the function of protein molecules [156, 180]. Protein dynamics contribute to the thermodynamic stability of functional states and play an important role in catalysis, ligand binding, molecular recognition and allostery [155, 181-183]. NMR has proved an excellent tool to study and characterize the protein dynamics at atomic level and on a wide range of time scales, from rapid bond fluctuations in the picoseconds to nanosecond (pn-ns) to slower collective motions in the micro to millisecond(μs-ms) regime (Figure 1.24) [156, 158].

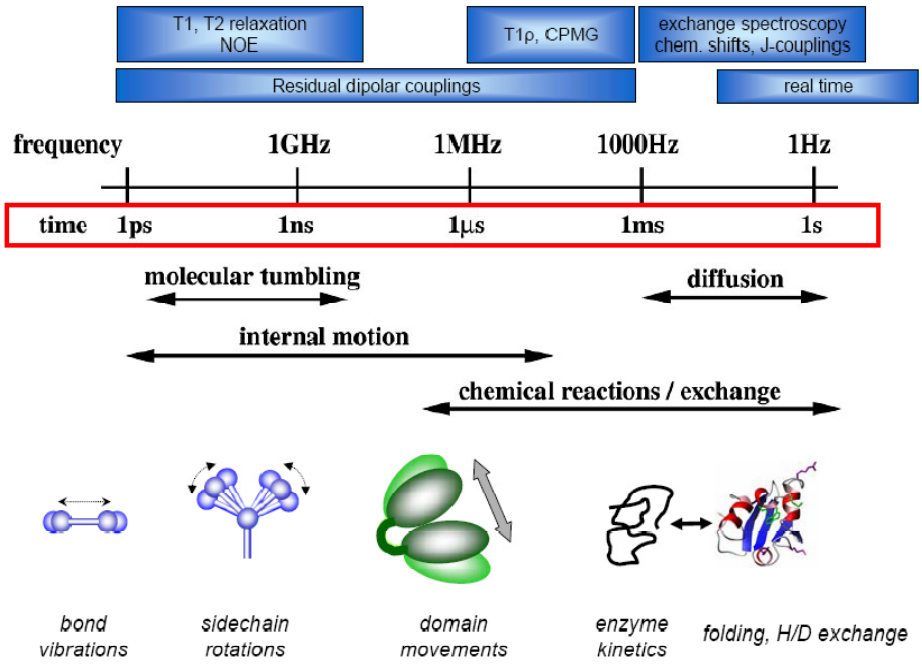

Figure 1.24: NMR time scales and dynamics in biology [144].

Many of the bonds in a protein can rotate and bend, and entire structural segments of the protein can move on a variety of timescales. Any of these motions may be functionally significant and directly related to ligand exchange and/or catalysis. Motions of backbone and side-chain atoms may be required for molecular recognition, loop motions may be required to exclude water or for repositioning of catalytic residues, and large-scale conformational rearrangements may be required to achieve the active form of the enzyme.

Fast protein dynamics (ps-ns). NMR relaxation has been extensively used to characterize molecular motions [155]. The longitudinal relaxation rate, R_1, the transverse relaxation rate, R_2, along with the heteronuclear ^{15}N-Nuclear Overhouse Effect (HetNOE) are the most universally measured NMR parameters for quantitating dynamics on fast timescales (ps-ns) [184, 185]. In the case of HetNOE the thermal fluctuations in a protein on a per residue basis are observed. As a rule of thumb, partially flexible parts, such as exposed loops can be easily distinguished from the folded core. Unstructured parts or unfolded proteins frequently yield ^{1}H-^{15}N NOE values of negative sign.

Slow protein dynamics (µs-ms). Many biological processes occur on the µs–ms timescale, including protein folding, substrate binding, allosteric regulation and catalysis. It becomes apparent the importance of studying slower timescale motion [153, 186].

Conformational changes alter the environment of a nuclear spin and modulate its chemical shift. When this process is on the µs-ms timescale and the chemical shift changes are large, the NMR signal broadens, leading to an increase in R_2. To measure the R_2 component that contributes to line broadening we measure the R_{ex}, factors which is the relaxation rate due to conformational exchange, as nuclei sample multi conformations

and magnetic environments. This process is most reliably identified by measuring R_2 as a function of the effective radiofrequency field strength using spin-lock ($R_{1\rho}$) or Carr-Purcell-Meiboom-Gill (CPMG) methods [157]. R_{ex} can be directly measured using these approaches.

I.3.1 Biological thermodynamics

All biological processes, such as enzyme function and signal transduction, depend on specific molecular interactions that are governed by thermodynamics [187]. An understanding of biomolecular recognition requires complete characterization of binding energetics.

The thermodynamics of association are characterized by the stoichiometry of the interaction (n), the association constant (K_a), the enthalpy change (ΔH), the entropy change (ΔS) the free energy change (ΔG) and the heat capacity of binding (ΔC_p). The energetics of binding combined with structural information, can provide a better understanding of the interaction mechanisms [188].

I.3.2 Basics of Binding Thermodynamics

Isothermal Titration Calorimetry (ITC) is the only technique that directly measures the enthalpy change upon binding and is widely used to characterize the binding interactions of macromolecules with ligands at constant pressure [189-191]. It allows the direct measurement of the enthalpy change (ΔH), the association constant (K_a) and stoichiometry (n) in a single experiment. The free energy (ΔG) and entropy changes (ΔS) of the binding reaction can be calculated after correction of ΔH for the presence of any linked equilibria to obtain ΔH from the relationship:

$$RT \ln K_d = \Delta G = \Delta H - T\,\Delta S = - RT \ln K \qquad (1.2)$$

where T is the absolute temperature and R the universal gas constant. The dissociation constant of the binding reaction, $K_d = 1/K_a$, is commonly used as a measure of the ligand affinity.

To have a complete thermodynamic analysis of a binding interaction it is essential to measure the ΔC_p, a fundamental thermodynamic quantity, that allows the prediction of ΔG, ΔH and ΔS as function of temperature.

$$\Delta C_p = d(\Delta H^o) / dT = T\, d(\Delta S^o) / dT = (\Delta H^o_{T2} - \Delta H^o_{T1}) / (T_2 - T_1) \qquad (1.3)$$

The ΔG of binding determines the stability of the biological complex and the direction which binding equilibrium will proceed with more negative values indicating higher binding affinity [192]. The total ΔG of binding includes a contribution associated with the formation of secondary and tertiary structure (van der Waals interactions, hydrogen bonding, hydration, conformational entropy), electrostatic and ionization effects, contribution due to conformational transitions, loss of translational and rotational degrees of freedom and others.

Interacting systems tend to compensate enthalpic and entropic contributions to ΔG, making binding free energy relatively insensitive to changes in the molecular details of the interactions process (Figure 1.25) [193]. Enthalpy–entropy compensation is characterized by a linear relationship observed between the enthalpy change and the entropy change in a binding reaction. Thus, consideration of ΔH and ΔS are crucial for a detailed understanding of the free energy of binding [194].

ΔH represents the changes in noncovalent bond energy occurring during the interaction. The measured enthalpy is the result of the formation and braking of many individual bonds e.g. protein-solvent hydrogen bonds, van der Waals interactions and solvent reorganization near protein surface. An overall increase in bonding is associated

with the release of heat or a negative enthalpy change and the reaction is termed exothermic. A negative value of ΔH indicates favorably enthalpic contribution to ΔG.

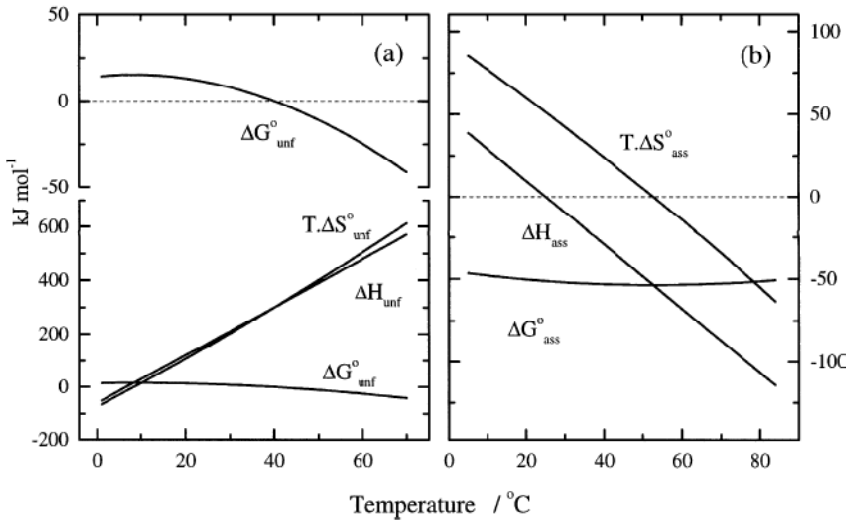

Figure 1.25: Thermodynamic parameters as a function of temperature for biomolecular processes determined from microcalorimetry. (a) ΔG^o_{unf}, ΔH_{unf} and $T\Delta S^o_{unf}$ of unfolding in solution of a typical globular protein, with ΔC_p = 9 kJ K^{-1} mol^{-1}. The free energy data are also shown expanded in the upper panel, for clarity. (b) ΔG^o_{ass}, ΔH_{ass} and $T\Delta S^o_{ass}$ of association interaction between protein subunits in solution, with ΔC_p = -1.9 kJ $K^{-1}mol^{-1}$ [193].

Entropy (S) is the measure of disorder and thus entropy increases with increasing disorder. The total entropy of binding represents the sum of ΔS_{sol} (the entropy change resulting from solvent rearrangement upon binding), ΔS_{conf} (a conformational term reflecting the reduction of rotational degrees of freedom around torsion angles of protein and ligand and $\Delta S_{r/t}$ (entails the loss of translational and rotational degrees of freedom when a complex is formed from two molecules free in solution) [195]. The entropy

change is associated with the disorder in a system, with an increase in bonding tending to decrease disorder. A positive value of ΔS indicates favorable entropic contribution to ΔG.

The Heat Capacity of a substance is the amount of heat required to raise the temperature of 1 mole of the substance by 1 degree K [196]. ΔC_p is measured accurately and directly from the change in enthalpy with temperature. Often, ΔC_p does not depend on temperature within small physiological temperature changes and is almost always negative when the complexed state of the macromolecule is taken as the reference state. A negative value for ΔC_p indicates that the complex has a lower heat capacity (less energy is required to cause an increase in temperature) than the free partners.

Any process that is accompanied by water release from the surface is thermodynamically characterized by a substantial ΔC_p, which is proportional to changes in solvent accessible surface area (ASA) involved. Negative contributions arise from burial of apolar surfaces (hydrophobic effect), while positive contribution from burial of polar surfaces (hydrogen bonding) (equation 1.4).

$$\Delta C_p = \mathbf{a}\ \Delta ASA_{ap} + \mathbf{b}\ \Delta ASA_{pol} \qquad (1.4)$$

where ΔASA_{ap} and ΔASA_{pol} are the changes in the apolar and polar ASA respectively and **a** (1.88 J K^{-1})and **b** (-1.09 J K^{-1}) are empirically determined coefficients derived from model compounds and unfolding data [197, 198]. The strong correlation between ΔC_p and the surface area buried upon complex formation provides a link between thermodynamic data and structural information [199].

Chapter II. Research rationale and objectives

The intriguing properties and the biological importance of the Sec system and especially of the SecA ATPase, prompted us to study in details this system and try to address fundamental questions related to its function. Allosteric communication among the various domains of SecA is essential for productive protein translocation. It will be of great importance to determine how the conformational and dynamic changes are transmitted among the domains and how their modulation controls the translocation process.

We have used NMR, ITC and biochemical approaches to characterize the *E. coli* SecA along the translocation pathway. Using modern NMR methodologies we were able to tackle the helicase-like motor of SecA as well as the full-length SecA. The specific aims of the current Thesis are:

(1) Characterize the functional conformational changes undergone by SecA along the catalytic pathway of ATP binding and hydrolysis. Explore how SecA and helicases couple the energy provided by ATP hydrolysis to protein translocation and DNA/RNA unwinding, respectively.

(2) Characterize the conformational changes that accompany the transition of SecA from its enzymatically inactive to the enzymatically active state.

(3) Determine the network of allosteric communication among the domains of SecA.

(4) Elucidate the interaction of SecA with regions of the translocation channel

Chapter III. Mechanisms of catalysis in the helicase motor of SecA

III.1 Introduction

The DEAD motor of SecA (NBD and IRA2) is located at the N-terminus of the protein. The rate limiting step in the ATPase cycle of SecA is the release of ADP which is controlled by protein-protein interactions and the translocation ligands [94, 97, 109, 200, 201] (Figure 3.26). A major unresolved question is how SecA and helicases convert the energy extracted from ATP hydrolysis to create locomotion required for protein translocation and RNA/DNA unwinding, respectively.

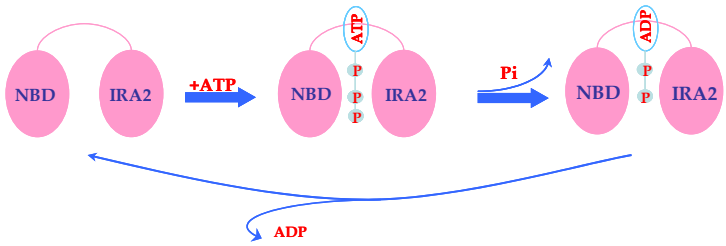

Figure 3.26: Catalytic cycle in the motor of SecA (apo, ATP- and ADP- bound)

All NTPase motor proteins (including G proteins) sense the presence of a γ-phosphate [202]. NTP hydrolysis and the subsequent loss of the γ-phosphate is thought to cause rearrangement of conserved structural elements flanking the NTP-binding site [202]. This rearrangement has mainly been considered to consist of a purely rigid-body movement of the two motor domains [120]. The vast majority of available crystal structures have shown rotations of the helicase motor domains that take place upon binding and release of the nucleotide [203-207], but not between the ATP- and ADP-bound states [208, 209]. This is somewhat surprising, because for many of these enzymes it is known that ATP hydrolysis rather than ATP binding regulates substrate affinity [132,

210]. For some mechanoenzymes [211-213], including SecA [73, 74, 100-103], crystal structures have suggested that no tertiary conformational changes are elicited by nucleotide binding at all.

The structural homology of SecA with SF2 helicases suggests that maybe these proteins use similar mechanisms to achieve translocation [73]. Here, we have combined NMR, thermodynamic and biochemical approaches to characterize the *E. coli* SecA and functional derivatives at key conformational states along the catalytic pathway (apo, ATP-bound and ADP-bound) (Figure 3.26).

III.1.1 ATPase activity of SecA

The ATPase activity of the cytoplasmic SecA is very low and is only stimulated when SecA is actively engaged in translocation [78, 80, 132, 214, 215]. Binding to the membrane switches SecA to the catalytically active state while maximum ATPase activity is stimulated by preprotein binding [68]. The activation mechanism involves a series of conformational changes in SecA that enables a part of the enzyme to insert and deinsert into the translocation channel, SecYEG [78]. The low ATPase activity of soluble SecA precludes the study of its catalytic cycle in solution. The activated state is only accessible in the presence of membranes and preproteins, which introduce in the system high complexity.

Several reports have shown that SecA can be studied using separate functional domains (Figure 3.27) [97, 105]. This approach simplifies the study of SecA and provides the opportunity to understand how domains function independently and how in the context of the intact protein (“divide and conquer” approach).

C domain truncated SecA (residues 1-610 in *E. coli*, hereafter SecAΔC) exhibits elevated ATPase activity at temperatures close to 37 °C, even in the absence of other translocation ligands, whereas at 0 °C behaves similarly to wild type SecA (Figure 3.27). Therefore, SecAΔC can be used as a mimic of the catalytically activated state of SecA [105, 106, 109, 216]. The low basal ATPase activity of cytoplasmic SecA is attributed to the presence of the C-domain, which acts as a suppressor by maintaining the protein in

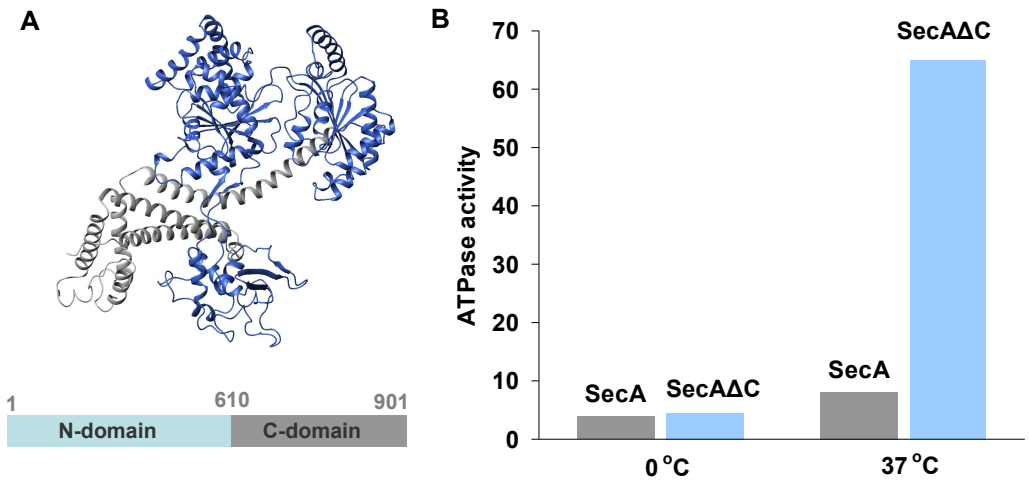

Figure 3.27: (a) SecA major domain separation, (b) Basal ATPase activity of SecA and SecAΔC. Basal ATPase activity is measured in the absence of membrane and translocation ligands [105].

an non-active state [105, 109]. The IRA1 domain is the key regulator of the ATPase by directly interacting with the SD, NBD and PBD domain thereby restricting the motor flexibility [109]. Functional isolation of the ATPase core (SecAΔC) in the absence of the C-domain provides us an excellent tool to study features of SecA ATP hydrolysis cycle.

III.2 Results

III.2.1 The helicase motor of SecA is highly dynamic

To characterize the intrinsic structural and dynamic properties of the helicase motor of SecA in the activated state we characterized SecAΔC by NMR spectroscopy (Figure 3.28a). SecAΔC is a stable, functional derivative of SecA and gel filtration shows that in the concentration used for our experiments (up to 0.8 mM) remain monomeric.

Despite the large size of SecAΔC (68 kDa, 610 residues) and the fact that the protein is fully protonated, the ^{1}H-^{15}N-TROSY-HSQC spectrum shows an unexpected dispersion of the resonance peaks which in addition appear relatively narrow (Figure 3.28a). This indicates that SecAΔC is highly dynamic and the subdomains, NBD, IRA2

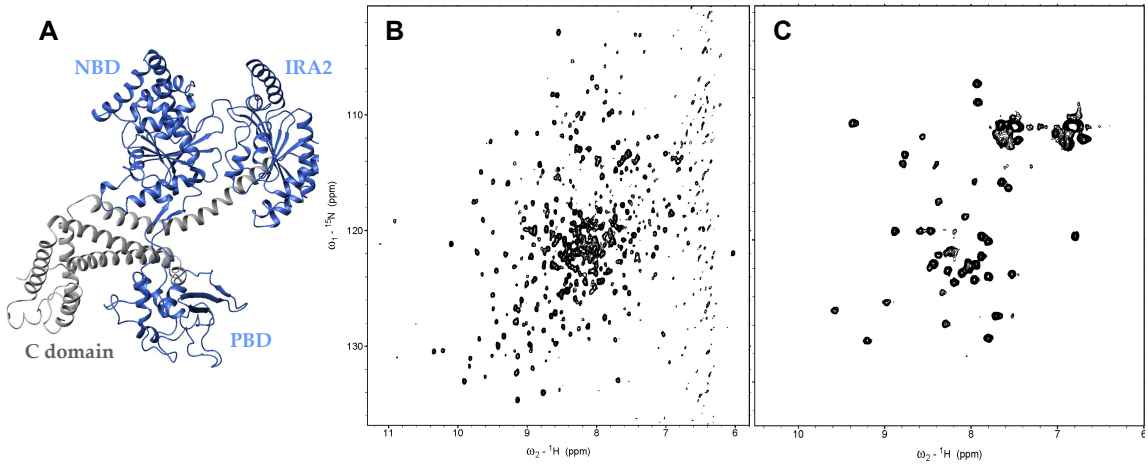

Figure 3.28: (a) Crystal structure of *E. coli* SecA colored according to major domain organization. SecAΔC is colored blue and C domain grey (b) ^{1}H-^{15}N TROSY-HSQC spectrum of ^{15}N-SecAΔC (monomeric, 68 kDa) recorded at 22 ^{o}C on an 800-MHz NMR instrument (c) ^{1}H-^{15}N HSQC spectrum of ^{15}N wt-SecA (dimeric, 204 kDa) recorded at 22 ^{o}C on a 600-MHz NMR instrument.

and PBD exhibit substantial flexibility and tumble independently of each other. For proteins with size similar to SecAΔC (68 kDa) we would have expected spectra characterized by severe line broadening because of very fast relaxation rates.

In contrast, the ^{1}H-^{15}N HSQC spectrum of intact SecA reveals extensive quench of the flexibility of the catalytic core (Figure 3.28b) with only few regions showing some mobility. These regions belong primarily to the very flexible crystallographically unresolved CTD domain of SecA. Therefore, binding of the C-domain suppresses drastically the inherent flexibility of the helicase motor.

III.2.2 Assignment strategy

To facilitate our studies, the helicase motor was further dissected in smaller functional fragments: the SecAΔC/ΔIRA2 (residues 1-420 in *E. coli*), the isolated IRA2 (residues 420-610 in *E. coli*) and the isolated PBD (residues 219-379 in *E. coli*) (Figure 3.29). The isolated domains remain folded, as can be concluded from the HSQC spectra. Moreover, overlaid spectra of the isolated domains with the SecAΔC spectrum indicate that the structure of the isolated domains is basically similar to that adopted in SecAΔC.

Working on the isolated domains simplified the assignment procedure whereas the good correspondence of the spectra enabled the assignment transfer to SecAΔC. Information regarding the behavior of the motor domains as isolated fragments and in the context of the motor assembly, SecAΔC, can prove useful in understanding the mechanisms underlying the catalytic cycle of SecA.

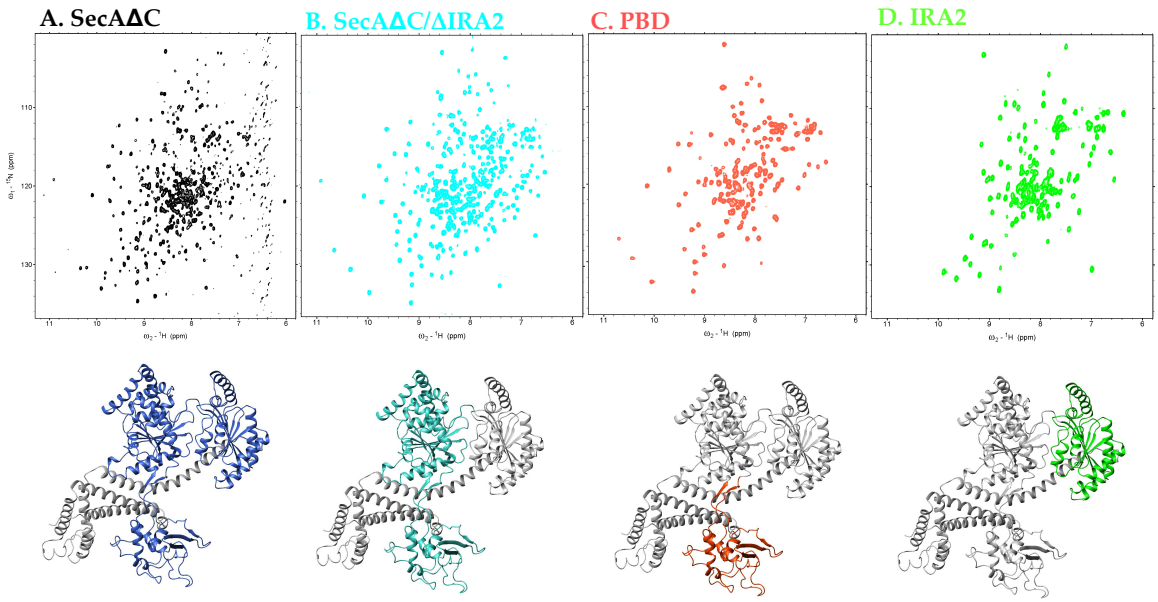

Figure 3.29: Each column in the figure displays a structural model of one of the protomers of SecA with the domain or fragment studied in isolation being highlighted, along with the corresponding backbone ^{1}H-^{15}N HSQC.

(A) SecAΔC (residues 1–610, comprising NBD, PBD, and IRA2)

(B) SecAΔC/ΔIRA2 (residues 1–420, comprising NBD and PBD)

(C) PBD (residues 220–379)

(D) IRA2 (residues 420-610)

The sequential assignment of ^{1}H, ^{13}C and ^{15}N protein backbone chemical shifts was performed using standard triple resonance experiments: HNCO, HN(CA)CO, HNCA, HN(CO)CA, HNCACB and HN(CO)CACB. To extend and confirm the assignment an auxotrophic *E. coli* CT19 strain was used to selectively label proteins with selected amino acids (Leu, Val, Phe, Ile, Tyr) [217] (Figure 3.30).

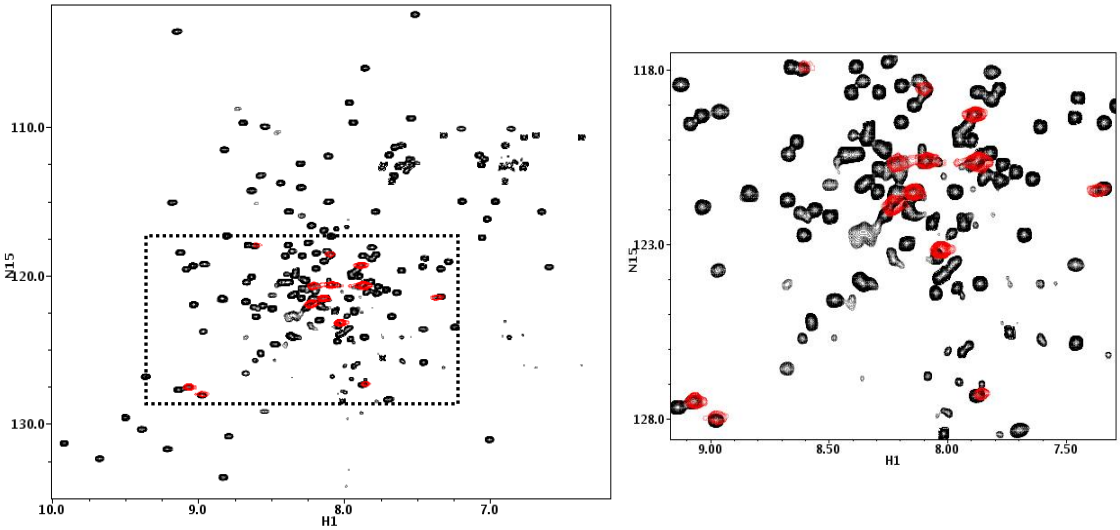

Figure 3.30: Selective isotopic labeling of IRA2 Ile residues (a) Overlaid ^{1}H-^{15}N HSQC spectra of IRA2 (black) and IRA2 with Ile residues ^{15}N labeled (red). Excerpt of the overlaid ^{1}H-^{15}N HSQC illustrating the usefulness of this approach.

III.2.3 The helicase motor domains interacts transiently

The highly dynamic nature of SecAΔC suggests that the bi-lobar motor adopts a dumbbell-like conformation in solution. The markedly 'open' conformation of the helicase motor has been previously reported in crystallographic studies for eIF4A [218], MjDEAD [219] and UAP56 DEAD-box proteins [212, 220] (Figure 3.31). These proteins are comprised of only the helicase motor core while SecA has two extra appendage domains (PBD and C-domain) that may provide stability to its catalytic core.

The spatial organization of the helicase motor in the absence of the nucleotide may be difficult to be defined by crystallography because of the inherent flexibility of the motor. The eIF4A structure represents a completely 'open' state; the MjDEAD adopts an intermediate state, whereas the catalytic core of UAP56 adopts the most compact conformation (Figure 3.31).

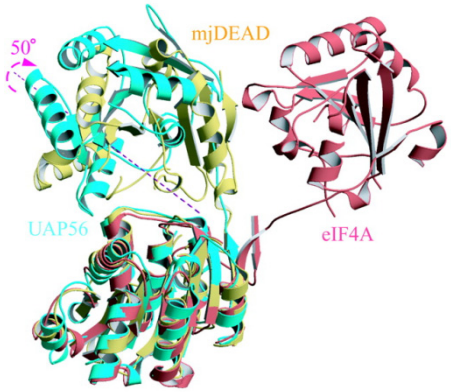

Figure 3.31: The UAP56 structure (cyan, PBD 1XTI) is superimposed with the structures of yeast eIF4A (red, PDB 1FUU) and mjDEAD (yellow, PDB 1HV8). The N-terminal domains were aligned. The dashed magenta line indicates the axis around which a rotation of 50° will superimpose the C-terminal domain of UAP56 with that of mjDEAD [212].

In contrast, NMR can be more informative as it determines the conformation of a protein in solution. Analysis of our spectra shows that the cross-peaks in the isolated IRA2 domain are not an exact subset of SecAΔC (Figure 3.32a, b). Instead, considerable chemical shift perturbations observed which is suggestive of a transient interaction between IRA2 and NBD in SecAΔC. The residues of IRA2 that are considerably affected by the presence of NBD are color mapped onto the structure of SecA (Figure 3.32c). All these residues cluster at the interface of the two domains where the nucleotide cleft is formed and include residues from helicase motifs V and VI that are essential for catalysis. The transient interaction between NBD and IRA2 is important because it provides some stability to the cleft in the absence of nucleotide while at the same time, allows flexibility to the cleft.

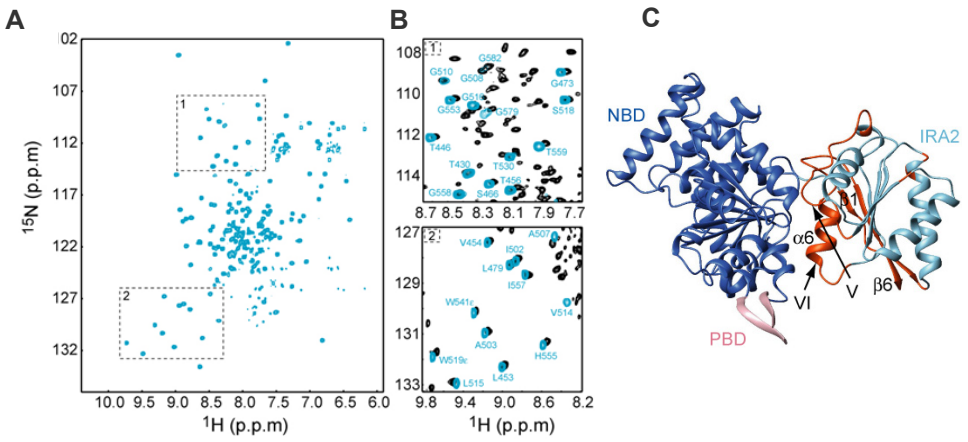

Figure 3.32: (a) ^{1}H-^{15}N HSQC NMR spectrum of the isolated IRA2 domain. (b) Excerpt of overlaid 2D ^{1}H-^{15}N HSQC spectra of isolated IRA2 (cyan) and SecAΔC (black). Assignment of the IRA2 residues is indicated. (c) IRA2 residues that change their chemical shift considerably upon interacting with the NBD, indicating a transient interaction between the two domains, are colored orange. Motifs V and VI, which are essential for ATP hydrolysis are indicated.

III.2.4 Reconstitution of the catalytic core from isolated fragment

To simplify our studies and gain further insights in the transient interaction of the catalytic core components the reconstitution of SecAΔC from isolated fragments was attempted (Figure 3.33). Protein reconstitution is an excellent tool to probe transient interactions. This strategy is based on the fact that the fragments will recombine noncovalently to regenerate the intact molecule [221].

$^{15-}$N labeled IRA2 was mixed with unlabeled SecAΔC/ΔIRA2 and complex formation was followed by observing the chemical shift changes in labeled IRA2. In agreement with our previous results, we observed small chemical shift and broadening in the resonance peaks of IRA2 upon interaction with SecAΔC/ΔIRA2 (Figure 3.34).

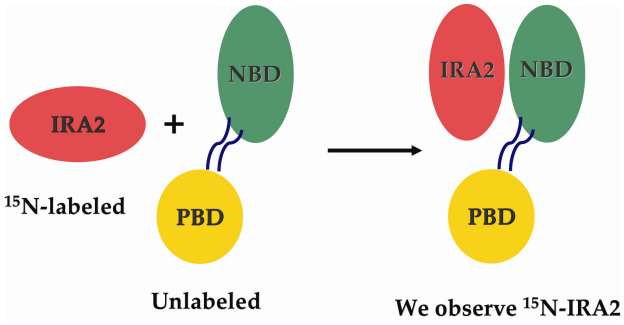

Figure 3.33: Reconstitution strategy of SecAΔC from IRA2 and SecAΔC/ΔIRA2

Residues of IRA2 that sense the presence of NBD are colored mapped on the SecAΔC crystal structure. The interface includes residues that face the nucleotide cleft and are very important for the catalysis. It is known that transient protein-protein interactions have key regulatory functions in many cellular processes [222]. The presence of transient interactions in the nucleotide cleft may be required to facilitate fast turnover in SecA.

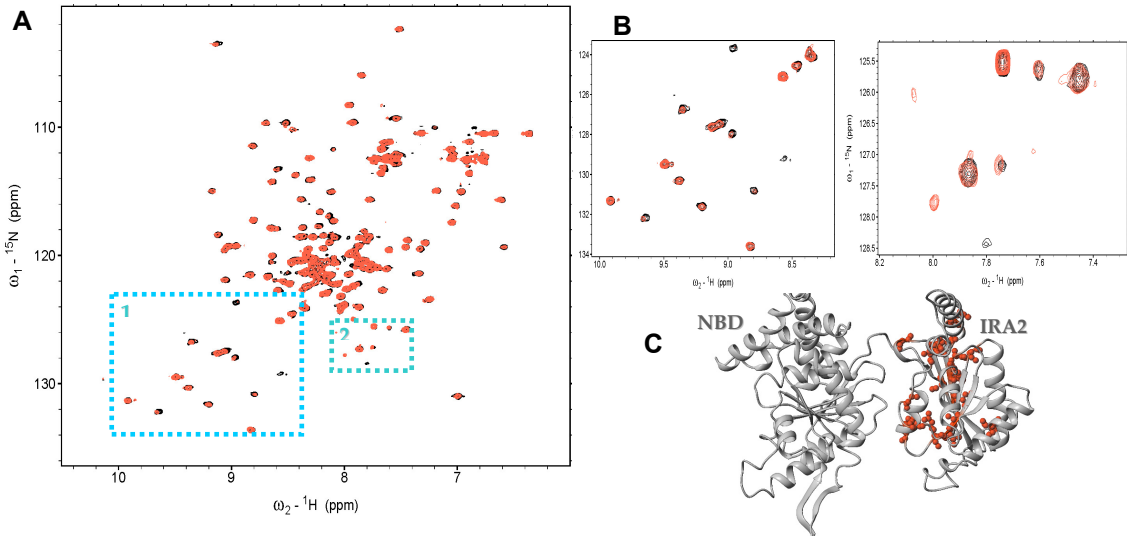

Figure 3.34: (a) Overlay of the ^{1}H-^{15}N HSQC spectra for the non-covalent complex of IRA2 (^{15}N labeled) with SecAΔC/ΔIRA2 (unlabeled). Black: IRA2 and orange: IRA2-SecAΔC/ΔIRA2 complex. (b) Excerpt of overlaid ^{1}H-^{15}N HSQC spectra. (c) IRA2 residues that change their chemical shift considerably upon addition of SecAΔC/ΔIRA2 are color mapped orange on the structure.

III.2.5 IRA2 region lining the cleft are inherently flexible

The core of the isolated IRA2 remains structured: The dynamic behavior of IRA2 and its potential mechanistic implications in the regulation of the motor properties during the catalytic cycle of ATP binding and hydrolysis prompted us to further characterize this domain. The dispersion of resonance peaks in the NMR spectrum for the isolated IRA2 suggests that the core of the domain remains structured (Figure 3.35a). In addition, superimposition of IRA2 and SecAΔC spectra shows that the core of the isolated IRA2 retains a conformation similar to the one adopted in the context of SecAΔC (Figure 3.35b).

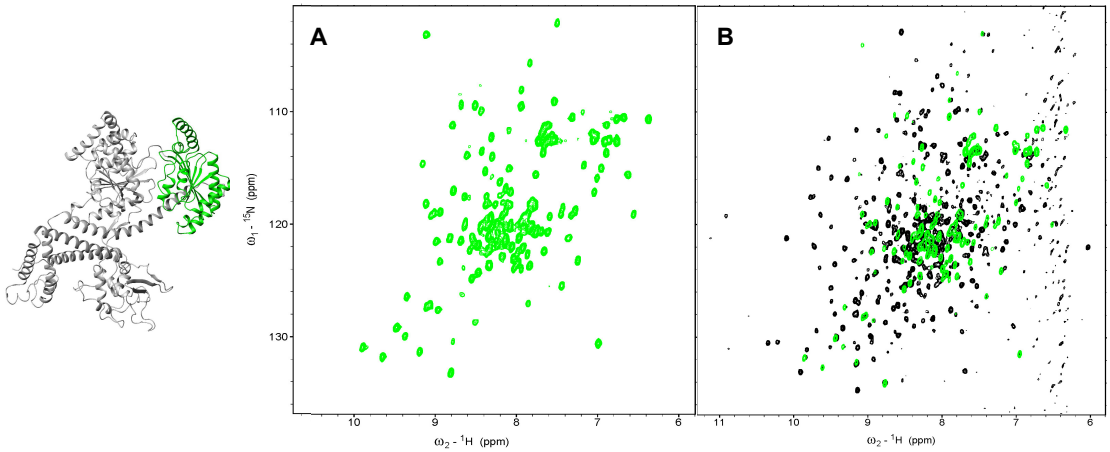

Figure 3.35: (a) ^{1}H-^{15}N HSQC NMR spectrum of the isolated IRA2 domain. (b) Overlaid 2D ^{1}H-^{15}N HSQC spectra of isolated IRA2 (green) and SecAΔC (black).

The IRA2 regions lining the cleft are disordered: Analysis of the secondary structural elements of IRA2 using NOE and Chemical Shift Index (CSI) reveals that β-strand 1 and 6, and α-helix 6 of the isolated IRA2 appear disordered in solution (Figure 3.36a, b). The same regions in full-length SecA appear very well structured in all of the available crystal structures of SecA. These regions (β-strand 1 and 6, α-helix 6) are

located at the interface of the nucleotide cleft and include residues essential for the catalysis. Previous NMR studies have suggested that α-helix 6 is dynamic in solution even in full-length SecA [223]. α-helix 6 is part of motif VI (DNQLRGRSGR), which is highly conserved in helicases and is involved in nucleotide binding and hydrolysis by providing the 'arginine finger'. Intrinsically disordered regions in proteins are implicated

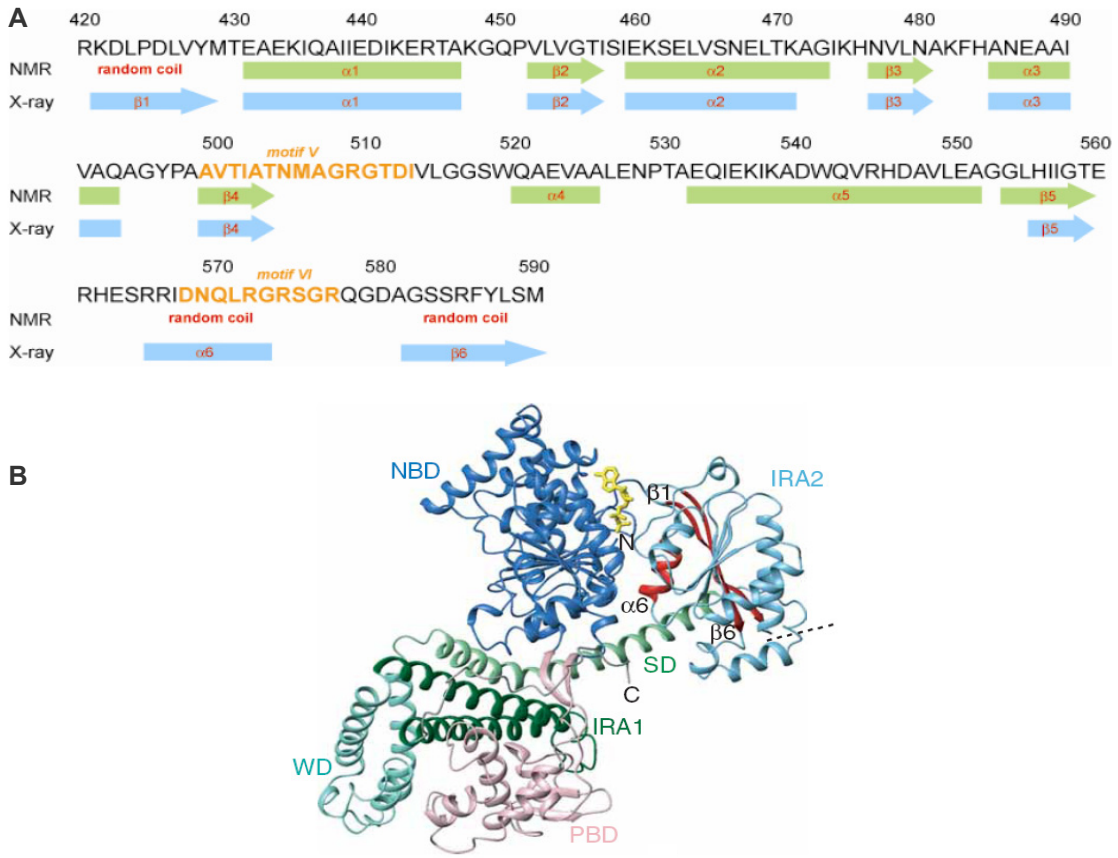

Figure 3.36: (a) Secondary structural elements of IRA2 in solution. The structural elements have been assessed based on NOE and CSI data. The NMR data are compared to crystal data from *B. subtilis* SecA. The *E. coli* IRA2 has an insertion of 29 non-conserved residues (residues 517-545) that, according to the NMR data, form two helices α4 and α5. (b) Crystal structure of *B. subtilis* SecA bound to ADP (yellow sticks), colored according to domain organization (PDB 1M74)

in several important cellular functions [224]. The intrinsic plasticity in SecA may have significant implications in the functional transitions between different conformational states along the catalytic cycle.

Dynamics of IRA2: To further characterize the dynamic character of IRA2 we determine the amplitude of fast scale (ps-ns). A sensitive and accurate way to characterize protein backbone dynamics is by recording heteronuclear ^{1}H-^{15}N NOE data. The measured values are plotted against residue number and are mapped on the crystal structure of IRA2 in a color coded manner (Figure 3.37a, b). The lower the NOE value, the higher the flexibility of the region, whereas the higher the NOE value the more rigid the region.

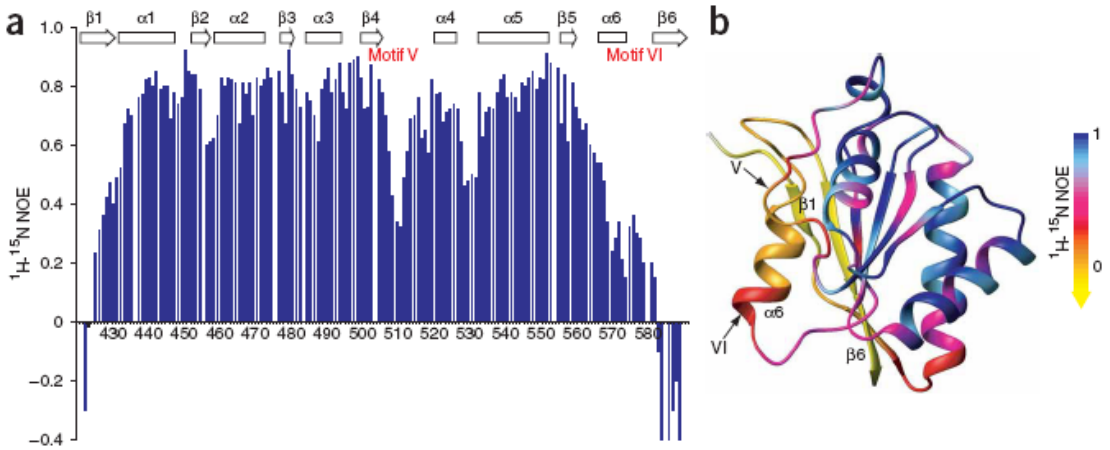

Figure 3.37: Fast backbone motions of isolated IRA2. (a) ^{1}H-^{15}N NOE values of IRA2 as a function of residue number. Low values indicate flexibility, higher values rigidity. (b) NOE values are mapped in continuous-scale colors on the structure of *B. subtilis* IRA2. Motifs V and VI are indicated.

From the plot we can clearly see that the motions of all residues in helicase motifs V and VI (encompassing α-helix 6) as well as β-strands 1 and 6 have large amplitudes (low NOE values), providing direct evidence for pronounced flexibility of these regions. Nevertheless, the NOE values suggest that motif VI retains some residual secondary structure, as opposed to strand 6, which appears entirely unfolded (negative NOE values). In contrast, the regions of IRA2 that face away from the nucleotide cleft remain well folded and show substantial rigidity (high NOE values). The observed differential flexibility of IRA2 may allow the rigid part to act as a scaffold to support the dynamic region that faces the nucleotide cleft.

III.2.6 Nucleotide binding stabilizes a folded yet dynamic IRA2

It would be of great importance to examine by NMR how nucleotide binding affects the structure and dynamics of the metastable regions of IRA2 that face the cleft. NMR analysis shows that ADP binding to the motor elicits widespread conformational changes in IRA2 (Figure 3.38a), with almost all IRA2 residues experiencing a pronounced chemical shift change. The resonances of several residues located close to the nucleotide interface showed particularly severe broadening, indicating the presence of conformational exchange phenomena (Figure 3.38b).

Under the experimental conditions used for the NMR studies (SecAΔC ~ 0.8 mM, ADP ~ 1mM, K_d ~ 0.3 μM), the contribution from ADP binding and dissociation to line broadening is negligible. We propose that IRA2 regions populate an ensemble of alternate conformations that interconvert on the μs-ms time scale, thereby causing significant line broadening.

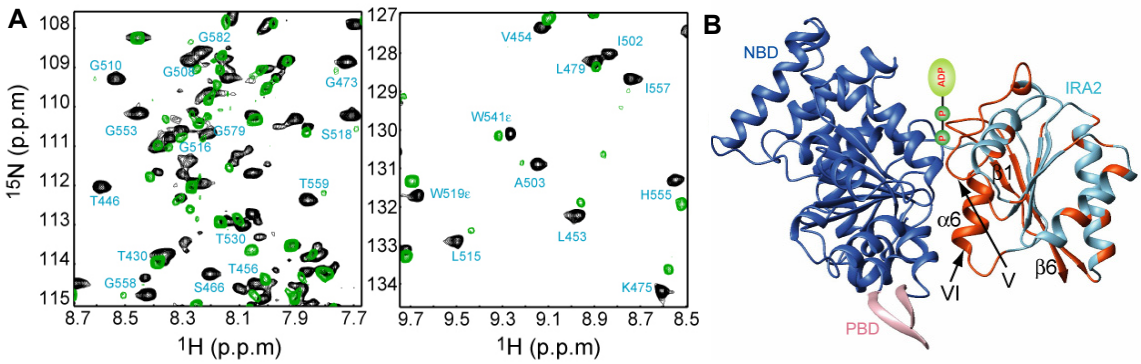

Figure 3.38: Effect on IRA2 induced by ADP binding to SecAΔC. (a) Excerpts of overlaid spectra of SecAΔC unbound (black) and bound to MgADP (green). Assignment of the IRA2 residues is indicated. (b) IRA2 residues whose resonance severely broadens upon ADP binding to SecAΔC are colored orange.

Notably, motifs V and VI also show enhanced slow dynamics upon ADP binding. Such slow domain motions are biologically very important because they are close to the time scales on which functional processes such as protein folding and allosteric transitions take place [153, 225, 226]. The slow motions shown by almost all residues of IRA2 that line the nucleotide cleft suggest that these regions, which are unfolded in the absence of the nucleotide, may undergo a nucleotide-coupled disorder-order transition and populate alternate conformations in the nucleotide-bound complex. The conformational plasticity of IRA2 is potentially of great significance, because it could allow different conformational states along the ATP hydrolysis pathway to be formed.

III.2.7 Equilibrium of disordered and ordered states in the motor

The NMR data shows that the nucleotide binding induces a more ordered form of the intrinsically metastable nucleotide cleft. A very sensitive and accurate approach to

characterize disorder-order transitions is to measure, by ITC changes in ΔH upon nucleotide binding as a function of temperature [227].

We have studied the nucleotide binding to SecAΔC over a wide range of temperatures and ΔC_p, a key thermodynamic parameter was determined (Figure 3.39).

$$\Delta C_p = (\Delta H_1 - \Delta H_2) / (T_1 - T_2) \qquad (1.5)$$

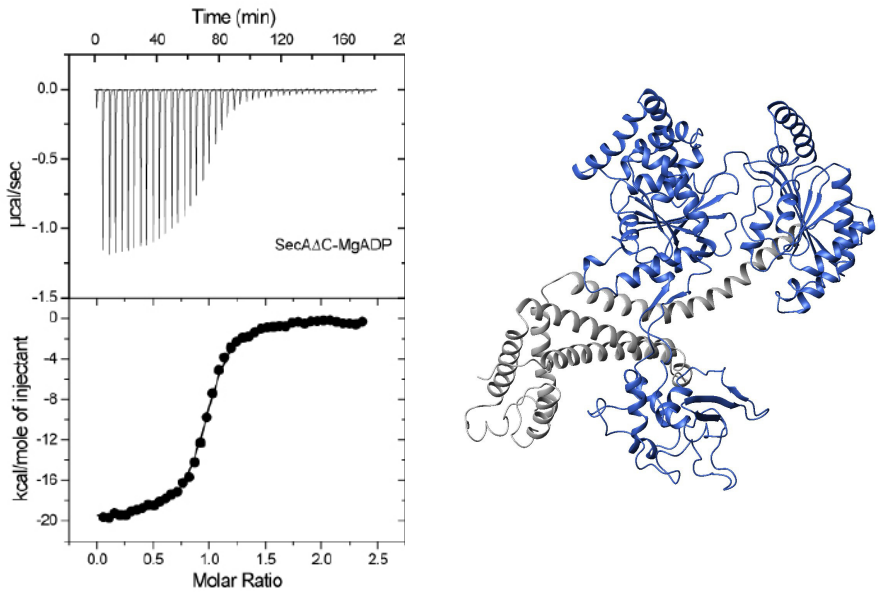

Figure 3.39: ITC trace and binding isotherm of the calorimetric titration of SecAΔC (colored blue on the SecA *E. coli* structure) with MgADP.

At low temperatures SecAΔC has high affinity (K_d= 0.15 µM) for ADP while as we approach temperatures higher than 25 ^oC we observe a ~ 6 fold decrease in the affinity (K_d = 1.0 µM). Moreover, at low temperatures (5-20 ^oC), the slope of ΔH versus temperature (T) correlation for ADP binding to SecAΔC is linear and the heat capacity change is not large (ΔC_p= -0.48 kcal mol^{-1} K^{-1}) (Figure 3.40a, solid blue line). This behavior is typical of protein-ligand interactions over experimental temperature ranges. Notably, at temperature higher than 21 ^oC (T_f, defined as the temperature at which

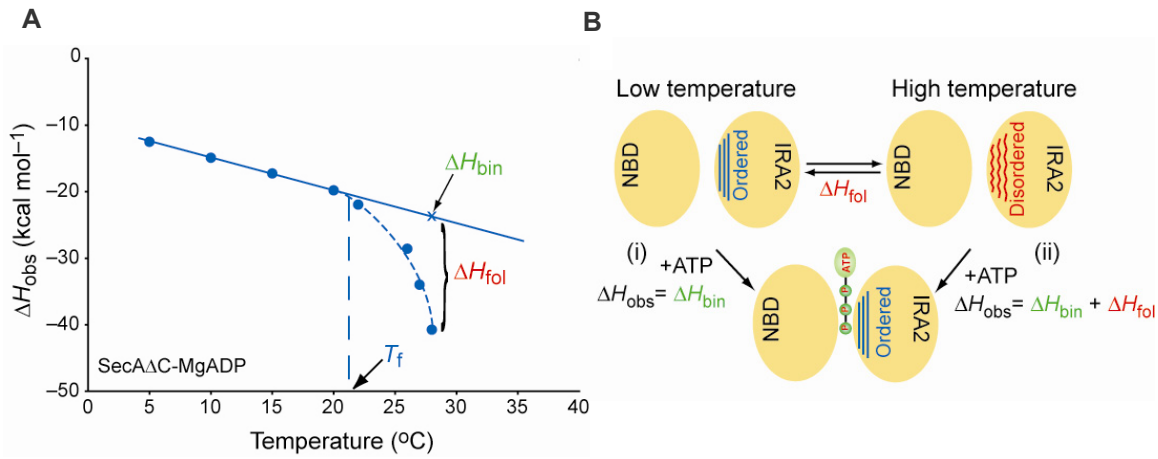

Figure 3.40: (a) ΔH_{obs} of MgADP binding to SecAΔC as a function of temperature. The broken line represents fit to the higher temperature points. (b) Schematic of disorder-order and binding equilibria in the nucleotide cleft. Nucleotide binding to the cleft at low temperatures (reaction i) will give rise to observed enthalpy change (ΔH_{obs}) that corresponds in its entirety to the intrinsic nucleotide binding ΔH (ΔH_{bin}). At higher temperatures, nucleotide binding (reaction ii) induces a disorder-order transition, and an additional enthalpic term, ΔH_{fol}, appears as a result of the folding process.

deviation from linearity is observed), ADP binding to SecAΔC is accompanied by an unusual nonlinear temperature dependence of the enthalpy, meaning that the heat capacity change is temperature dependent (Figure 3.40a, dashed blue line).

To exclude the possibility that ionization phenomena are coupled to nucleotide binding, we conducted a series of similar ITC experiments in buffers with different ionization enthalpies [228]. The enthalpy of reaction in Tris buffer, which has large ionization enthalpy (ΔH_{ion}= 11.4 Kcal mol^{-1}), and in phosphate buffer, which has small ionization enthalpy (ΔH_{ion}= 1.2 Kcal mol^{-1}), is very similar. Thus, no ionization phenomena are coupled to nucleotide binding.

The origin of the nonlinear temperature dependence of ΔH can be rationalized in terms of the observed disorder-order transition with a simple model (Figure 3.40b). The nucleotide cleft in SecAΔC exists in an equilibrium of disordered and ordered states. At lower temperatures, the ordered states predominate, as suggested by NMR; thus the experimentally observed ΔH (ΔH_{obs}) upon ADP binding at temperatures below ~21 ^{o}C corresponds in its entirety to the intrinsic binding enthalpy (ΔH_{bin}). As temperature increases, the fraction of the protein that populates the disordered states also increases. In this case, ADP binding would induce folding of the nucleotide cleft, in full agreement with the NMR data. As a consequence, an additional enthalpic term (ΔH_{fol}) appears as result of the folding process. A nonzero ΔH_{fol} is what causes ΔH_{obs} to deviate from linearity and can be attributed to the folding of the unstructured region of IRA2 that line the nucleotide cleft and ΔH_{fol} can be used as a measure of the extent of the nucleotide-induced disorder-order transition.

Our NMR and thermodynamic data are consistent with the existence of a temperature dependent equilibrium of disordered-ordered states in the nucleotide cleft of the apo-SecAΔC. The increased negative ΔC_p upon nucleotide binding at high temperatures is a characteristic of a coupled folding event [229], arising from the burial of hydrophobic surface areas as the IRA2 regions that line the cleft become more ordered. In fact, temperature dependent heat capacity is the thermodynamic signature of a preexisting conformational equilibrium in the unliganded state of a protein [227, 230-232]. It should be emphasized that rigid body opening and closure of the NBD-IRA2 interface cannot give rise to temperature-dependent heat capacity [227, 229].

III.2.8 Interactions among helicase motifs stabilize IRA2

The characteristic temperature T_f at which ΔH_{fold} becomes appreciable, thus causing ΔH_{obs} to deviate from linearity provides an additional probe of the disorder to order transition. For ADP binding to SecAΔC, T_f is 21 ^oC. Therefore, at temperatures below T_f the flexible regions of IRA2 exist in a more stable conformation in the context of SecAΔC. On the other hand, NMR shows that these regions in the isolated IRA2 remain unfolded and flexible even at temperatures as low as 15 ^oC. Our observations suggest that these IRA2 regions may gain some stability in the context of SecAΔC because of the presence of NBD.

The entire NBD-IRA2 interface is predominantly mediated by salt bridges formed by highly conserved residues at the helicase motifs (Figure 3.41a). R566 (motif VI) forms three salt bridges with D212, D217 and E397 (motif III) whereas R509 (motif V) forms salt bridge with D212 and E210 (motif II). Interestingly, the overall electrostatic surface of the contact area displays optimal complementarity (Figure 3.41b).

To test the hypothesis that the structural integrity of the nucleotide cleft depends on NBD-IRA2 interaction, the strength of the electrostatic contacts was modulated by changing the salt concentration in the ITC buffer. Increase of salt concentration from 100 to 550 mM K^+ caused a pronounced reduction of T_f, which approached a value of 13 ^oC (Figure 3.42a). Therefore, substantial unfolding of IRA2 takes place ~ 8 ^oC lower in the high-salt buffer compare to low-salt buffer. The increased concentration of salt confers ‘screening’ in the coulombic interaction network between NBD-IRA2. As a result the interactions in the catalytic core are now weakened and the flexible IRA2 regions that face the nucleotide cleft are no longer stabilized and, thus, populate unfolded states.

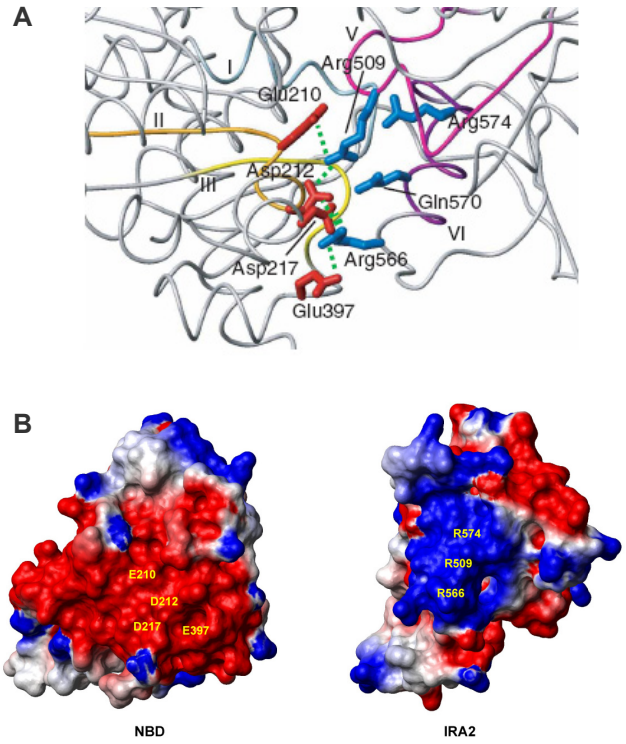

Figure 3.41: (a) Highly conserved salt bridges (green dotted lines) formed at the NBD-IRA2 interface stabilize the interaction between the domains (*E. coli* numbering). Latin numbers indicate helicase motifs (b) Electrostatic potential in the motor interface, positively and negatively charged residues are colored blue and red respectively.

The effect of the increased salt concentration becomes also evident in the affinity of the motor for ADP (Figure 3.42b). At low temperatures the K_d is similar for both low and high salt concentration, ~ 0.15 μM. At temperatures that approach the T_f of the motor the affinity for ADP at high salt concentration decreases dramatically. This is in accordance with the observation that the motor now is largely dissociated resulting in lower affinity for ADP.

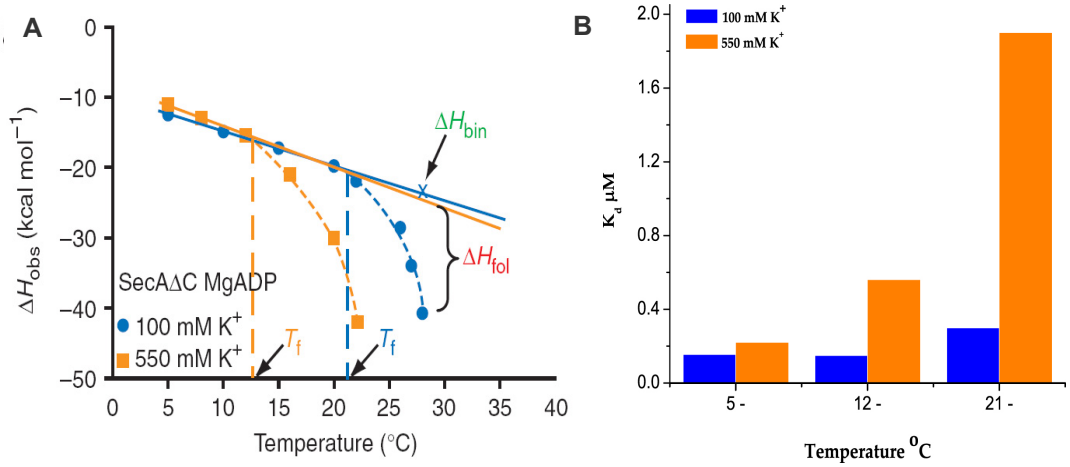

Figure 3.42: (a) ΔH_{obs} as a function of temperature for MgADP binding SecAΔC in 100 mM K^+ and 550 mM K^+ buffer. (b) Effect of salt concentration in the dissociation constant (K_d) of ADP binding to SecAΔC.

Control of folding transitions at the nucleotide cleft by interdomain NBD-IRA2 interactions provides a mechanism to regulate the structure and dynamics of the helicase motifs as SecA undergoes conformational changes during the translocation process.

III.2.9 Full-length SecA undergoes disorder-order transitions

Next, we conducted a detailed thermodynamic and biochemical study in full length SecA and its interaction with different nucleotides to investigate whether the disorder-order transition phenomena observed in SecAΔC are influenced by the presence of the C domain in full-length SecA (Figure 3.43).

SecA has high affinity for ADP (K_d ~ 0.1 µM at 8 °C) with the affinity decreasing as temperature increases (K_d ~ 1.5 µM at 38 °C). The same behavior has been observed for SecAΔC with the exception that this decrease occurs at even lower temperatures (K_d ~ 1.0 µM at 25 °C).

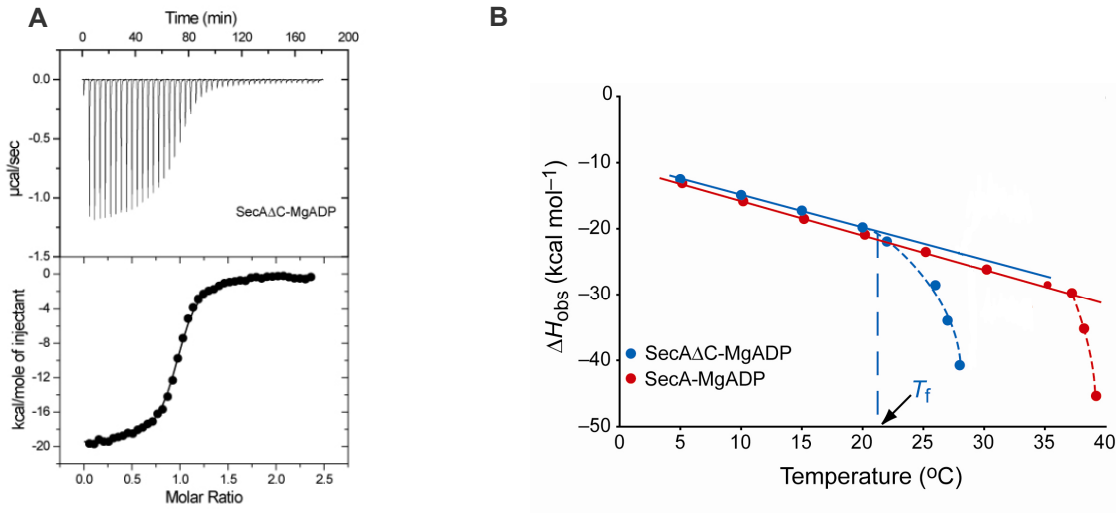

Figure 3.43: (a) ITC trace and binding isotherm of the calorimetric titration of SecA with MgADP. (b) ΔH_{obs} of MgADP binding to SecA (red line) and SecAΔC (blue line) as a function of temperature

Very interestingly, we found that ADP binding to SecA is coupled to a folding transition at the nucleotide cleft, similar to that identified previously for SecAΔC (Figure 3.43b). However, in full-length SecA the IRA2-NBD interface becomes unstable only at temperatures close to physiological ones (~37 ^{o}C). This striking difference can be attributed to the presence of C domain in full-length SecA. Apparently, in accordance with our NMR data and previous biochemical and biophysical observations [97, 105, 109], the C domain physically restricts the NBD and IRA2 domains from moving apart, resulting in higher stability of the regions lining the nucleotide cleft.

Similarly to SecAΔC, in high salt buffer the folding transition occurs at a temperature (T_f = 35 ^{o}C) much lower than that in the low salt buffer (T_f = 37 ^{o}C) (Figure 3.44). It appears that the nucleotide driven transitions in SecA are salt-dependent, indicating that they rely upon electrostatic interaction mediated by the helicase motifs.

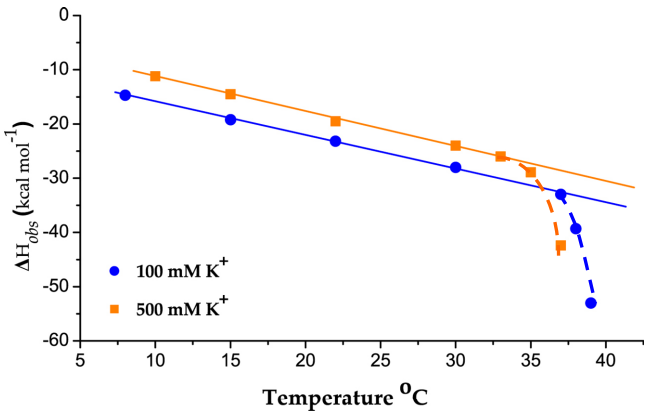

Figure 3.44: ΔH_{obs} as a function of temperature for MgADP binding to SecA in 100 mM K^+ and 550 mM K^+ buffer.

III.2.10 The γ-phosphate modulates the disorder-order transition

To test the hypothesis that the equilibrium of disorder-ordered states at the nucleotide cleft is modulated during the catalytic cycle, we studied the binding of ATP to SecA. To this end, in addition to ADP, which probes the post hydrolysis state (or product-like), we used ATP-γ-S, a nonhydrolyzable ATP analogue, to probe the substrate-like state (Figure 3.45).

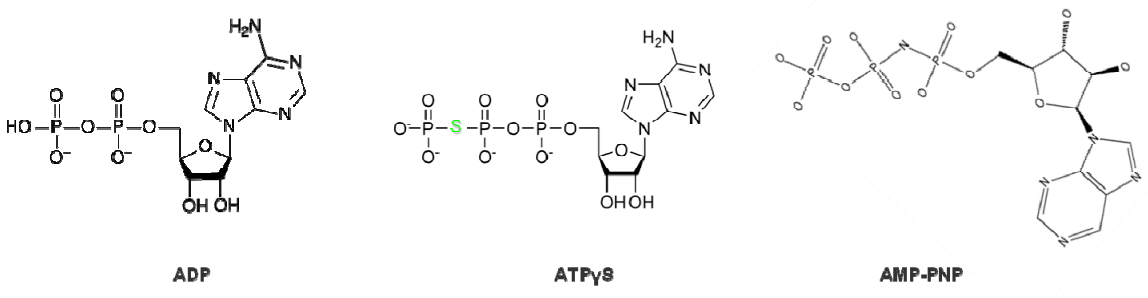

Figure 3.45: Adenosine 5′-diphosphate (ADP), Adenosine 5′-(γ-thio) triphosphate (ATP-γ-S) and Adenylyl-imidodiphosphate (AMP-PNP).

At the physiological temperature of 37 ^{o}C, ADP binding to SecA does not induce the folding transition, because $\Delta H_{fol} = 0$ (Figure 3.65b, blue line). In contrast, at the same temperature, ATP-γ-S binding to SecA results in $\Delta H_{fol} = -4.5$ kcal mol^{-1} owing to induced folding (Figure 3.46b, green line). Therefore, although at 37 ^{o}C the fraction of SecA with the nucleotide cleft in the disordered state is appreciable, only ATP-γ-S binding is capable of inducing local folding of IRA2 regions.

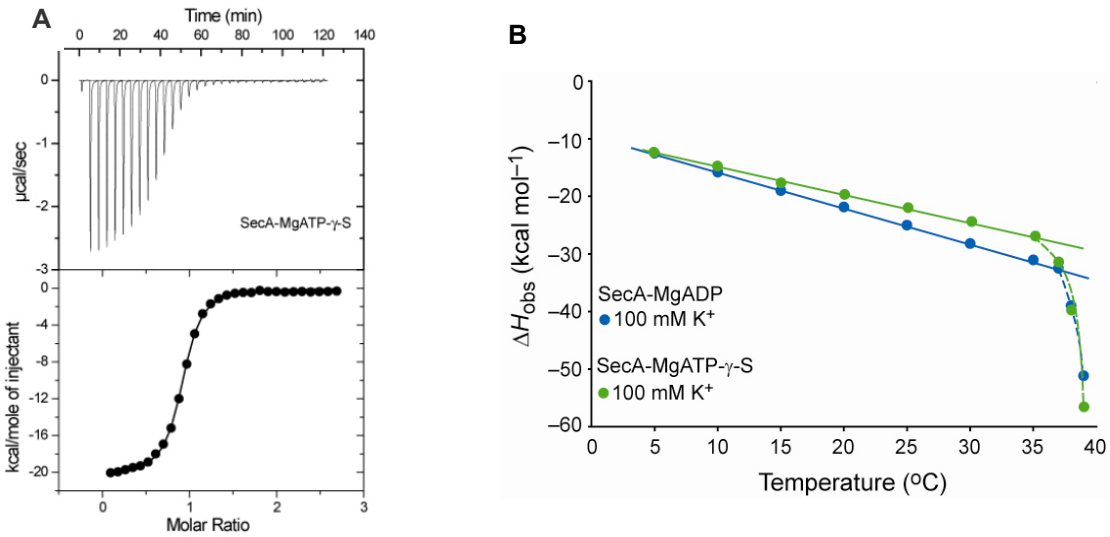

Figure 3.46: (a) ITC trace and binding isotherm of the calorimetric titration of SecA with MgATP-γ-S. (b) ΔH_{obs} of MgADP (blue line) and MgATP-γ-S (green line) binding to SecA as a function of temperature.

At higher salt concentrations, where the nucleotide cleft exists in a disordered state at low temperatures, ATP-γ-S binding induces folding of the flexible regions at a T_f of just ~ 25 ^{o}C whereas ADP does so only at T_f ~ 32 ^{o}C (Figure 3.47a). These results indicate that ATP binding to SecA favors a compact conformation rather than a relaxed one as it has been previously suggested [72] by studies using AMP-PNP (5'-adenylyl-beta,gamma-imidodiphosphate) as a nonhydrolyzable analogue of ATP.

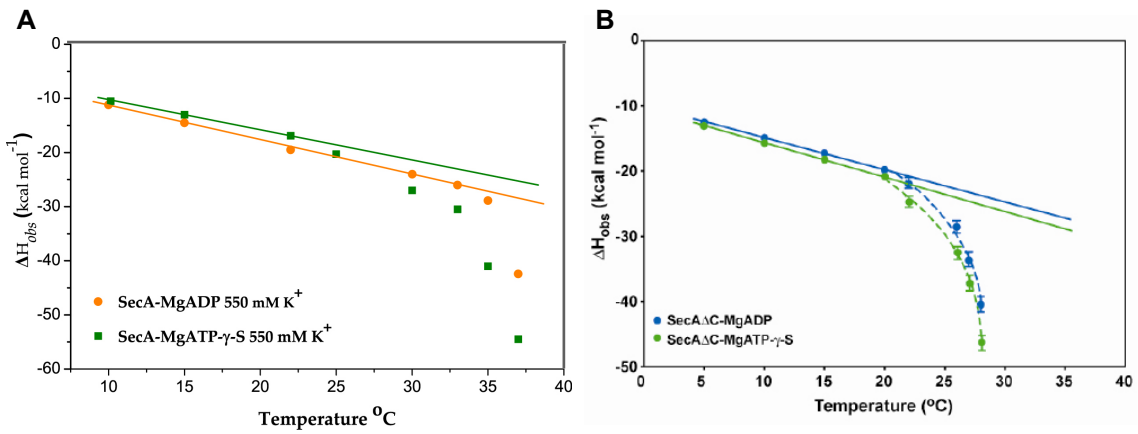

Figure 3.47: ΔH_{obs} as a function of temperature for MgADP and MgATP-γ-S binding to SecA (a) and SecAΔC (b) in 550 mM K^+ buffer

Our thermodynamic analysis shows that AMP-PNP binds very weakly to SecA (100 μM) while ATP and ADP have μM (~0.1 μM) affinities. At low temperatures (~10 °C) the thermodynamic parameters for ATP and ADP binding to SecA are similar (Table 1) whereas for AMP-PNP are very different. Thus, AMP-PNP is not a faithful mimic of ATP as it fails to reproduce the binding properties of ATP and results obtained using this analogue must be interpreted with great caution [110, 200]. Overall, our thermodynamic data clearly show that the extent of the disorder-order transition depends on the nucleotide identity.

Table 1: Energetic of SecA interaction with nucleotides (10 °C)

	ΔG (kcal mol^{-1})	*ΔH (kcal mol^{-1})*	*-TΔS (kcal mol^{-1})*
ADP	-8.9	-15.8	6.9
ATPγS	-8.3	-15.1	6.8
AMP-PNP	-5.0	-1.5	-3.5

Distinct nucleotide-induced folding events are also observed in SecAΔC, where the interface is even more flexible. As in the case of SecA, the characteristic temperature of the folding transition is much lower for ATP (T_f = 19 ^oC) than for ADP (T_f = 21 ^oC) (Figure 3.47b). The difference can be attributed to the presence of the γ-phosphate that provides extra contacts between the nucleotide and the motor subdomains and thus induces a local folding of the intrinsically unfolded elements.

The NMR results suggest that at ~22 °C only the IRA2 regions facing the cleft are disordered. Based on the amount of non-polar and polar surface [229] of these regions we estimate that complete folding of IRA2 and closure of the nucleotide cleft would give rise to a ΔC_p of ~-1 kcal mol^{-1} K^{-1}. ΔC_p due to folding (estimated by correcting for the intrinsic ΔC_p of binding at lower temperatures) is 1.4 kcal mol^{-1} K^{-1} for ATP and 1.0 kcal mol^{-1} K^{-1} for ADP. Thus, ADP binding appears to stabilize a much smaller fraction of the folded regions of IRA2 than ATP does.

Overall, ATP and ADP modify the conformational ensemble at the NBD-IRA2 interface in a distinct way, with ATP favoring a locally more folded state. It appears that the γ-phosphate in ATP provides additional contacts to the flexible regions of IRA2, thus improving their stabilization.

III.2.11 'Arginine fingers' regulate the disorder-order transition

'Arginine fingers' serve to neutralize developing charges in the transition state, thereby stimulating catalytic activity [99, 124, 233]. Based on SecA crystal structures [73, 74, 102], and, in accordance with structural and mutagenesis studies of relevant helicases [99], both Arg574 (motif VI) and Arg509 (motif V) in *E. coli* SecA, two highly

conserved residues, could act as "arginine finger" by coordinating the γ-phosphate of ATP (Figure 3.48).

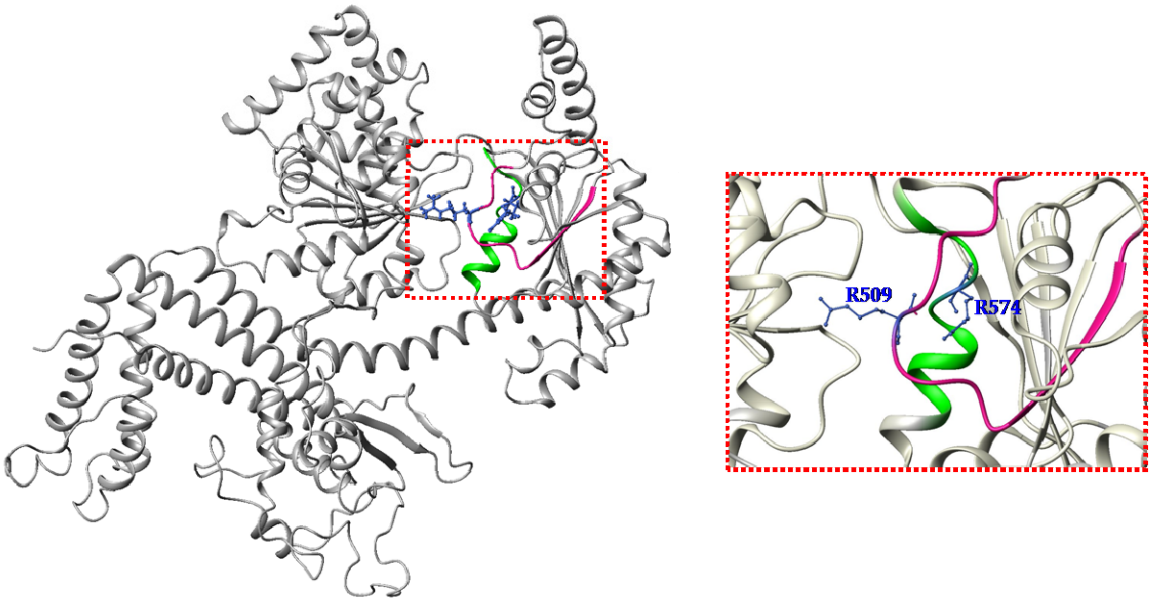

Figure 3.48: R509 and R574 are putative "Arginine fingers" in *E. coli* SecA. Motifs V and VI are colored pink and green respectively.

To test this hypothesis, we mutated these arginine residues to lysine (R509K and R574K), a positively charged amino acid that still can interact with the negatively charged phosphate but has shorter side chain compare to arginine. Both mutants, R509K and R574K, compromise the elevated basal ATPase activity of SecAΔC and exhibit ATPase activity similar to that of wild-type SecA. Moreover, the ATPase activity of SecA-R509K and SecA-R574K mutants is not stimulated upon addition of preprotein and SecYEG-containing membranes (Figure 3.49) [68, 75].

To test whether SecA-R509K and SecA-R574K mutants can function as trigger for conformational changes in SecA during the catalytic cycle, we measured ΔH of

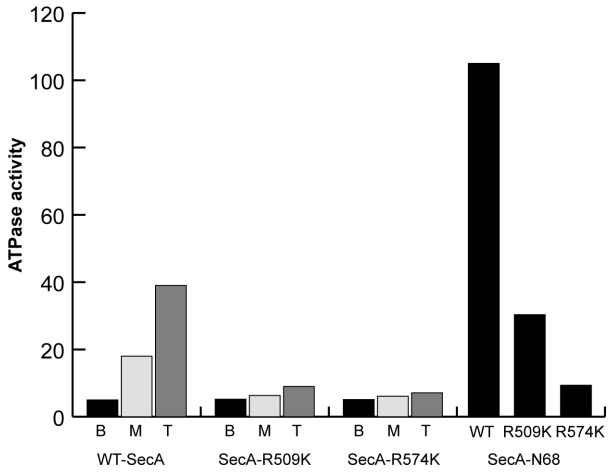

Figure 3.49: ATPase activity of SecA, SecAΔC and their R509K and R574K mutants. Basal (B), membrane (M), and translocation (T) activities of SecA are shown.

nucleotide binding to SecA-R574K and SecA-R509K as a function of temperature (Figure 3.50a). ATP-γ-S binding to either SecA-R574K or SecA-R509K at 37 ^{o}C does not induce folding of the nucleotide cleft (ΔH_{fol} = 0), in contrast to wild type (wt)-SecA (ΔH_{fol} = -4.5 kcal mol^{-1}). At higher temperatures, nucleotide binding to the amino acid substituted proteins promotes some local folding, but this is to a much lesser extent than seen in wt-SecA.

In addition, the association constant (K_a) of either SecA-R509K or SecA-R574K with ATP-γ-S decreases four-fold at 37 ^{o}C, whereas it remains invariable for their complexes with ADP (Figure 3.50b). Apparently, the contact between the guanidinium group of Arg509 and Arg574 with the γ-phosphate is of great importance for the catalysis as it regulates the disorder-order transition. The electrostatic interaction of R509 and R574 with the γ-phosphate of ATP results in the stabilization of the helix of motif VI, which in turn may further stabilize the salt bridges between NBD and IRA2. Therefore,

Arg509 and Arg574 can differentiate between ATP-γ-S and ADP and are central determinants of the alternate conformational states generated during the ATPase cycle.

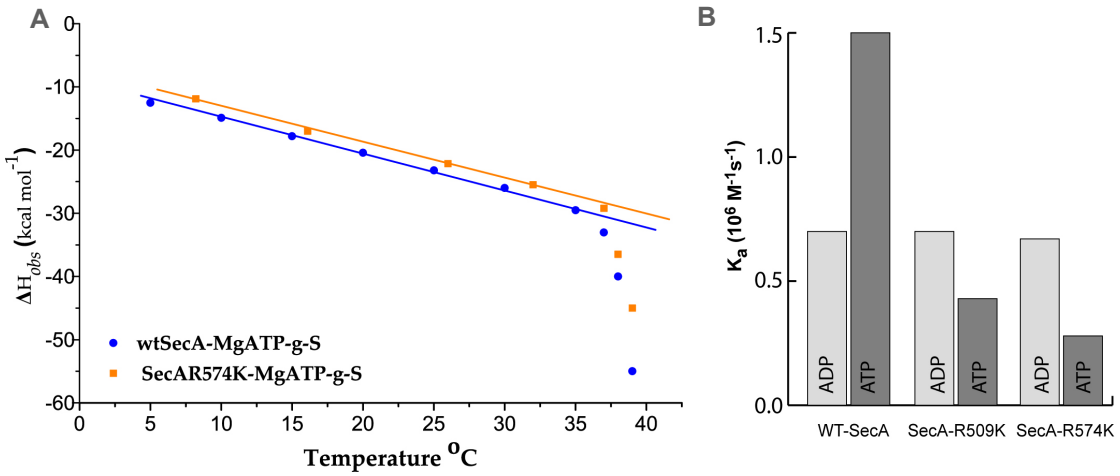

Figure 3.50: (a) ΔH_{obs} of MgATP-γ-S binding to SecA (blue line) and SecAR574K (orange line) as a function of temperature. (b) Association constant (K_a) for the interaction of SecA and its R509K and R574K mutants with MgADP and MgATP-γ-S, at 37 °C, measured by ITC.

III.2.12 Control of SecA ATP hydrolysis through a novel 'gate' in the DEAD motor

SecA has a complex mechanism that controls the physical interaction between NBD and IRA2, thereby regulating the opening/closure of the nucleotide cleft and modulating the ATPase activity of the motor [68, 73, 97, 105, 109, 234].

One structural element that is involved in this mechanism is ''Gate 1'', a salt bridge formed between D217 and R566 (Figure 3.51) [234]. D217 lies at the end of the α helix (orange) that harbors the catalytic helicase Motif II at its other end and R566 is located at the beginning of Motif VI (green). Gate 1 connects NBD and IRA2 at the

bottom of the nucleotide cleft and allows conformational and functional cross-talk between the catalytic Motif II and Motif VI.

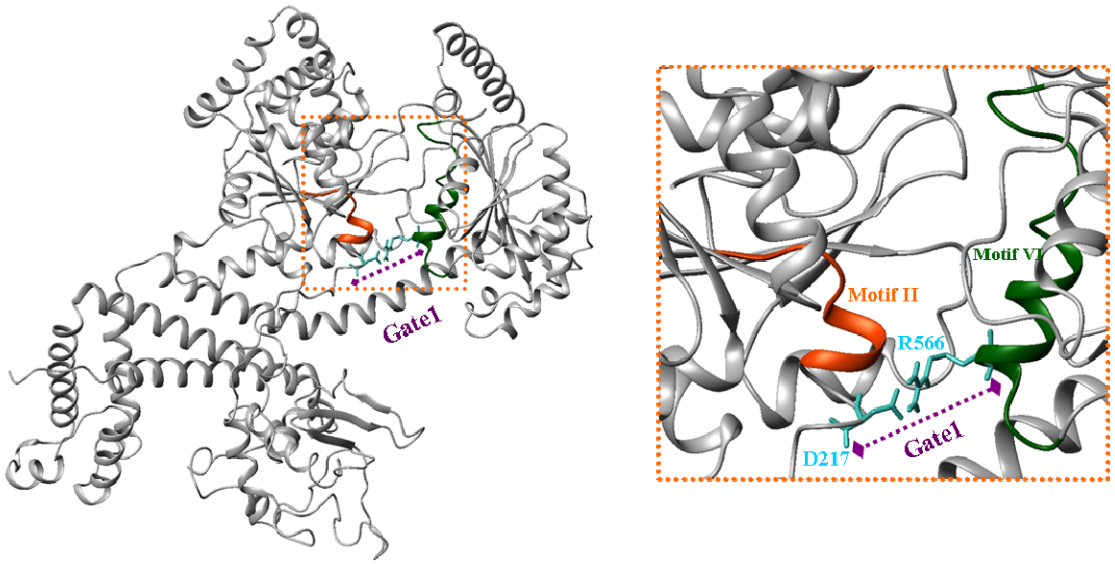

Figure 3.51: The "Gate1" region of *E. coli* SecA. Motifs II and VI are colored orange and green respectively. D217 and R566 are the residues that form Gate 1 and are colored blue.

To assess the importance of this salt bridge we mutated Arg566 and Asp217 to Ala. Interestingly, both mutants display 'early' ATPase activation with optima at 26 ^{o}C for SecAΔC(R566A) and 28 – 29 ^{o}C for SecAΔC(R566A) whereas for wt-SecAΔC is ~ 37 ^{o}C (Figure 3.52a). In agreement with this, salt-bridge weakening by increased salt buffer concentration downshifts the wt-SecAΔC ATPase to early activation (~ 28 ^{o}C). 'Gate 1' opening seems to be coincident with early thermal activation of the DEAD motor ATPase and its role is critical for the integrity of the nucleotide cleft.

Previously, we showed that IRA2 structural elements facing the nucleotide cleft undergo a nucleotide driven disorder- order transition [110]. To assess the effect of 'Gate 1'-mediated catalytic activation of the DEAD motor ATPase to the catalytically essential

disorder-order transition in the nucleotide cleft, we measured by ITC the temperature dependence of ΔH caused by nucleotide binding to SecAΔC-R566A (Figure 3.52b). Interestingly, T_f value for ADP binding to SecAΔC-R566A is 16 ^oC, much lower than that of wt-SecAΔC (~21 ^oC). This indicates that the nucleotide cleft becomes significantly destabilized after disruption of D217-R566 salt bridge.

The 'Gate1' salt bridge stabilizes ADP-driven IRA2 folding. Through control of IRA2 conformation, 'Gate1' controls ADP release, the rate-limiting step for multiple ATP turnovers [97, 200]. 'Gate1' opening results in a remarkable loss of ADP affinity, leading to activation of SecA ATPase; in contrast, Gate1 closure stabilizes the ADP state.

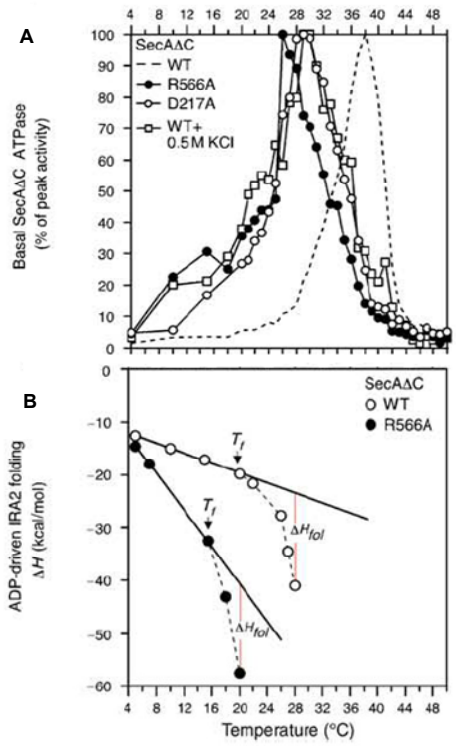

Figure 3.52: (a) Basal ATPase activities of SecAΔC(R566A), SecAΔC(D217A) and SecAΔC. SecAΔC basal ATPase activity was also determined in the presence of 550 mM KCl. (b) ΔH_{obs} as a function of temperature for the SecAΔC and SecAΔC(R566A) interaction with MgADP [234].

III.3 Discussion

Our results demonstrate that the helicase motor of SecA uses a novel mechanism that acts independently of potential rigid-body movements during the catalytic cycle. We show that, at physiological temperatures, the nucleotide cleft of SecA exists in a metastable state characterized by an equilibrium of disordered-ordered conformational states. This highly dynamic conformational ensemble has different responses to ATP binding and hydrolysis, giving rise to alternate conformations during the ATPase cycle (Figure 3.53).

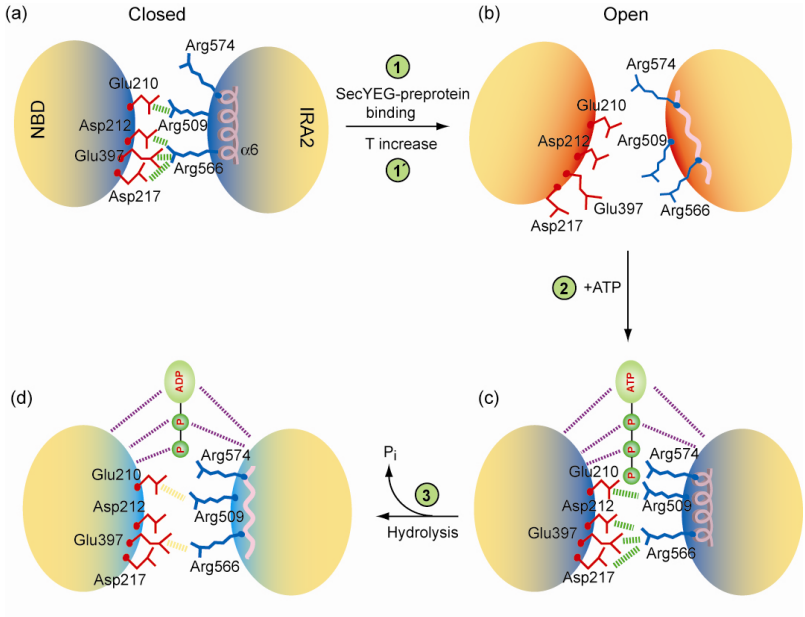

Figure 3.53: Model of conformational and dynamic changes in the helicase motor of SecA as a function of the nucleotide state, as suggested by the present NMR, thermodynamic and biochemical data. Green and yellow dotted lines indicate strong and weak salt electrostatic interactions, respectively. NBD-IRA2 interface is colored according to its flexibility: dark blue, light blue and red indicate increasing flexibility.

In the ‘closed’ conformation of the motor (Figure 3.53a), consolidated by the extensive contact surface between SD and the motor and by lower temperatures, NBD-IRA2 contacts are optimal and all IRA2 regions facing the cleft are well folded. Because SD is the structural ‘switch’ that modulates the mutual interaction of the NBD-IRA2 interface, it may then control the response of SecA to translocation ligands. Factors that loosen the SD-motor interaction will shift the conformational equilibrium at the cleft toward the disordered state (Figure 3.53b). The strong effect of SD in promoting the interaction between NBD and IRA2 is illustrated by the pronounced flexibility gained by SecA upon removal of the C domain (SecAΔC) (Figure 3.28). The flexible conformation of the motor in SecAΔC is expected to resemble the functionally relevant relaxed conformation of SecA seen at physiological temperatures. However, even when SecA adopts a completely loose, dumbbell-like conformation, NBD and IRA2 still interact transiently (Figure 3.32, 3.34).

Temperature is the main determinant of the interconversion of the helicase motor between the closed and open conformations when the C domain is detached (Figure 3.53b). Whereas at elevated temperatures ADP binds to SecAΔC with much lower affinity than to SecA, at low temperatures the affinities for both SecAΔC and SecA binding to ADP are very similar. Furthermore, at low temperatures the ATPase activity of SecAΔC is suppressed. These measurements suggest that, whereas the helicase motor of SecAΔC is widely open at higher temperatures, drastically reducing the affinity for nucleotide, while at very low temperatures it exists in a closed conformation, even in the absence of the C domain.

SecA is known to undergo an endothermic transition at temperatures slightly above physiological [72, 106, 200]. Because this transition is modulated by a variety of mutations in both SecA and SecG [200, 235, 236], as well as by the presence of nucleotides [73, 97, 109, 235] and preproteins [106], it has been hypothesized that it is important for the preprotein translocation reaction. On the basis of combined biophysical and biochemical data, it has been proposed that this transition may involve the dissociation of the α-helical wing domain (WD), resulting in globally cooperative changes in domain-domain interactions and the opening of the nucleotide cleft [72, 73]. The present results suggest that the disorder-order transitions at the nucleotide cleft are the primary contributor to the thermodynamics of the endothermic transition in SecA.

ATP binding to the helicase motor would bring closer the NBD and IRA2 domains by providing contacts to both of them (Figure 3.53c). The γ-phosphate may be coordinated by Arg574 and Arg509 only when IRA2 is folded (Figure 3.49, 3.50). Therefore, ATP binding induces a disorder-order transition resulting in the α-helix of motif VI and the other flexible regions of IRA2 becoming folded. Subsequent ATP hydrolysis and release of pyrophosphate (P_i) would disrupt the contacts of the arginine fingers to the phosphate moiety of the nucleotide, resulting in a less stable conformation (Figure 3.53d). In this state, the helicase motor is occupied by ADP and still exists in a closed conformation, as suggested by the present thermodynamic data. This conclusion is further corroborated by earlier observations that the linker connecting NBD and IRA2 becomes protease resistant in the presence of either ATP or ADP [105]. However, it is clear from our data that, in contrast to the ATP-bound state, in the ADP-bound state the

interdomain interactions are not optimal and regions of IRA2 facing the cleft are partially disordered.

The arginine fingers are of tantamount importance in controlling the disorder-order equilibria, as, when they are mutated, the resulting SecA proteins cannot differentiate between ATP and ADP. The overall motor conformation in the ATP-bound state of these mutant SecAs presumably resembles the ADP-bound state of wild-type SecA, as suggested by the ΔC_p values. These results reveal a previously uncharacterized role of the arginine fingers in helicase motors: their ability to modulate the degree of the conformational disorder-order transitions undergone by regions lining the nucleotide cleft. In principle, this novel mechanism may or may not be accompanied by rigid-body rotation of the motor domains, as is the mechanism described in PcrA helicase [203].

The motor domain-2 (corresponding to IRA2 in SecA) of another helicase (Hepatitis C virus, HCV) [237] seems to undergo disorder-order transitions as a function of the ligation state (Figure 3.54). A salt bridge between the helix of motif VI and the

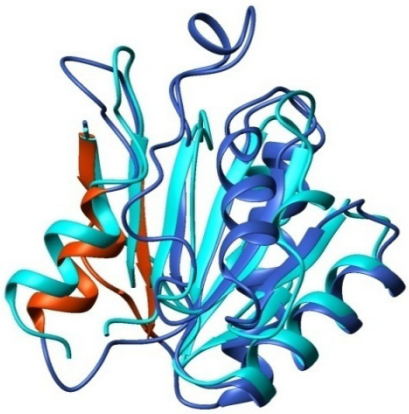

Figure 3.54: *B subtilis* IRA2 (blue) is superimposed with the corresponding region from HCV (turquoise). The disordered regions of IRA2 identified in this study are colored red.

rigid scaffold of domain 2 confers stability to this region in HCV. This salt bridge is not present in IRA2 of SecA, whose stability is instead regulated through interdomain interactions with the NBD and SD. Disruption of this salt bridge in HCV by mutagenesis results in the unfolding of motif VI and two β-strands located at very similar positions to the ones seen to unfold in IRA2. This observation suggests that both SecA and the HCV helicase may exploit the conformational ensemble of the helicase motor through similar mechanisms to translocate entirely different biopolymers.

In conclusion, the presence of extended regions of intrinsic plasticity at the motors of helicases provides these proteins with a very sensitive and malleable 'allosteric scaffold' that can be distinctly modified during the ATPase cycle. The outcome achieved by this mechanism is the coupling of nucleotide-driven cycles of helicase motor motions to cycles of binding, conformational alteration and release of the translocated aminoacyl or nucleic acid polymer.

Chapter IV. The activation mechanism of SecA's ATPase activity

IV.1 Introduction

SecA has very low ATPase activity which is stimulated only after its interaction with the preprotein and the protein conducting channel SecYEG [78, 80, 132, 214, 215]. Once at the membrane, SecA actively drives translocation and a part of SecA inserts into the channel. The exact mechanism by which SecA is activated remains unknown. It has been proposed that the membrane-bound SecA is nucleotide free and adopts an open/relaxed conformation [72] while in the ADP-bound state, as it is found in the cytosol, adopts a closed/compact conformation [238]. The conversion of SecA from the inactive to the activate state is believed to be accompanied by large conformational change.

SecA uses the C domain to regulate the futile ATPase activity. In fact, the ATPase activity of SecA is under the strict control of C domain which controls the physical interaction of the motor domains, thereby regulating its opening/closure and, thus, modulating the ATPase activity of the motor.

To better understand the mechanism underlying the activation of SecA, we studied by NMR the full-length SecA.

IV.2 Results

IV.2.1 The C-domain alters the NBD – IRA2 interface

The only C domain structural element that physically interacts with the motor and holds the subdomains of SecA in a closed compact conformation is SD (Figure 4.55). In section III.1.1 we show that SecAΔC (a construct with the C domain truncated) exhibits elevated ATPase activity. Most likely the SD helix is a regulatory element of the ATPase activity of SecA by regulating the opening/closure of the motor.

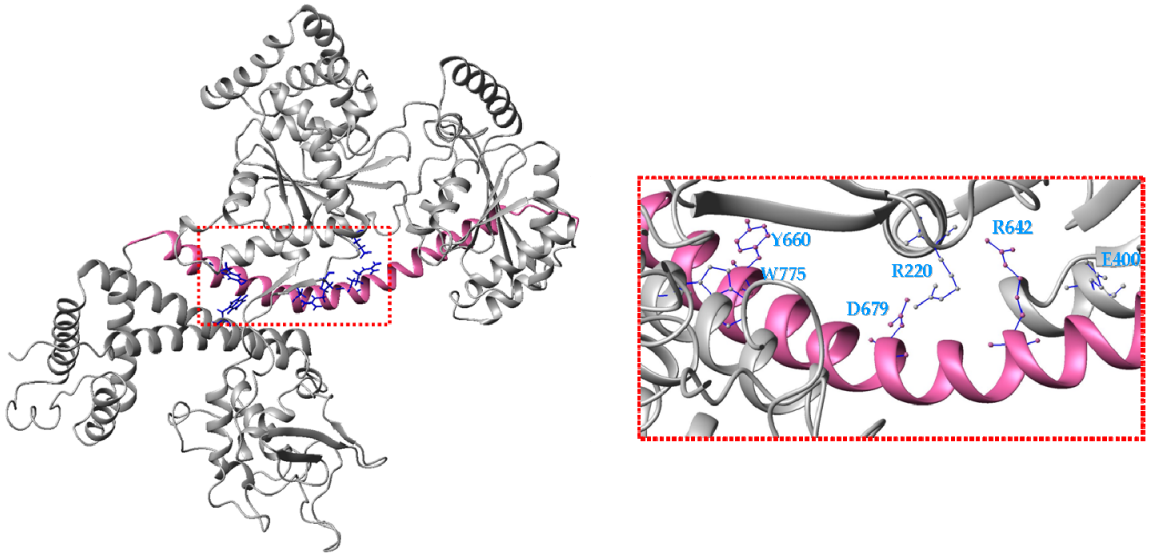

Figure 4.55: The long α-helix SD (pink) in SecA participates in two strong salt bridges with the NBD (Asp649 with Arg220 and Arg642 with Glu400) and a hydrophobic interaction with IRA1 (Tyr660 with Trp775).

In all available SecA crystal structures, the long SD α-helix appears to participate in two strong salt bridges with the NBD (D649 with R220 and R642 with E400) and a hydrophobic interaction with IRA1 (Y660 with W775) (Figure 4.55). These interactions are responsible for retaining SecA in a compact conformational state. To test the

hypothesis that the integrity of the NBD-IRA2 interface is regulated by SD we disrupted these interactions by mutating R642, D649 and W775 to A.

We first introduced a single mutation, D649A, which disrupts the salt bridge between D649 and R220. The SecA-D649A is functional as shown by *in vivo* genetic complementation assays involving the chromosomal thermosensitive *secA* gene (Figure 4.56a). Furthermore, this mutant is able to carry out efficient protein translocation in vitro in a degree similar to that of wild-type SecA as revealed by protein translocation assays

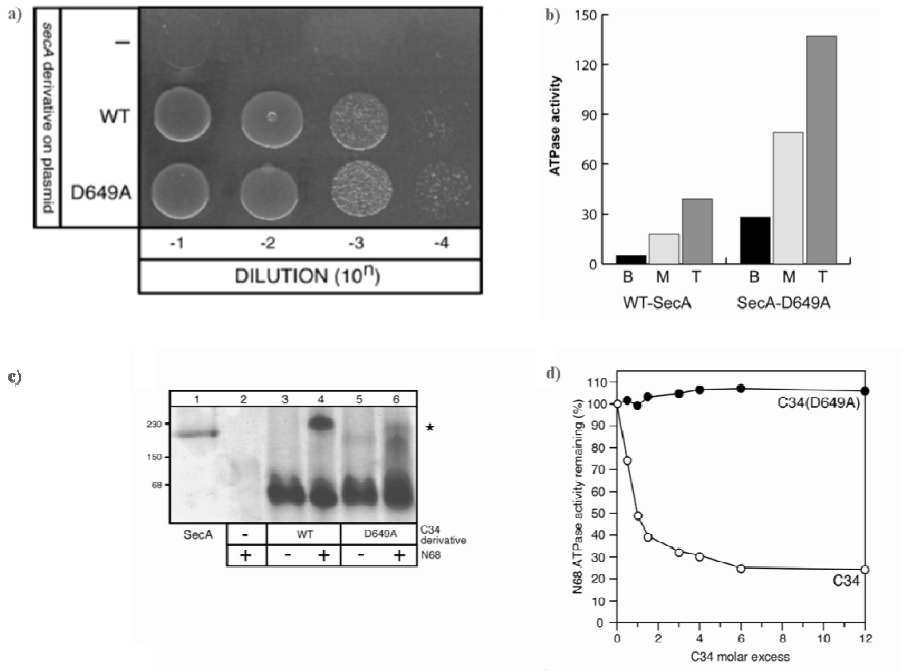

Figure 4.56: (a) Genetic complementation of the *secAts* strain BL21.19 by pET5 or pET5 carrying cloned secA or secA-D649A. Indicated culture dilutions (grown at 30 °C) were spotted on LB/ampicilin plates and incubated (42 °C). (b) Basal (B), membrane (M) and translocation (T) ATPase activity of wt-SecA versus SecA-D649A. (c) Native PAGE of wt-C34 interaction with SecAΔC to yield 'reconstituted SecA' (indicated with an asterisk). C34-D649A binds SecAΔC very weakly. (d) C34-D649A does not suppress the ATPase activity of SecAΔC, in contrast to wild-type C34.

(Figure 4.56b). In addition, we introduced the mutation D649A to C34, an isolated polypeptide that encompasses the C-domain of SecA. We attempted to reconstitute SecA from the isolated component SecAΔC and C34-D649A and the degree of association was assessed by native PAGE assay (Figure 4.56c).

Our results demonstrate that the wild type components, C34 and SecAΔC form a reconstituted SecA complex that migrates more slowly (200 kDa) than either SecAΔC or C34 alone. In contrast, the C34-D649A is severely compromised in its ability to form stable complexes with SecAΔC because of the disruption of SD-NBD interaction. In agreement with these results C34-D649A is unable to suppress the elevated ATPase activity of SecAΔC as the wt-C34 does (Figure 4.56d). As expected, SecA-D649A exhibits higher basal ATPase activity compare to wt-SecA. Notably, a single mutation in the SD helix is capable of strongly affecting the ATPase regulation of SecA.

To assess the effect of the D649A mutation on the integrity of the nucleotide cleft, we measured ΔH of ADP binding as a function of temperature (Figure 4.57). We found that ADP binding to SecA-D649A is characterized by a much lower T_f (~24 ^oC) than SecA (~37 ^oC). In fact, the T_f of SecA-D649A approaches the characteristic T_f of SecAΔC (~21 ^oC). Thus, we suggest that SecA-D649A resembles the activated state of SecA, wherein the C domain has been detached from the motor. Therefore, our thermodynamic and biochemical data suggest that the SecA C-domain is an additional regulator of helicase motor folding and ATP catalysis.

To further explore the importance of the C-domain in regulating the integrity of the motor we disrupted additional interactions of the SD helix with NBD and IRA1 (Figure 4.55). The R642A and W775A mutations were introduced in a stepwise manner

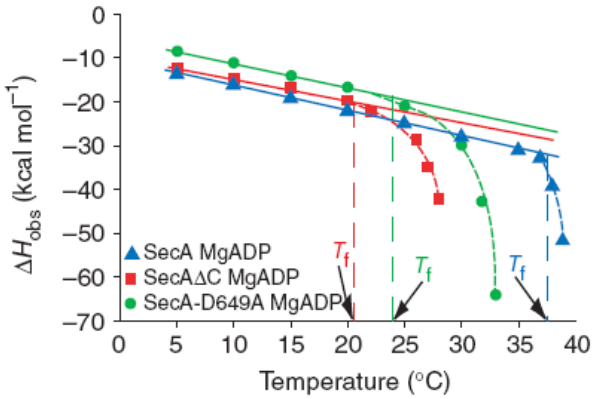

Figure 4.57: Enthalpy change (ΔH_{obs}) as a function of temperature for the interaction of SecA, SecAΔC and SecA-D649A with MgADP in 100 mM K+.

to SecA-D649A and T_f values were measured by ITC for the resulting mutants (Table 2). Following the same trend observed for SecA-D649A, disruption of more interactions between SD and NBD or IRA1 result in a drastic decrease of the T_f values that now are either lower from that of the hyper-activated SecAΔC (~ 21 ^oC) for SecA-R642A-D649A (~ 18 ^oC) or even lower for SecA-R642A-D649A-W775A (~ 14 ^oC).

In summary, with this strategy we manage to construct a mutant that resembles the activated state of SecA and can be used as a tool to study the activation mechanism in the context of full-length SecA without the need of other translocation ligands that make the task almost impossible.

Table 2: T_f values for wt-SecA and derivatives

SecA derivative	**T_f (^oC)**
SecA	37
SecAΔC	21
SecA-D649A	23
SecA- R642A-D649A	18
SecA- R642A-D649A-W775A	14

IV.2.2 Methyl-TROSY studies of 204 kDa SecA ATPase

A major challenge in studying SecA by NMR spectroscopy is its large size (204 kDa). The use of conventional NMR methodologies can only provide limited information; in a simple ^{1}H-^{15}N-HSQC spectrum only a small fraction of peaks shows up, from the flexible CTD (Figure 4.58).

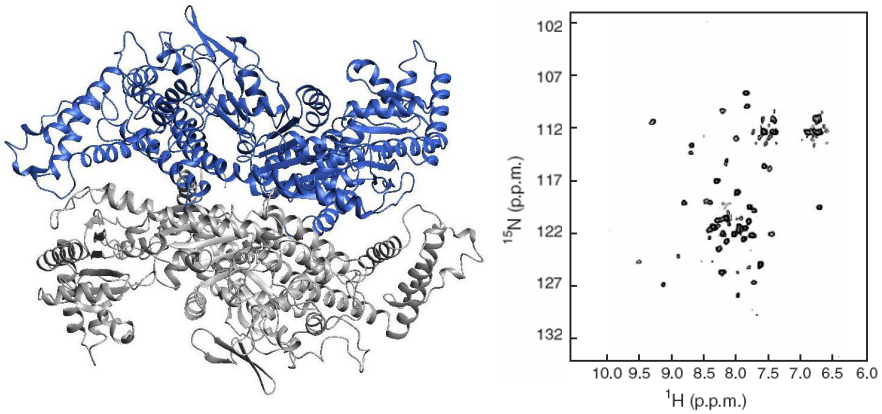

Figure 4.58: ^{1}H-^{15}N HSQC spectrum of SecA (dimeric, 204 kDa) recorded at 22 ^{o}C on a 600-MHz NMR instrument.

A very attractive methodology for studying large macromolecular systems by NMR has been introduced by Lewis Kay and is based on specific labeling of methyl groups in an otherwise entirely deuterated background [166, 168, 169, 174].

We initially produced SecA with the δ_1 methyl groups of Ile residues ^{1}H-^{13}C labeled in an otherwise completely deuterated background (Figure 4.59). We use methyl-TROSY to optimize both sensitivity and resolution [129, 168, 169, 174, 239]. SecA has in total 54 Ile residues, which are distributed throughout the SecA structure that provide excellent probes for studying the interactions and the dynamics of full-length SecA with different ligands. The recorded ^{1}H-^{13}C heteronuclear multiple quantum (HMQC)

spectrum (methy-TROSY) is of exceptional quality as we are able to observe all 54 Ile-δ_1 methyl resonances (Figure 4.59) .

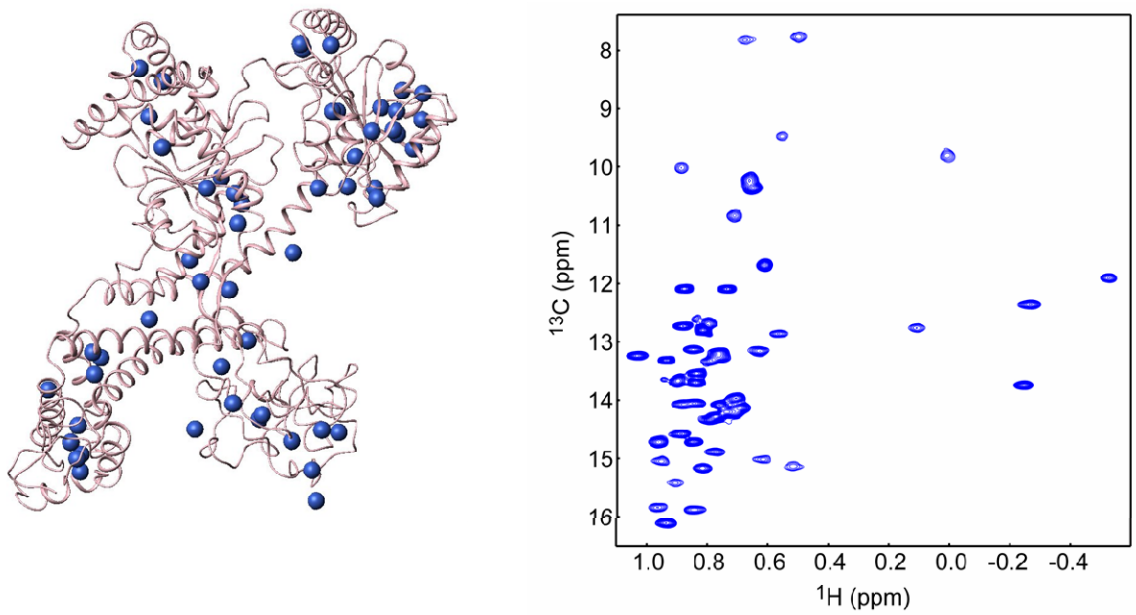

Figure 4.59: SecA protomer with the Ile-δ_1 methyls displayed as blue spheres. ^{1}H-^{13}C HMQC spectrum of SecA U-[^{2}H, ^{12}C], Ile-δ_1-[$^{13}CH_3$] recorded at 25 ^{o}C on a 600 MHz NMR instrument.

IV.2.3 Assignment strategy of methyl resonances

The large size of SecA precludes the use of traditional assignment protocols. For this reason, we followed a domain-parsing strategy. All domains of SecA and a number of fragments comprising continuous domains have been isolated and characterized by NMR as we describe in chapter III [110]. Assignment of the methyl groups on these relatively small domains was straightforward with standard methodologies (Figure 4.60). Comparison of the ^{1}H-^{13}C-HMQC spectra of the various domains with that of the full-length SecA demonstrates very good resonance correspondence (Figure 4.61). Therefore,

the majority of the assignment of the methyl cross peaks performed in the isolated domains and fragments could be readily transferred to full-length SecA.

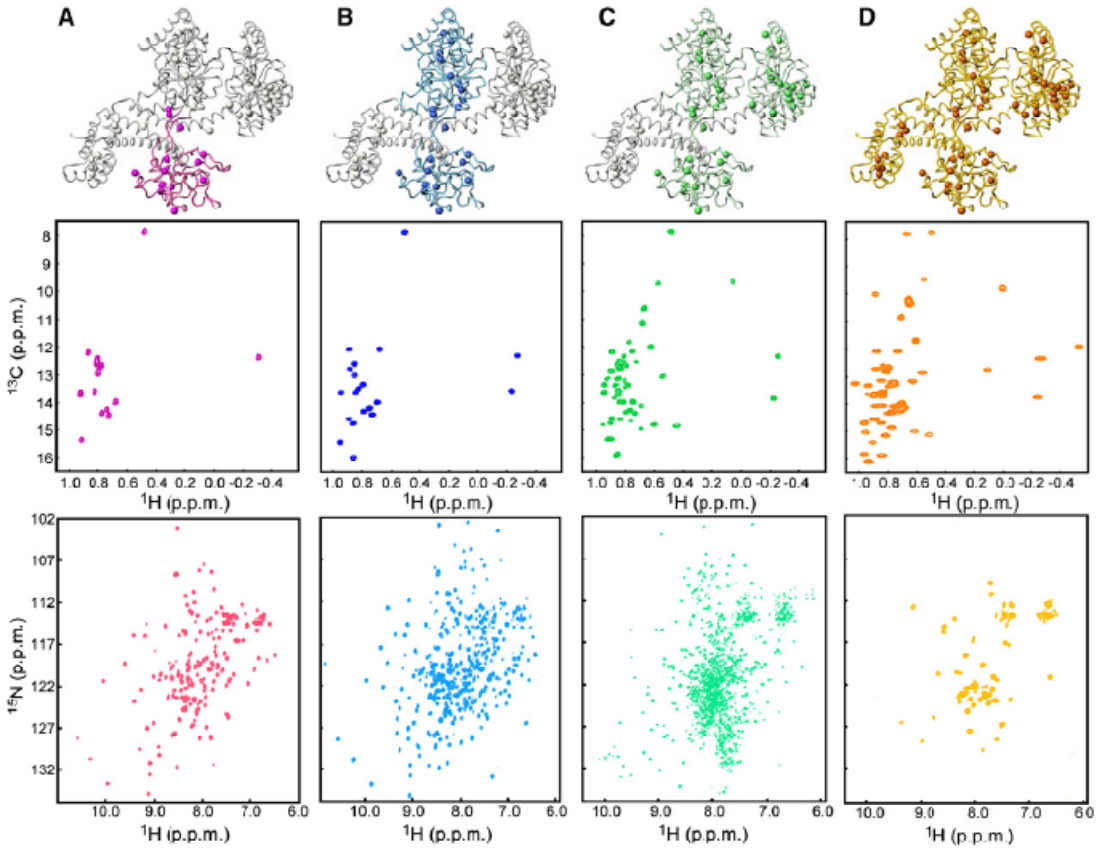

Figure 4.60: Strategy for the assignment of methyl correlations of SecA. Each column in the figure displays the protomers of SecA with the domain or fragment studied in isolation being highlighted, along with the corresponding ^{1}H-^{13}C HMQC of Ile-δ_1 methyls (displayed as spheres) and the backbone ^{1}H-^{15}N HSQC. (A) PBD, (B) SecAΔC/ΔIRA2 (comprising NBD and PBD), (C) SecAΔC (comprising NBD, PBD, and IRA2), (D) Full-length SecA.

Assignment was completed with 3D NOESY (^{13}C-HMQC-NOESY-HMQC) spectra recorded on full-length SecA (Figure 4.62. The use of a perdeuterated sample, combined with long mixing times (~0.3-0.4 sec) enabled the detection of NOEs between methyl groups located as far as 7 Å. Because the structure of SecA is known, the NOESY data were very helpful in assigning the methyl side chains of full-length SecA. We also used mutagenesis to resolve ambiguities that primarily existed for residues located at the interface of domains. For example, in the Ile spectra, Ile304 shifts significantly from SecAΔC-ΔIRA2 to full-length SecA (indicated by the grey line in Figure 4.61). The reason being that, in SecA, this residue is located at the interface between PBD and

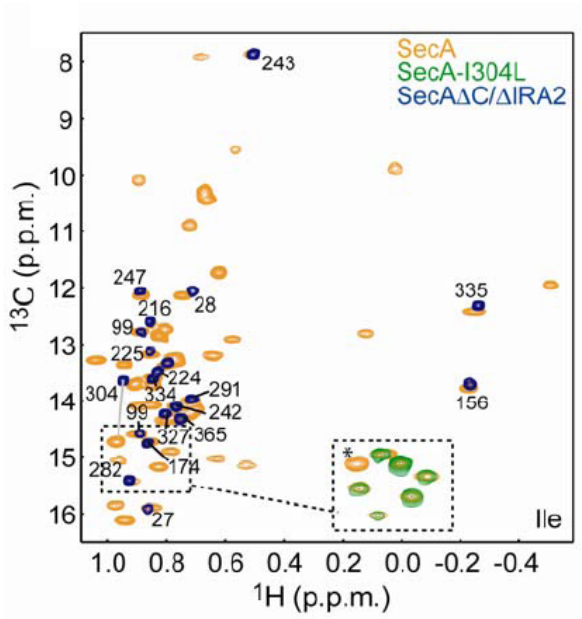

Figure 4.61: The Ile-δ_1 methyl spectra, of SecA (orange), SecAΔC/ΔIRA2 (blue) are overlaid. The excellent correspondence of the spectra permitted the transfer of the assignment from the isolated domain/fragment to full-length SecA. Ambiguities exist only for residues located at the interface of domains, for example I304 which we mutated to Leu (green).

IRA1. To resolve this ambiguity, Ile304 was mutated to Leu and the spectrum of the mutant (green peaks in the insert in Figure 4.61) was recorded, clearly identifying the chemical shift of Ile304 in full-length SecA (denoted by an asterisk in the insert, Figure 4.61).

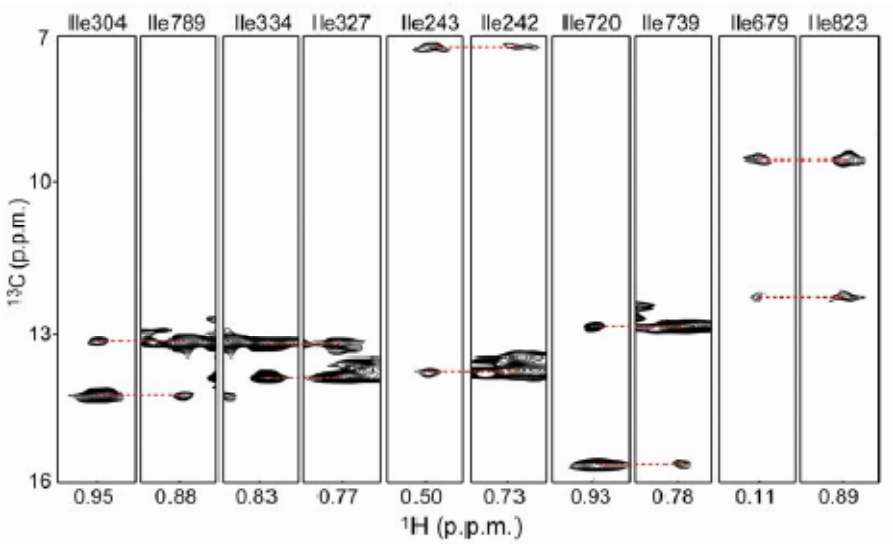

Figure 4.62: Selected strips from SecA ^{13}C-HMQC-NOESY-HMQC spectra are shown.

IV.2.4 Conformational changes of SecA upon activation.

To determine the conformational changes that accompany SecA activation, we studied SecA-D649A mutant by methyl-TROSY NMR. As we described previously, the D649A substitution stimulates SecA ATPase. To monitor the conformational changes accompanying this transition, we recorded the Ile-δ_1 methyl spectrum of SecA-D649A and compare it to that of wt-SecA (Figure 4.63).

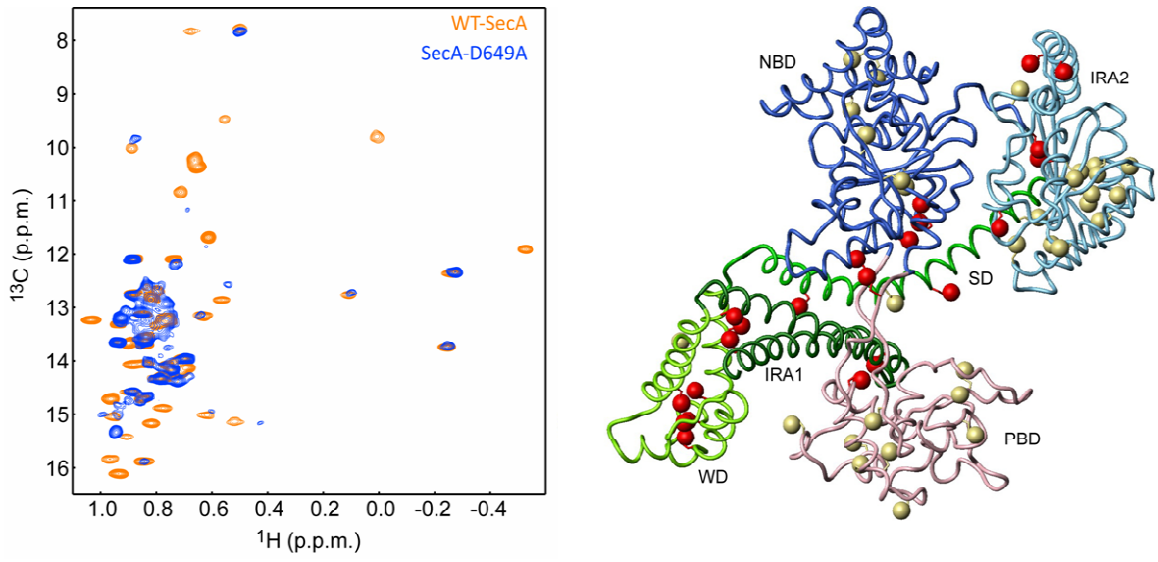

Figure 4.63: ^{1}H-^{13}C HMQC spectrum of SecA Ile-δ_1-[$^{13}CH_3$] (orange) and SecA-D649A (blue) recorded at 25 ^{o}C on a 600 MHz NMR instrument. SecA-D649A protomer with the Ile methyl groups that experience severe broadening displayed as red spheres.

Interestingly, many signals of SecA-D649A are broadened beyond detection. Mapping of these residues onto SecA structure reveals that the majority of them are located at the C-domain and at the interface between the helicase motor and the C-domain (Figure 4.63). Protein conformational dynamics on µs-ms timescales is manifested as chemical exchange line broadening in NMR spectroscopy [185, 240]. The combined NMR and thermodynamic data (section VI.2.1) suggest that C domain continuously binds and releases the motor.

To better understand the structural and dynamic properties of the C domain, we recorded the Ile-δ_1 methyl spectrum of isolated C34 fragment (Figure 4.64). Only few peaks appear in the spectrum, which cluster in the center, indicating that the isolated C-domain behaves like an unfolded/molten globule protein.

We propose that C domain is detached from the motor exists in a metastable state. It is likely that this metastable state of C domain facilitates its insertion and deinsertion in the membrane embedded protein conducting channel SecYEG during the actual translocation process.

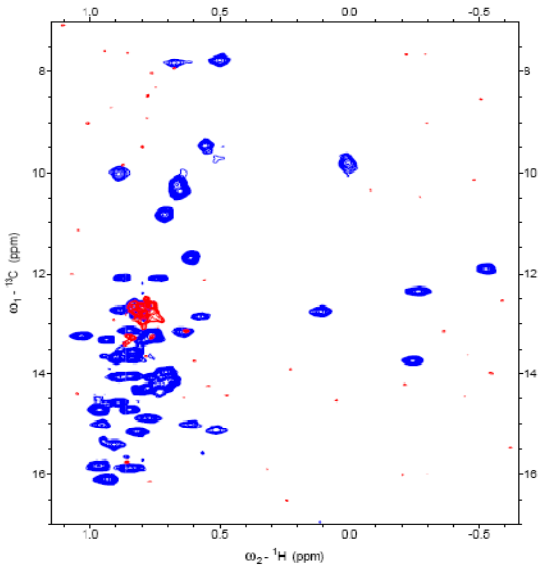

Figure 4.64: ^{1}H-^{13}C-HMQC spectrum of SecA Ile-δ_1-[$^{13}CH_3$] (blue) and C34 (red) recorded at 25 ^{o}C on a 600 MHz NMR instrument.

IV.3 Discussion

Our results demonstrate that even a single mutation on SD that disrupts a salt bridge between SD and NBD suffices to stimulate the basal ATPase activity of SecA to values similar to those of the translocation ATPase (Figure 4.56b). The strong effect of SD in promoting the interaction between NBD and IRA2 is illustrated by the pronounced flexibility gained by SecA upon removal of the C domain (SecAΔC) (Figure 3.28). The flexible conformation of the motor in SecAΔC is expected to resemble the functionally relevant relaxed conformation of SecA seen at physiological temperatures [105].

However, even when SecA adopts a completely loose, dumbbell-like conformation, NBD and IRA2 still interact transiently because of the presence of C-domain (Figure 3.32, 3.34). The opening/closure of the nucleotide cleft is directly linked with the ATPase activity of SecA and is controlled from the C-domain.

The C-domain is a highly dynamic element in SecA that binds and release the helicase motor on the μs-ms timescale (Figure 4.63, 4.65). This time regime is very important in biological processes such as enzymatic catalysis and product release, ligand binding, or protein folding. For several enzymes, the frequency of motion is comparable to the overall turnover rate, raising the possibility that conformational rearrangement may be the rate limiting for catalysis in these enzymes [180].

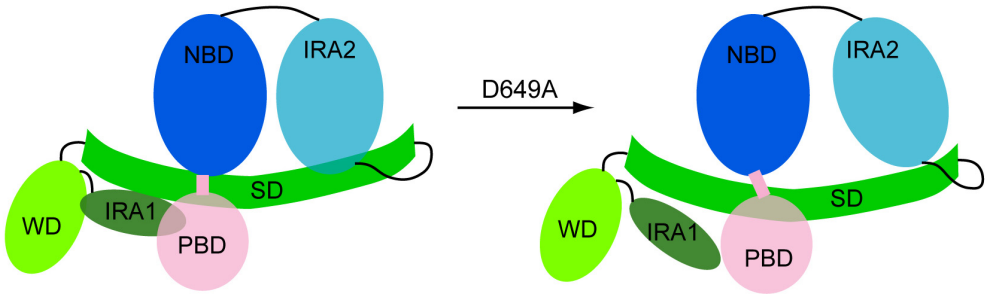

Figure 4.65: Model of conformational changes in SecA as result of activation induced by a single mutation (D649), as suggested by the present NMR, thermodynamic and biochemical data. Activated SecA adopts a loose conformation which facilitated by domain rearrangement.

SecA becomes activated when the contacts between the motor and the C-domain are loosen, a process which is probably facilitated by the membrane (Figure 4.65). The key event in SecA activation is the release of the motor from the C-domain followed by a cascade of events that result in large turnover number of the enzyme.

Here, we provide direct evidence that the C-domain, once released from the motor, exists in a metastable state, a state that promotes ADP release (rate limiting step) and initiates a new catalytic cycle of ATP hydrolysis and insertion into the channel (Figure 4.63,4.64). On the other hand, the C-domain in the resting inactive state of SecA is well structured and acts as the structural component that holds the motor from moving apart, thereby conferring stability to the entire SecA (Figure 3.28, 3.43). Our data demonstrate that the C-domain is both a central stabilizing element in SecA and a regulator of catalysis.

Our solution NMR data reveal that the nucleotide binding, hydrolysis and release of the product is a dynamic process which is governed by the intrinsic flexibility of the helicase motor (disorder-order transition in the helicase motor) and the inherent plasticity of the C-domain. The cross-talk between these two elements controls the ATPase activity of SecA and consequently the translocation process.

Chapter V. Allosteric communication in SecA

V.1 Introduction

SecA is a multidomain protein involved in a remarkable array of activities/interactions in the cell that results in productive protein translocation. SecA is the key player of the translocase. It interacts with all of the translocation ligands and, thus proper communication among the various domains is important for the function (Figure 5.66) [241].

DEAD motor helicases couple the free energy of ATP binding and hydrolysis while translocating vectorially along their substrates. The affinity/specificity of a helicase for its substrate is modulated allosterically by NTP binding, hydrolysis or product release, which is central in helicase catalyzed DNA/RNA unwinding [242, 243] and SecA catalyzed protein translocation.

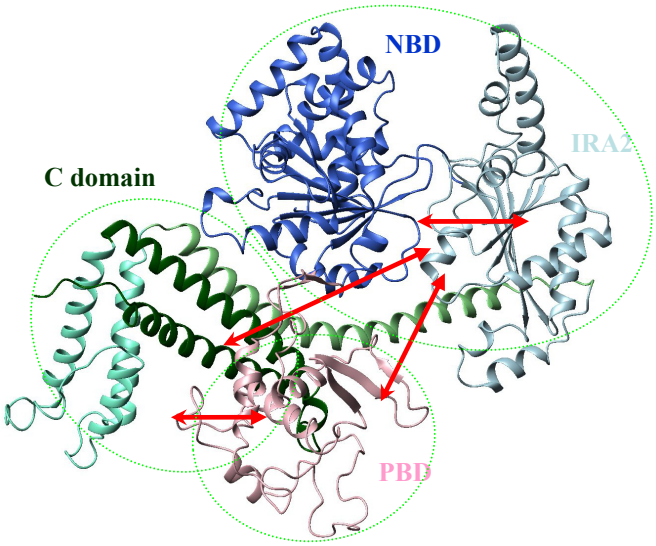

Figure 5.66: Allosteric network of interactions among the subdomains of SecA. Red arrows indicate communication and green circles the main subdomains of SecA.

Many biochemical studies have suggested the presence of such allosteric communication, that facilitates the functional "cross-talk", within SecA [97, 104, 106, 109, 234]. In an attempt to shed some light on coupling of protein translocation and the ATPase reactions cycle of SecA we studied the effect of nucleotide and signal peptide binding on its conformational transitions, by NMR and ITC.

V.2. Results

V.2.1 Nucleotide binding affects allosterically PBD.

Our NMR spectra revealed that ADP binding to SecAΔC causes PBD to undergo significant conformational changes, as evidenced by extensive chemical shift changes, and slower dynamics, as evidenced by resonance broadening (Figure 5.67). This demonstrates that the binding signal generated at the NBD-IRA2 cleft is allosterically transmitted to PBD. Several residues are affected from ADP binding, among them Tyr326 and Trp349, which have been implicated in preprotein binding [106, 244]. Interestingly, the nucleotide and preprotein-binding sites are located more than 50 Å apart.

The substantial slow dynamics on the μs-ms timescale that are induced to PBD by ADP binding to the remote helicase motor could have a great impact on the binding energetics and the promiscuous specificity of SecA for its translocation substrates.

In an attempt to further assess the effect of nucleotide binding on the conformation and dynamics of PBD, we studied the effect of nucleotide binding on full-length SecA (Figure 5.68). The SecA Ile-δ_1-[$^{13}CH_3$] spectra revealed that indeed nucleotide binding in SecA, except of the obvious local changes in the motor domain, is

able to affect not only PBD but also residues at the C-domain (659I, 789I). This is indicative of the allosteric regulation that is present in SecA even in interesting inactive solution state.

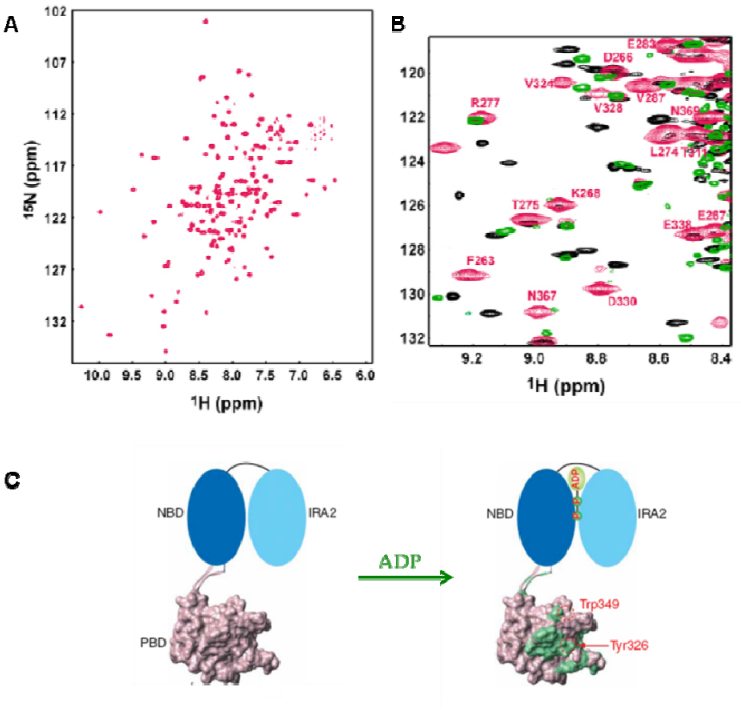

Figure 5.67: Allosteric effect of ADP binding to SecAΔC on PBD. (a) ^{1}H-^{15}N HSQC spectrum of isolated PBD (pink), (b) Excerpt of overlaid ^{1}H-^{15}N HSQC spectra of SecAΔC (black), SecAΔC-MgADP (green) and PBD (pink), assignment of PBD residues is provided. (c) Schematic showing structural changes in PBD after binding of ADP in the remote DEAD motor of SecA. Green surface coloring indicates residues in PBD that are affected upon ADP binding. Tyr326 and Trp349, important for preprotein binding to SecA, are indicated.

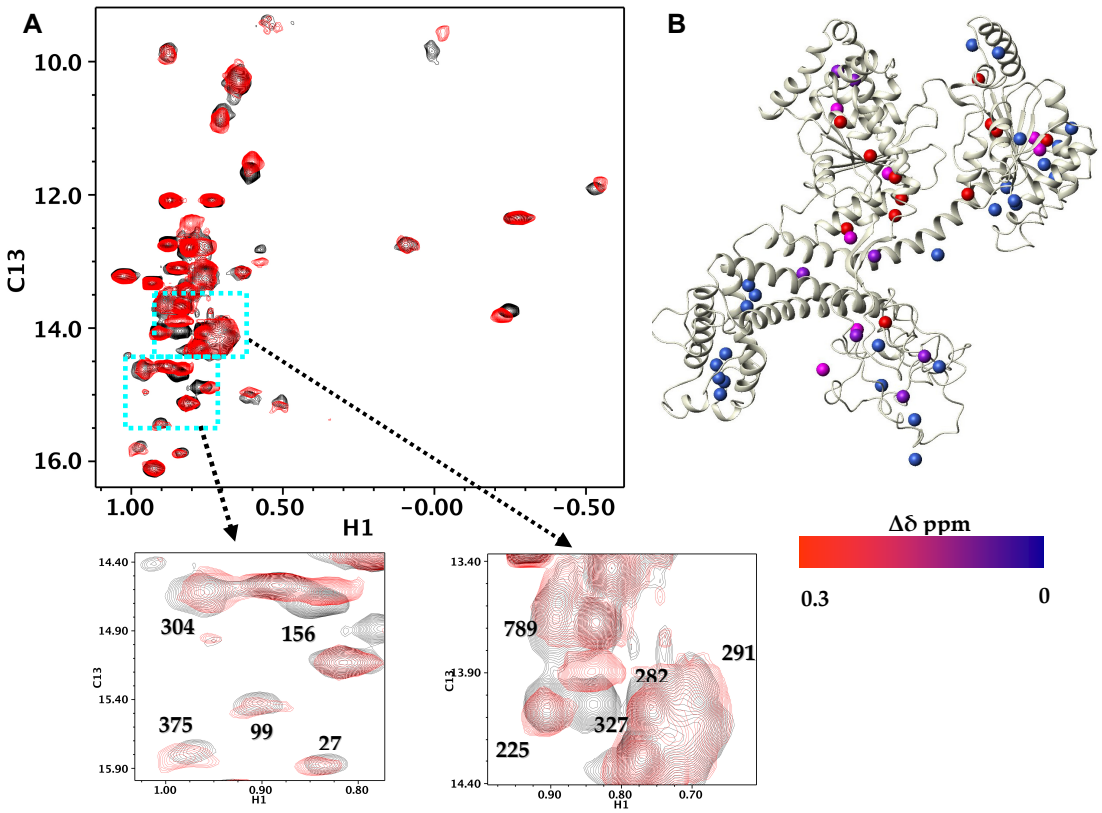

Figure 5.68: (a) Overlaid ^{1}H-^{13}C HMQC spectra of SecA Ile-δ_1-[$^{13}CH_3$] free (black) and after MgADP addition (red) recorded at 25 ^{o}C on a 600 MHz NMR instrument. (b) Mapping of the residues affected from MgADP onto SecA protomer with the Ile-δ_1 methyls displayed as spheres and colored according to the chemical shift difference between apo and ADP-bound SecA.

V.2.2 IRA2 presence affects allosterically PBD

Next we explored whether IRA2 is capable of inducing conformational changes in the remote PBD. Comparison of the NMR spectra of SecAΔC with those of SecAΔC-ΔIRA2 (a polypeptide encompassing NBD and PBD but not IRA2) shows that the presence of IRA2 strongly influences the conformation of PBD, even when the nucleotide cleft is vacant (Figure 5.69). Therefore, in addition to its role as an ATPase regulatory domain, IRA2 seems capable of affecting the preprotein binding site at PBD even though it interacts only transiently with NBD.

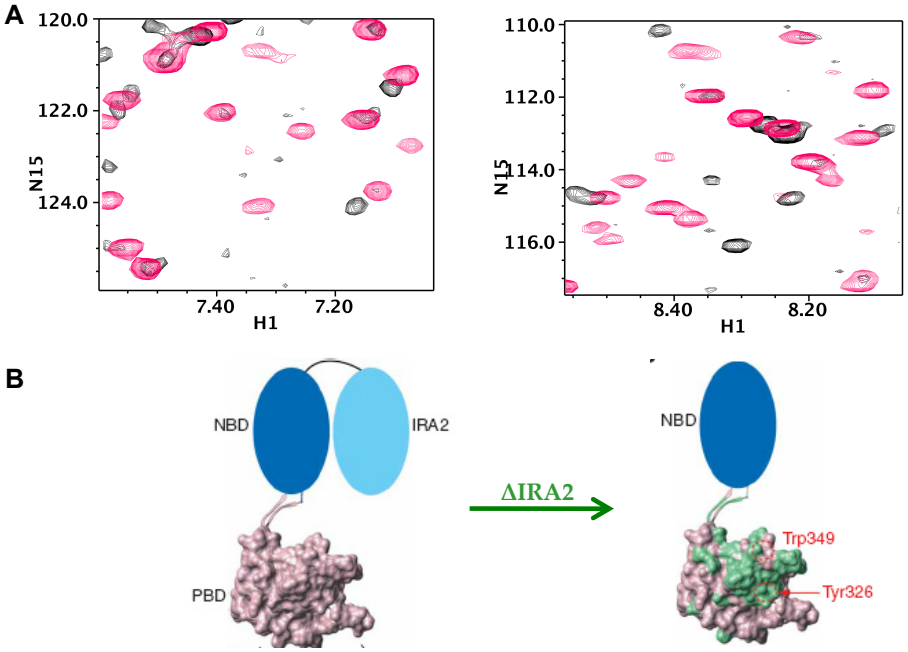

Figure 5.69: Allosteric effect of the presence of IRA2 on PBD. (a) Excerpt of overlaid ^{1}H-^{15}N HSQC spectra of SecAΔC (black), SecAΔCΔIRA2 (pink) (b) Schematic showing structural changes in PBD. Green surface coloring indicates residues in PBD that are affected in the presence of IRA2. Tyr326 and Trp349, important for preprotein binding to SecA, are indicated.

To summarize, we conclude that nucleotide binding and IRA2 allosterically control both the conformation and the dynamics of the preprotein binding site, thus providing a functional link between the ATPase cycle and preprotein binding.

V.2.3 Signal Peptide Binding affects the stability of the motor domain

To further characterize the intriguing allosteric network of communication in SecA, we explored the impact of signal peptide binding on the conformation and the inherent plasticity of the helicase motor.

We found that signal peptide binding to SecA-D649A has similar thermodynamic behavior as with binding to wt-SecA within the temperature range of 5 to 25 ^{o}C (Figure 5.70, blue line). At temperatures higher than 25 ^{o}C we observe a large enthalpy release which clearly suggests the presence of a coupled folding process that is linked to the signal peptide binding (Figure 5.70, blue dashed line).

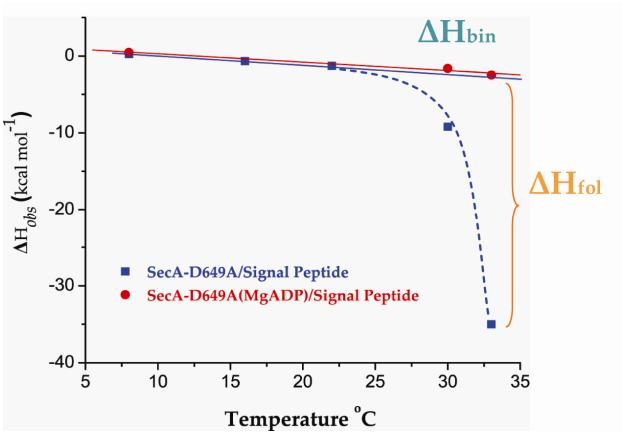

Figure 5.70: ΔH_{obs} of signal peptide binding in SecA-D649A in the absence (blue line) and in the presence MgADP (red line) as a function of temperature.

As we extensively discussed in chapter III, deviation from linearity and large negative ΔC_p are anticipated when binding is coupled to temperature dependent structural transitions. The catalytically activated SecA-D649A undergoes disorder-order transition in the helicase motor upon nucleotide binding starting at the characteristic temperature T_f~ 25 ^oC (Figure 4.57).

To explore the origin of the large amount of heat released upon signal peptide binding to SecA-D649A, we perform a series of ITC experiments, at different temperatures while having the nucleotide cleft saturated with MgADP (Figure 5.70, red line). Under these conditions, signal peptide binding to SecA-D649A does not give rise to non-linear ΔC_p, even at temperatures higher than 25 ^oC.

This implies that any excess ΔH observed upon signal peptide binding at temperatures higher than 25 oC originates from conformational changes that take place at the distal nucleotide binding site (disorder-order transition in IRA2) Our data suggest that signal peptide binding to SecA affects the motor domain and can potentially regulate ATP hydrolysis (Figure 5.71).

V.3 Discussion

SecA undergoes structural rearrangements that include large domain movements or local changes in secondary structure such as the disorder-order transition in the cleft, required for its functionality. Such dynamic processes are characteristic for enzymes as they regulate the catalytic process by directly coupling conformational changes throughout the macromolecule to the catalytic process [186].

Here we found that signal peptide binding directly affects the motor by inducing local folding of the unstructured regions that face the nucleotide cleft (Figure 5.70). It is remarkable how signal peptide binding to the PBD/IRA1 interface has such an impact on IRA2 conformation, while this two sites share no immediate physical connection. On the other hand, nucleotide binding and IRA2 allosterically control both the conformation and the dynamics of PBD, thus providing a functional link between the ATPase cycle and preprotein binding (Figure 5.67, 5.68).

We show that conformational 'cross-talk' between the DEAD motor, PBD and the C-domain is central to a productive protein translocation (Figure 5.71). Maybe this is the basis to explain how SecA uses the energy extracted from ATP hydrolysis to move polypeptide chains through the translocation channel. Nucleotide-driven conformational changes in the motor are transmitted to the specificity domains, thereby modulating their interaction with the preprotein.

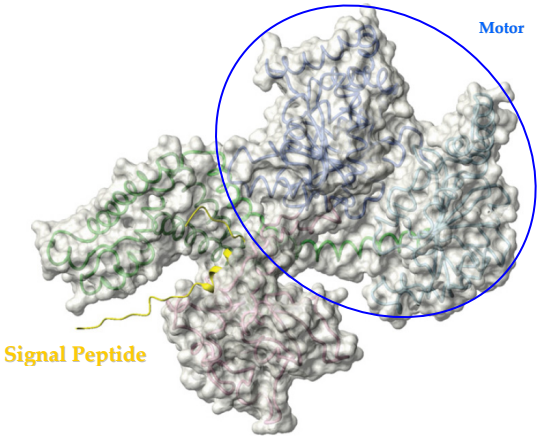

Figure 5.71: Allosteric communication between the preprotein binding site and the DEAD motor. The signal peptide is colored yellow and the motor domain blue [96].

Understanding allosteric communication in SecA, the process by which the signals originated at one site of the protein is propagated reliably to affect distant functional sites will be important for ultimately understanding how SecA functions.

Chapter VI. Interaction of SecA with the extreme C-terminal tail of SecY

VI.1 Introduction

The interaction of SecA with the protein conducting channel SecYEG is very crucial for the initiation of protein translocation [132]. This interaction induces conformational changes to both SecA and SecY that result in the activation of SecA ATPase activity [68, 127, 131, 132] and opening of the channel [21] by weakening the interactions of the plug with the center of the channel [19, 52, 245].

As we extensively discussed in paragraph *I.4.4.4*, the main contacts between SecA and SecY are mediated by the cytosolic loops C4, C5 and C6 of SecY that protrude out of the membrane bilayer (Figure 6.72ab) [21, 48, 54-58].

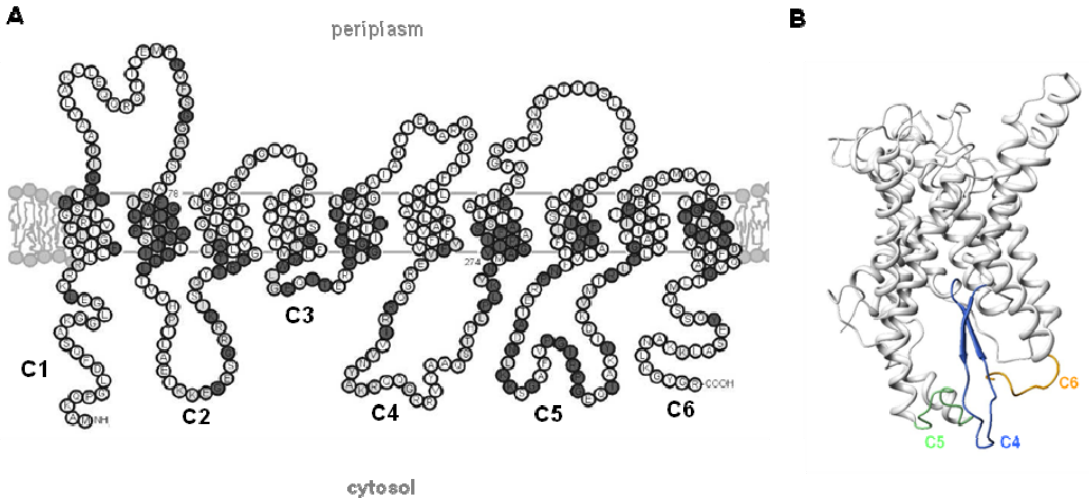

Figure 6.72: (a) Schematic overview of the topology and conservation of integral membrane protein SecY. The amino acid residues of SecY are displayed to indicate cytoplasmic (C1–C6), transmembrane, and periplasmic regions [192] (b) SecY structure from *M. jannaschii*. The cytoplasmic loops C4, C5 and C6 are highlighted to illustrate the docking site for the cytoplasmic partners.

In the crystal structure of the SecA – SecY complex, the last eight amino acids of the SecY extreme C terminus are unresolved (424 - 431 residues in *T. maritima* numbering) (Figure 1.18) [57]. One the other hand, the importance of this amino acid stretch has demonstrated by biochemical and genetic studies. Mutations or truncations in this region have a severe effect on or even abolish protein translocation [140, 141].

We have used NMR to elucidate the interaction of SecA with the extreme C-tail of SecY and provide a better understanding of its role in the protein translocation process.

VI.2 Results

VI.2.1 SecA interacts specifically with the extreme C terminus of SecY

To study the interaction of *E. coli* SecA with the extreme C terminus of *E. coli* SecY we use a synthetic peptide composed of the last 23 amino acids of SecY (hereafter C6 peptide) (Figure 6.73a). First, ITC was used to characterize the binding of C6 with SecA (Figure 6.73b).

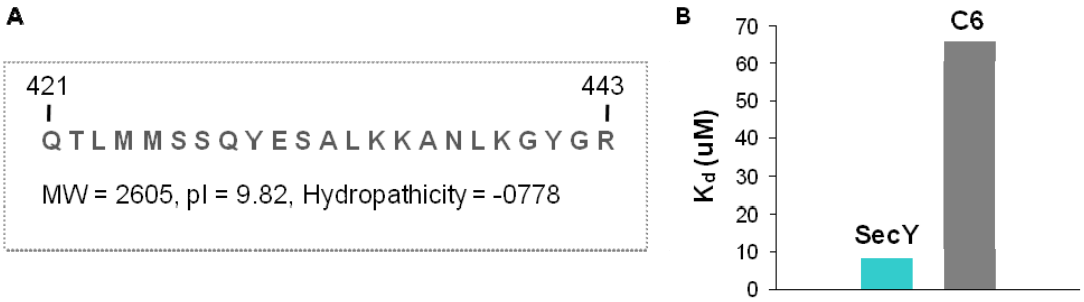

Figure 6.73: (a) The synthetic peptide C6 used accompanied by its basic physicochemical properties (b) Dissociation constant (K_d) for the interaction of SecA with intact SecY (green bar) and C_6 peptide (grey bar), at 8 °C, measured by ITC.

The affinity of the C6 for SecA is low (~ 66 μM) compared to the affinity of SecA for the full-length SecY (~ 4-5 nM) [132]. Apparently, the high affinity of SecA for SecY results from the multitude of interactions between SecA and SecY. As mentioned in section *I.1.4.4.* there are three cytoplasmic loops of SecY, (C4, C5 and C6), involved in this interaction. Moreover, the channel is formed from two SecY copies that both interact with SecA [57, 65, 93].

To further characterize the interaction between SecA and the SecY C6 peptide we used NMR. SecA labeled with Ile-δ_1 $^{13}CH_3$ was titrated with C6 peptide (Figure 6.74). The spectrum suggests a specific, localized interaction between the two partners since only few SecA resonances shift upon C6 binding while some of them experiencing line broadening. Notably, chemical shift perturbation shows that C6 peptide has two binding sites on SecA (Figure 6.74a). One is located at the motor domain and includes IRA2 residues. The second site involves residues from the C domain and PBD. The second site is in full agreement with the interaction between SecA and SecY seen in the crystal structure.

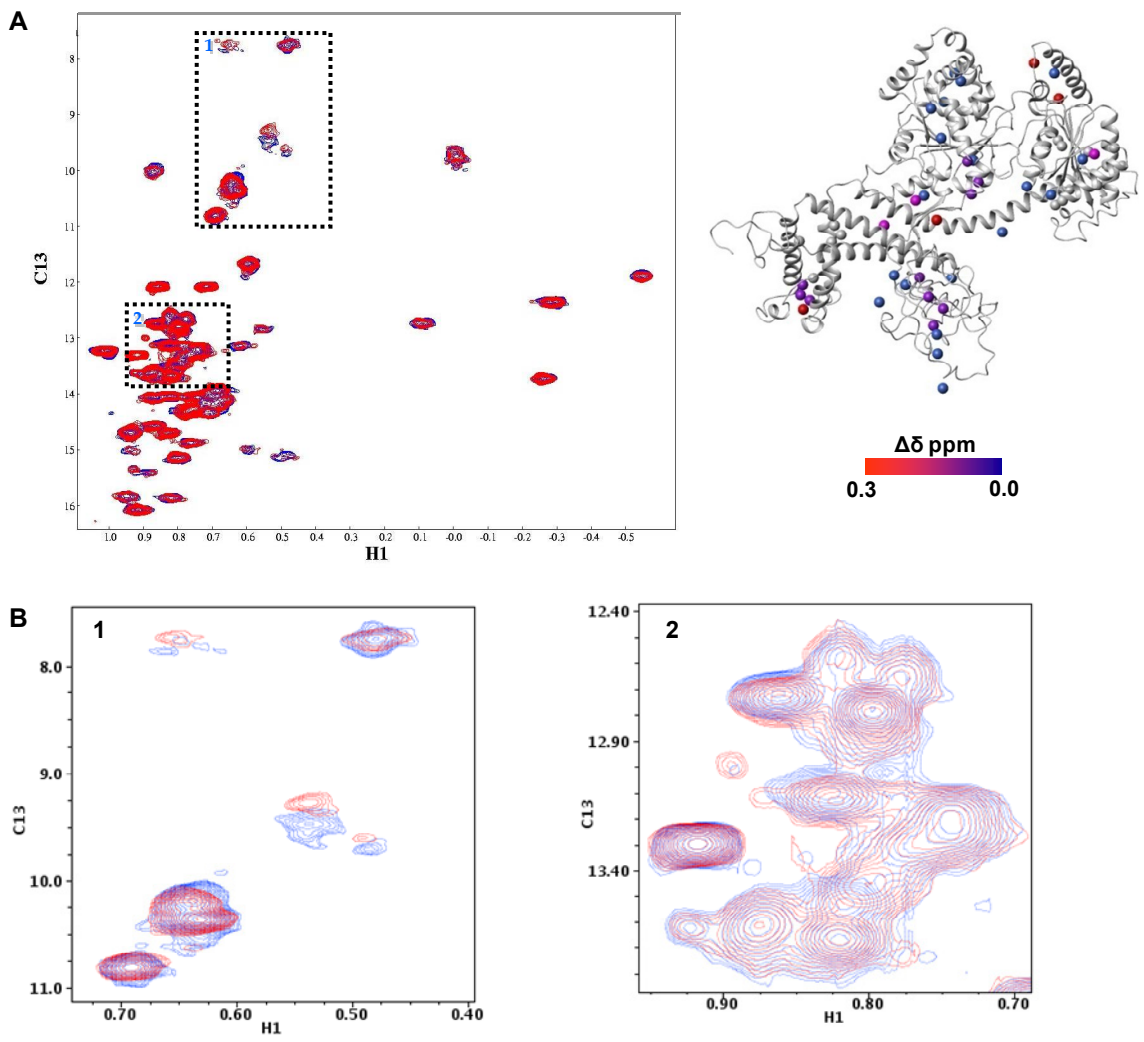

Figure 6.74: (a) Overlaid ^{1}H-^{13}C HMQC spectra of Ile-δ_1-SecA unliganded (blue) and bound to C6 peptide (red). Ile residues that are affected upon the interaction are colored mapped onto SecA structure (b) Excerpts of the overlaid ^{1}H-^{13}C HMQC spectra shown in (a), assignment of SecA residues is indicated.

VI.2.2 Differential broadening revealed the interaction site on C6 peptide

Biochemical and genetic studies [133, 137, 140, 141, 246] suggested that Y429 and the amino acid stretch ^{433}LKKANL^{438} are crucial for the interaction of SecY with SecA as point mutations or truncation in this region abolish the binding and interfere with protein translocation.

To gain more insight into the C6 recognition by SecA, we measured diferential line-broadening of the C6-peptide resonances upon interaction with SecA. This experiment is suitable for studying weak interacions of small ligands with proteins in the fast exchange regime (Figure 6.76). Upon binding of a rapidly tumbling peptide to a large protein that rotates slowly (the corelation time of the dimeric SecA is ~100ns) the transverse relaxation rate R_2 of the small peptide significantly increases. This is manifested in the spectrum of the peptide, where in resonances, characteristic of fast tumbling molecules, in the prssence of the large protein [152]. In the fast exchange regime, the chemical shift is similar both for the free and the bound states and the NMR signal is very sensitive to the relaxation rate of the bound state [247].

The interaction of SecA with the C6 is weak (K_d = 66 μM) as determined by ITC (Figure 6.73) and is a fast process as juged by NMR (Figure 6.74). To proceed with the differential-line broadening experiment, first, sequencial assiggnment of C6 peptide was sucsesfully completed by using standard 2D experiments (^{1}H-^{1}H-TOCSY, ^{1}H-^{1}H-NOESY and ^{13}C-HSQC) (Figure 6.75) . The recorded specta showed that the C6 is unstructured in solution and its conformation does not appear to change appreciably when bound to SecA.

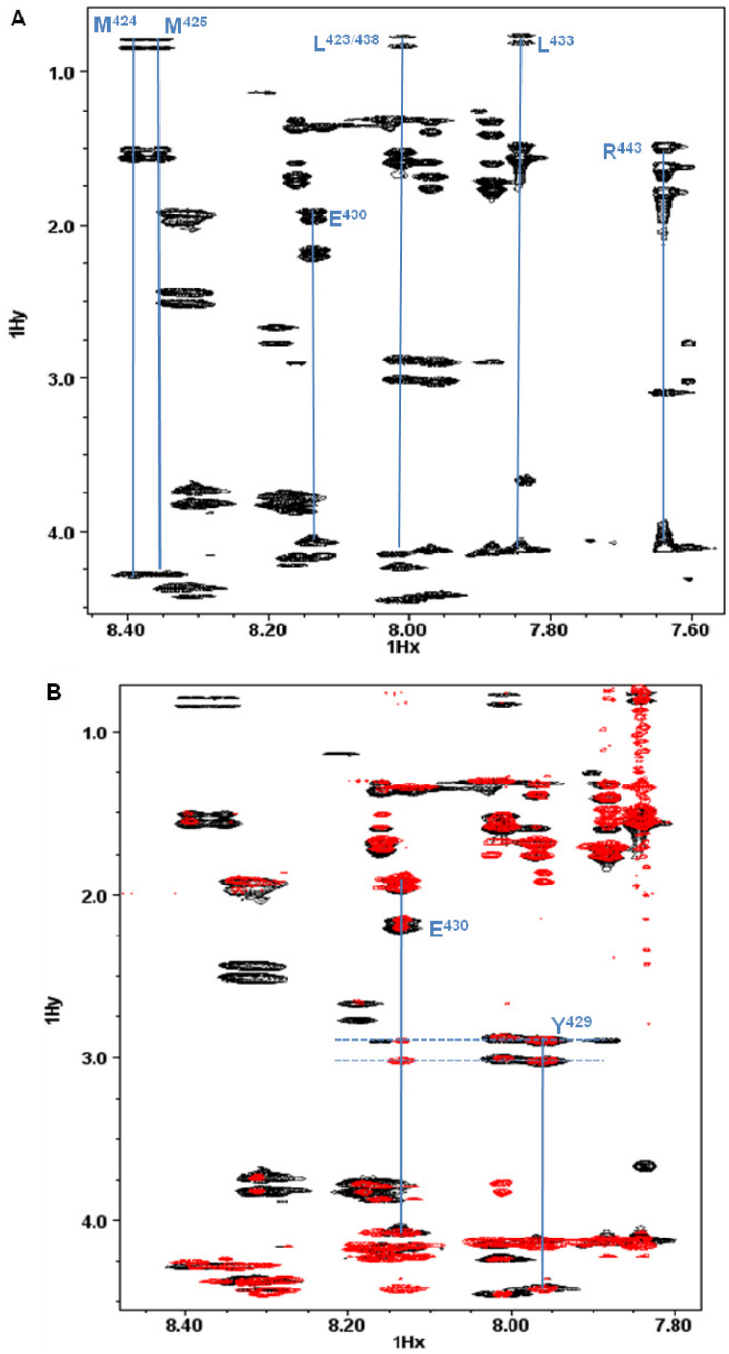

Figure 6.75: Assignment of the C6 peptide (a) ^{1}H-^{1}H TOCSY (black) spectrum with mixing time 70 ms used to identify individual spin systems (b) Overlaid ^{1}H-^{1}H TOCSY (black) and ^{1}H-^{1}H NOESY (red) with mixing time 100 ms used to perform the sequential assignment. Spectra recorded at 900 MHz instrument at 25 ^{o}C. Indicative assignment is provided.

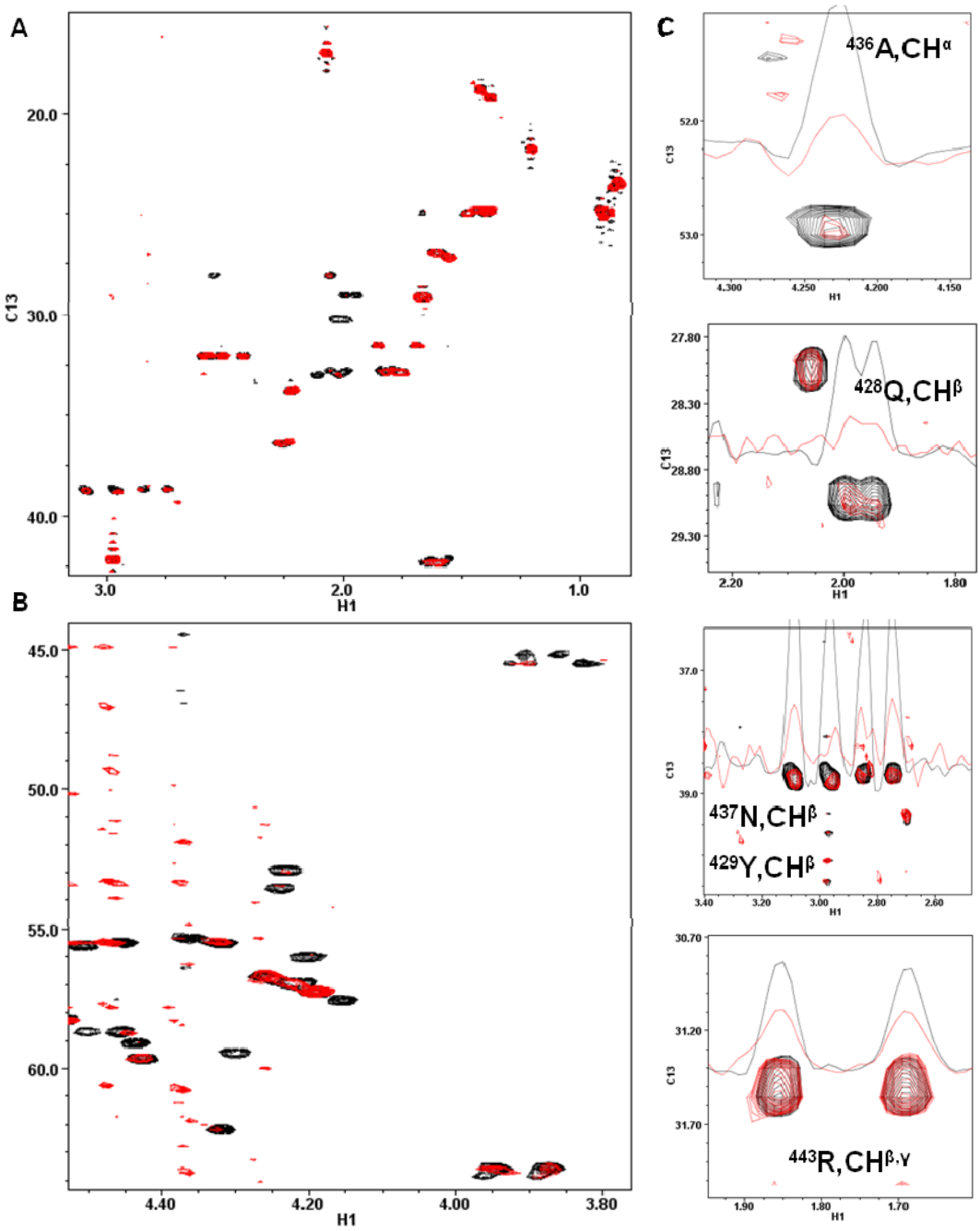

Figure 6.76: (a) and (b) overlaid ^{1}H-^{13}C HSQC spectra of C6 peptide free (black) and after addition of SecA (red) at a ratio 20:1. Column (c) illustrates selected excerpts of ^{1}H-^{13}C HSQC spectra showing residues that severely affected by the presence of SecA (A436, Q428, Y429 and N437) and residues, such as R443, that are not affected.

Diferential-line broadening was performed with C6 at a concentration of 1.5 mM and by titrating increased amounts of unlabeled SecA to yield ratios of 20:1 and 15:1 for C6 peptide/SecA. The effect was followed by observing the effect of unbound C6 by recording ^{1}H- ^{13}C-HSQC spectra (Figure 6.76). Our data indicate that the residues with the greater resonance broadening, such as Q428, Y429 interact with SecA whereas the ones experience less broadenning, such as R443, do not form a direct contact with SecA. By using this methodology, we identified two amino-acid stretches on C6 that appear to make direct contacts with SecA (Figure 6.77). These results are in agreement with previous genetic and biochemical studies [133, 137, 140, 141, 246]. However, our results provide more specific information and demonstrate that additional C6 residues contact SecA.

421- Q T L M M S S Q Y E S A L K K A N L K G Y G R - 443

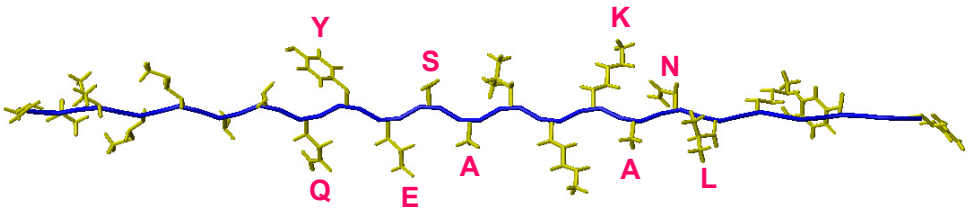

Figure 6.77: Schematic representation of C6 peptide. Red-colored residues amino-acids are residues mainly affected upon addition of SecA.

VI.3 Discussion

SecA interacts specifically with SecY and this interaction is essential for protein translocation [19, 21, 52, 68, 127, 131, 132, 245]. Here, we found that the extreme C-terminus of SecY contacts both the motor and the C-domain of SecA. Furthermore, we

identified important residues from the cytosolic loop C6 of SecY that mediate this interaction. The functional pore is formed from two SecY copies with one copy forming the translocation pore and the other copy providing constitutive contacts for SecA [65]. Moreover, the dimensions of SecA are consistent with the proposal that one SecA molecule interacts with two SecY complexes [92, 248]. According to these observations, our results can be explained using the model proposed for the dimeric pore (Figure 6.78).

The interaction sites for SecA are likely different for the two SecY copies. The crystal structure of SecA-SecY most likely represents the interaction of SecA with the translocating copy of the channel [57]. In this structure, the part of C6 loop that has been resolved approaches the WD domain whereas the C4 and C5 loops are in contact with the PBD and IRA1 (Figure 1.18). Our chemical shift perturbation results show that C6 peptide affects also the WD domain.

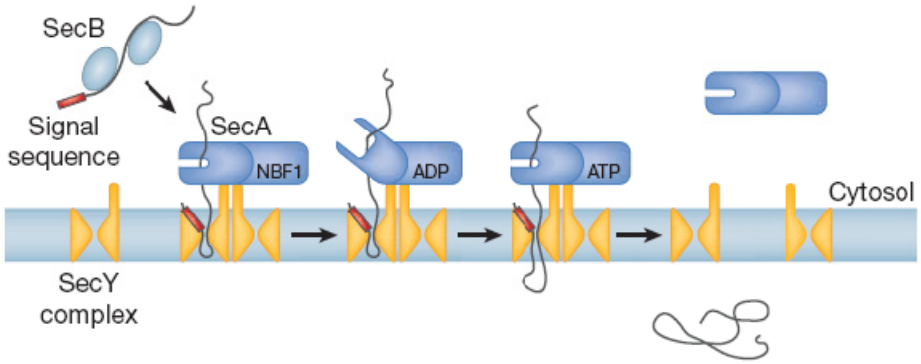

Figure 6.78: The translocation pore is formed by two copies: one serves as a SecA-docking site and the other functions as a translocation pore. Both the motor and the C domain of SecA the contact SecY channel. The orientation of SecY protomers is shown arbitrarily [10].

It would be of great importance to gain more detail insight in the interaction of SecA with the non-translocating copy. A crystal structure of SecY complexed with an anti-SecY Fib C fragment was proposed to represent the interaction of SecA with the non-translocating SecY copy [93]. In this structure, the main contacts between SecY and Fib are mediated by the C4 and C5 loops and most likely this interaction is involved in the ATPase activation of SecA [133]. It is noteworthy that the C6 loop is not resolved in this structure and that the motor has been replaced by an antibody. Thus, whether Fib antibody faithfully mimics SecA or what is the role of C6 loop in this interaction remains unknown.

Our data suggest that the C6 loop approaches SecA not only in its WD domain but also in its motor domain. This is in agreement with a previous study showing that SecA contacts the non-translocating copy via NBD (NBF1 in Figure 6.78) [65]. Here, we show that the C6 loop mainly affects residues from IRA2 domain. We suggest that most likely the whole motor is in close contact with the non-translocating copy of SecY with the C4 and C5 loops contacting NBD and the C6 loop the IRA2 d0main.

Differential-line broadening shows that C6 loop contacts SecA through two major amino acid stretches (Figure 6.76). One includes amino acids in the vicinity of Y429, 428QYESA432, which is highly conserved (Figure 6.79) and has been reported to be important for protein translocation. The second interacting amino acid stretch is located close to the end of C6 loop and includes the residues 435KNAL438. Interestingly, this region is not resolved in the SecA-SecY complex structure and includes highly conserved residues.

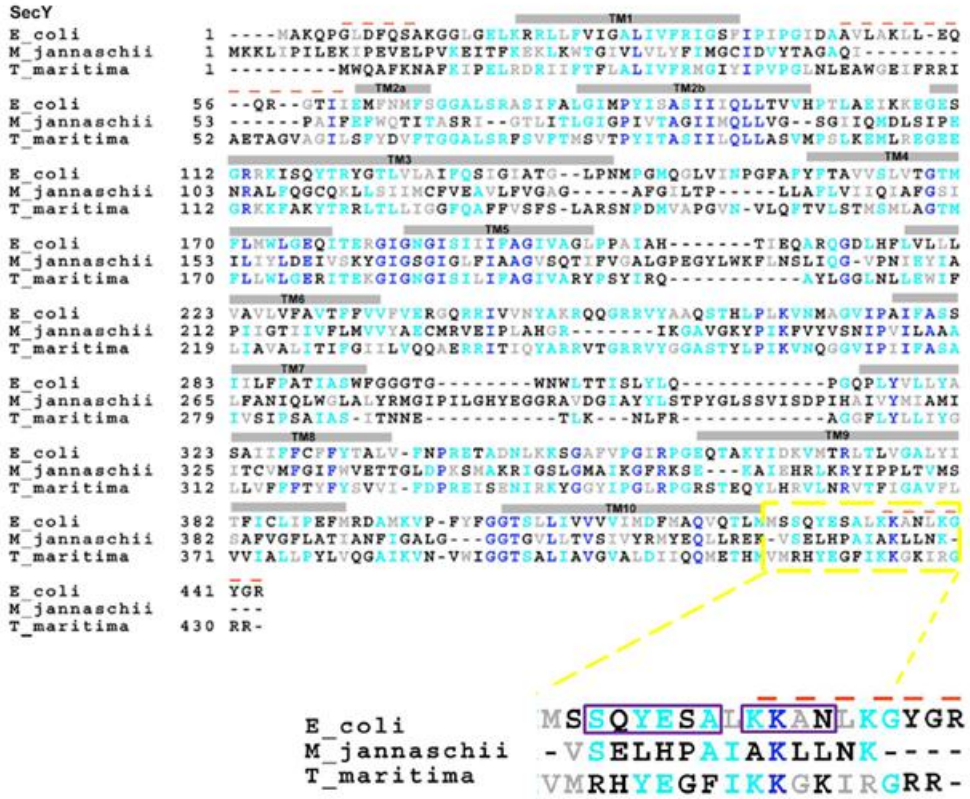

Figure 6.79: Sequence alignment of the SecYs from *E. coli, M. jannaschii and T. maritima*. TM-helices are indicated by gray bars, and regions not modeled in the SecY-SecA crystal structure are indicated by red dashed lines. Lower panel illustrates the last 20 aminoacids of SecY. Purple boxes indicate the residues that we identified from differential-line broadening to be in contact with SecA [57].

Clearly, more studies are needed to characterize and assess the importance of the interaction of the C6 loop with SecA. Ideally, a structure composed of both SecY copies and the motor SecA would provide valuable insight into the interaction of the translocation channel with its cognate receptor SecA. However, our results in combination with the existing structural and biochemical data show that SecA may interact with both SecY copies that assemble the translocation pore with extreme C terminal tail of SecY (C6) playing an important role in this association.

Chapter VII. Materials and methods

VII.1 Protein expression

His-tagged *E. coli* SecA, SecAΔC, SecAΔC-ΔIRA2 and isolated PBD and IRA2 domains were constructed as described previously (Table 1) [97, 105].

The BL21(DE3) or BL21(DE3)/ply's strain containing the selected protein-coding plasmid were grown overnight on Luria Broth (LB)- agar plate supplemented with the appropriate antibiotics (ampicilin,100 go/ml and/or chloroamphenicol, 25μg/ml). The following day, a 5 ml LB/antibiotics liquid culture was inoculated with a single colony and grown for 6 h in a shaking incubator. The 5ml culture was transferred in 100ml LB or minimal medium (Table 3) in the presence of the appropriate antibiotic and grown overnight in a shaking incubator. The next day the cell culture was transferred in 1 lt culture media and grown up to the desired Optical Density (O.D.), measured at 600 nm. For the induction of plasmid encoded genes under control of an IPTG inducible promoter, exponentially growing cultures were supplemented with IPTG (isopropyl β-D-1-thiogalactopyranoside) at the appropriate concentration.

Cultures for full-length SecA and its mutants were grown at 30 ^{o}C and protein synthesis was induced at the same temperature by addition of 0.5 mM of IPTG at A_{600} OD~0.4 and the cultures were allowed to grow for 3-5h. Cells were harvested at A_{600} OD~0.75. Isolated IRA2, PBD and SecAΔC-ΔIRA2 were produced by growing their cultures at 30 ^{o}C to an A600 OD~0.3. At that point, the temperature was decreased to 22 ^{o}C and IPTG was added 1 h later. SecAΔC was produced similarly, but IPTG was added at 16 ^{o}C and the culture was allowed to grow for 2 h before harvesting. Cells were re-

suspended in 50 mM Tris.HCl (pH 8.0), 1M NaCl, 10% glycerol, 2 mM PMSF, 5 mM imidazole, 10 mM β-mercaptoethanol.

For sequential assignment and NMR studies SecAΔC, SecAΔC-ΔIRA2, IRA2, and PBD were prepared as ^{15}N-, ^{13}C, -labeled samples using minimal media (Table 3) containing a combination of $^{15}NH_4Cl$ and $^{1}H_7$-$^{13}C_6$-glucose (2 g l^{-1}) in H_2O.

For isotope labeling of intact SecA, minimal media containing $^{15}NH_4Cl$ and [^{2}H,^{12}C] or [^{2}H,^{13}C]-glucose in 99.9% $^{2}H_2O$ were used. For the production of U-[^{2}H], Ile-δ_1-[$^{13}CH_3$] samples, 50 mg l^{-1} of alpha-ketobutyric acid (methyl - $^{13}CH_3$) were added to the culture 1 hr prior to addition of IPTG. Alpha-ketobutyric acid is commercially available in the protonated form at position 3. To achieve deuteration in this position, 50 mg of alpha-ketobutyric acid (methyl - $^{13}CH_3$) were dissolved in 16 ml $^{2}H_2O$. The pH corrected at 10.5 with ^{2}HCl or $NaO^{2}H$ and the solution incubated at 45 ^{o}C for 24 h prior to use.

Table 3: Composition of Minimal Media used for isotopic labeling

Minimal Media	Concentration
Na_2HPO_4	5.8 g l^{-1}
KH_2PO_4	3.0 g l^{-1}
NaCl	0.5 g l^{-1}
NH_4Cl	1.0 g l^{-1}
$MgSO_4$	1 mM
$CaCl_2$	1 μM

VII.2 Protein purification

Cells were disrupted with sonication (Misonix 3000) and the cytosolic fraction was separated from the membrane fraction by centrifugation at 50.000 x g. Purification for all proteins was performed in three steps. First, the lysate was loaded on a nickel-nitrilotriacetic acid agarose resin (Amersham), pre-equilibrated with 50 mM Tris-HCl (pH 8.0), 1 M NaCl, 10% (v/v) glycerol, 10 mM β-mercaptoethanol and 10 mM imidazole. The protein was eluted with the loading buffer, containing 50–450 mM imidazole. Next, the sample was loaded, after dialysis, on a Mono-Q ion exchange column (Amersham) and the protein was eluted with a 0–2 M NaCl linear gradient.

For the final purification step, the sample was dialyzed against gel filtration buffer (50 mM Tris·HCl, pH 8.0, 400 mM NaCl, 10% glycerol and 10 mM β-mercaptoethanol). After dialysis the sample was concentrated and applied to a Superdex-200 size exclusion column (Amersham) equilibrated in the same buffer.

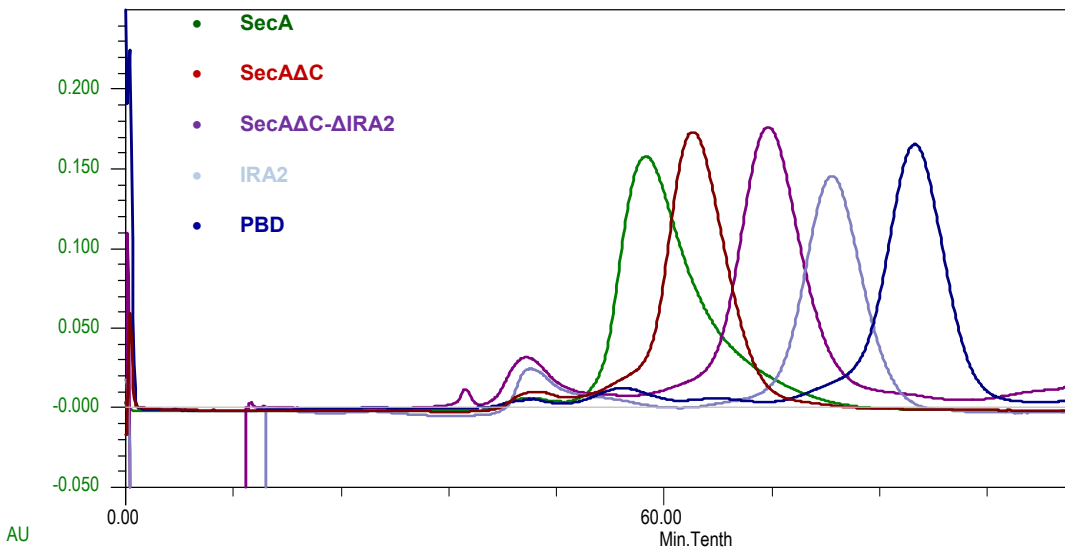

Figure 7.80: Size exclusion chromatography profiles for the proteins used in this study. Separation is based on the molecular weight (see Table 4).

Gel filtration confirmed the dimeric state of full-length SecA and the monomeric state of SecAΔC (Figure 7.80). The latter behaved as a monomer even at concentrations as high as 0.8 mM. Buffer exchange was performed in between the steps using Amicon Ultra-4 and -15 centrifugal units at 4 ^{o}C. The buffers used were filtrated using membrane filters (pore size 0.45 μm) and thoroughly degassed for 15 min by passing Helium. All purification steps were performed at 4 ^{o}C.

The expression and the purity throughout the different purification steps of constructs were assessed with SDS-Page (Figure 7.81). Protein concentration was determined spectrophotometrically (Beckman DU800) using the corresponding molecular extinction coefficient M^{-1} cm^{-1} (Table 4) at 280 nm.

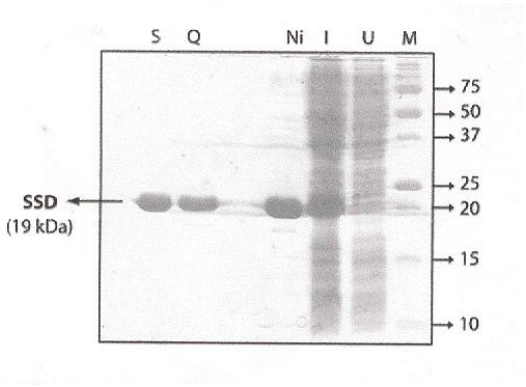

Figure 7.81: SDS-PAGE of PBD expression (BL21(DE3)/pLysS strain) and purification. M: molecular weight marker (size is indicated in kDa), U: before IPTG, I: after IPTG, after purification on Ni: Ni-NTA column, Q: ion-exchange Mono-Q, S: superdex column. SDS-PAGE was stained with Coumassie Blue.

Table 4: SecA constructs and mutants used in the current study along with their basic physicochemical properties

	MW (kDa)	Number of aa	pI	Extinction coefficient ($M^{-1}cm^{-1}$, 280nm)
SecA (1-901)	102.000	901	5.43	75750
SecAR509K	101.995	901	5.43	75750
SecAR574K	101.995	901	5.43	75750
SecAD649A	101.979	901	5.46	75750
SecAD649A-R642A	101.894	901	5.43	75750
SecAD649A-R642A-W775A	101.779	901	5.43	70500
SecAΔC (1-610)	68.275	610	5.621	40340
C34 (610-901)	33.765	291	5.17	35410
SecAΔC/ΔIRA2 (1-420)	47.559	420	5.41	24870
IRA2 (420-610)	20.891	191	6.60	15470
PBD (219-376)	17.734	157	513	9970

VII.3 NMR spectroscopy

NMR experiments were performed on Varian 600- and 800- MHz and Bruker 900 MHz spectrometers. Sequential assignment of the ^{1}H, ^{13}C and ^{15}N protein backbone chemical shifts was achieved by means of through-bond heteronuclear scalar correlations using the following 3D pulse sequences:

- HNCO, HN(CA)CO
- HNCA, HN(CO)CA
- HNCACB and HN(CO) CACB.

Side chain assignment was performed using 3D C(CO)NH and 3D H(CCO)NH spectra. NOEs were assigned and collected on the basis of 3D ^{15}N NOESY HSQC and ^{13}C NOESY HSQC spectra.

All NMR samples in chapter III were prepared in 50 mM KCl, 50 mM potassium phosphate, 1 mM DDT and 1 g l^{-1} NaN_3 (pH 7.5). Concentrations were 0.5 mM for full-length SecA, 0.8 mM for SecAΔC, 0.5 mM for IRA2, 0.7 mM for PBD and 0.15 mM for SecAΔC-ΔIRA2. All spectra were recorded at 22 ^{o}C.

The spectra of C6 peptide were recorded in 25 mM KCl, 25 mM potassium phosphate, 1 mM DDT and 1 g l^{-1} NaN_3 (pH 7.5) at 25 ^{o}C. The concentration of C6 peptide was 1.5 mM. TOCSY experiment was recorded using mixing time 70 ms while for NOESY experiment the mixing time was 100 ms. Titration of C6 peptide to SecA Ile-δ_1 [$^{13}CH_3$] was performed at the same conditions. The differential-line broadening was performed my recording ^{1}H-^{13}C HSQC for the free peptide and after adding SecA in a ratio C6peptide/SecA: 20/1 or 15/1.

The combined chemical shift change of a particular residue upon ligand binding was calculated as

$$\Delta\delta = [(\omega_{HN}\Delta\delta_{HN})^2 + (\omega_N\Delta\delta_N)^2]^{1/2} \text{ in ppm,}$$

where ω_i denotes the weight factor of nucleus i, $\omega_{HN} = 1$, $\omega_N = 0.154$ [182].

Methyl chemical shift changes upon ligand binding was calculated as

$$\Delta\delta = [(\Delta\delta_H)^2 + (\Delta\delta_C)^2]^{1/2}, \text{ in hertz [249]}$$

Spin relaxation measurements. The heteronuclear cross-relaxation ^{1}H-^{15}N NOE data were obtained by recording interleaving pulse sequences with and without proton saturation. One spectrum was recorded with a 3 sec recycle delay followed by 3 sec

saturation and another spectrum with no saturation and a 6 sec recycle delay. The heteronuclear ^{1}H-^{15}N NOE was determined from the ratio of peak heights for experiments with and without ^{1}H-saturation pulses.

All spectra were processed using the NMRPipe software package and analyzed with NMRView.

VII.4 Isothermal titration calorimetry

ITC was used to measure ΔH, ΔS and ΔG changes of nucleotide, signal peptide and C6 peptide binding to SecA and its functional derivatives (Figure 7.82). The reaction stoichiometry, dissociation constant, K_d, and ΔH are directly measured in a single ITC experiment, whereas ΔG and ΔS are calculated from standard thermodynamic equations (1.2, 1.3). The ΔC_p of the reaction was determined from the temperature dependence of enthalpy change (equation 1.5).

At least two independent measurements of the reaction were made at lower temperatures and four or five for the reactions at higher temperatures. All experiments were performed on a VP-ITC microcalorimeter (MicroCal).

For ITC experiments with different nucleotides (Sigma-Aldrich), protein samples were extensively dialyzed against ITC buffer, typically containing 50 mM Tris- HCl (pH 7.5), 50 mM KCl (or 500 mM KCl for experiments in high salt), 5 mM $MgCl_2$ and 1 mM TCEP. The heat of binding in the Tris buffer was very similar to that observed in potassium phosphate, indicating a weak coupling of binding to changes in protonation [228] of the protein, the ligand or both. Nucleotide solutions were prepared in the flow-through of the last buffer exchange and their concentration was determined

spectrophotometrically using a molecular extinction coefficient of 14,650 M^{-1} cm^{-1} at 259 nm.

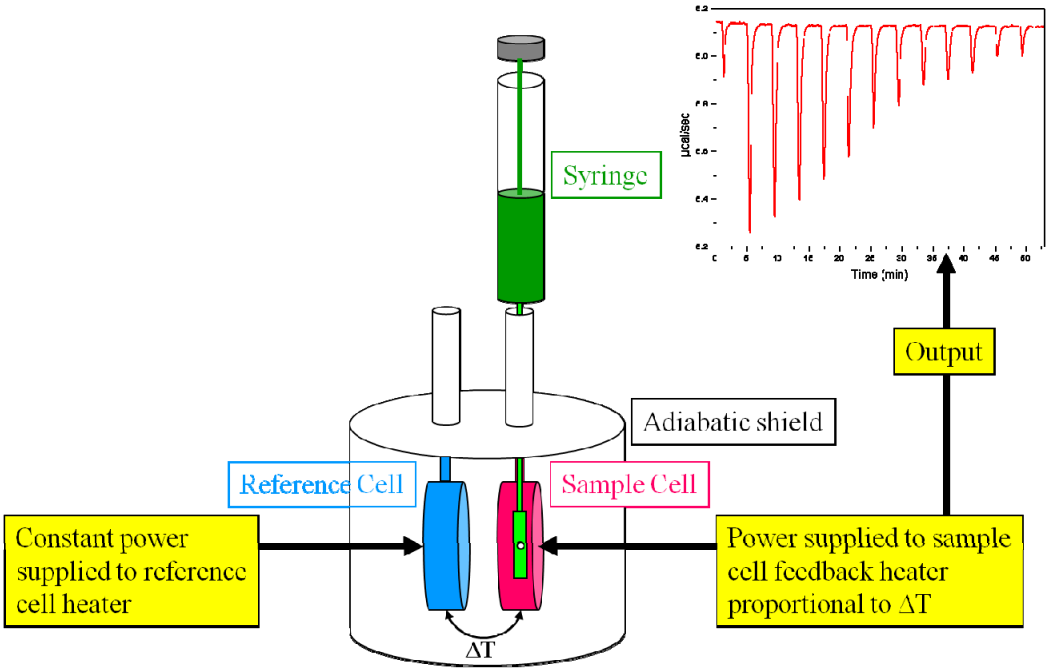

Figure 7.82: Schematic representation of an Isothermal Titration Calorimeter. In ITC, a syringe containing a "ligand" solution is titrated into a cell containing a solution of the "macromolecule" at constant temperature. When ligand is injected into the cell, the two materials interact, and heat is released or absorbed in direct proportion to the amount of binding. As the macromolecule in the cell becomes saturated with ligand, the heat signal diminishes until only background heat of dilution is observed.

Calorimetric titrations of the LamB signal peptide (MMITLRKRRKLPLAVA) with SecA-D649A were performed in buffer containing 20 mM KP_i (pH 7.5), 20 mM KCl, and 1 mM TCEP. SecA-D649A concentration was in the range of 50 μM and the ligand solution was prepared by dissolving peptide in the flow through of the last buffer

exchange in the desired concentration. We use the KRR- modified version of LamB porin signal peptide. The KRR-LamB peptide was chemically synthesized by GeneScript (Piscataway, NJ).

ITC experiments with C6 peptide were performed in buffer containing 25 mM KP_i (pH 7.5), 25 mM KCl, and 1 mM TCEP. SecA concentration was in the range of 100 μM and the ligand solution was prepared by dissolving peptide in the flow through of the last buffer exchange. The concentration of C6 peptide was determined spectrophotometrically at 280 nm using the molecular extinction coefficient of 2980 M^{-1} cm^{-1}. The C6 peptide was chemically synthesized by GeneScript (Piscataway, NJ).

All solutions were filtered using membrane filters (pore size 0.45 μm) and thoroughly degassed for 15 min by gentle stirring under vacuum. In a typical experiment (e.g. nucleotide titration to SecA), the 1.35 ml sample cell was filled with a 10 - 40 μM solution of protein and the 250-μl injection syringe with 100 - 400 μM of the titrating nucleotide. Each titration typically consisted of a preliminary 2-μl injection followed by 25 subsequent 10 μl injections. Data for the preliminary injection, which are affected by diffusion of the solution from and into the injection syringe during the initial equilibration period, were discarded. The heat effects which are not directly related to the binding reaction, such as dilution of the injectant and viscous mixing, was corrected by a control titration of the injectant into the experimental buffer. Data were analyzed using the ITC version of Origin 5.0 with embedded calorimetric routines.

VII.5 Construction of SecA mutants

We generated point mutations in SecA by using the site direct mutagenesis methodology (Stratagene, QuikChange site-directed mutagenesis):

(1) A temperature cycler for the polymerase chain reaction (PCR, Eppendorf),

(2) *PfuTurbo* DNA polymerase (2.5 U/µl) (Stratagene),

(3) Plasmid vector bearing the wild-type SecA gene (50 ng / reaction). The plasmid was isolated using a plasmid isolation/purification kit (Qiagen)

(4) Two synthetic complimentary oligonucleotide primers (forward and reversed) containing the desired mutation (125 ng each primer / reaction).

We constructed the following mutants by using the corresponding primer pairs:

- **His-SecA-D649A-W775A**

  F: 5' GCAAACGCTTGACTCCCTG**GCC**AAAGAGCACCTGGCAGCGATG 3'

  R: 5' TCGCTGCCAGGTGCTCTTTG**GCC**AGGGAGTCAAGCGTTTGCAG 3'

- **His-SecA-D649A-W775A-R642A**

  F: 5' GTAACTTCGACATTCGTA**GCC**AACTGCTGGAATATGATG 3'

  R: 5' CATCATATTCCAGCAGTT**GGC**TACGAATGTCGAAGTTAC 3'

- **His-SecA-I304L**

  F: 5' GCAAACGCTTGACTCCCTG**GCC**AAAGAGCACCTGGCAGCGATG 3'

  R: 5' TCGCTGCCAGGTGCTCTTTG**GCC**AGGGAGTCAAGCGTTTGCAG 3'

- **His-SecA-I513L**

  F: 5' GGTCGTGGTACAGAT**CTG**GTGCTCGGTGGTAG 3'

  R: 5' CTACCACCGAGCAC**CAG**ATCTGTACCACGACC 3'

Upon completion of the temperature cycling the reaction mixture was treated with *Dpn* I to digest the parental DNA template (wt-SecA plasmid) that is dam methylated in almost all *E. coli* strains and to select for mutation-containing synthesized DNA. The plasmid containing the desired mutation was transformed to BL21(DE3) cells. Selected colonies were tested in the ability to produce the desired protein and finally, all point mutations verified with DNA sequencing.

VII.6 Biochemical assays

SecA ATPase activity measurements were carried out in buffer consisting of 50mM Tris-Cl, pH:8.0, 50mM KCl, 5mM $MgCl_2$, 1mM DTT, with 1mg/ml BSA, supplemented with 1mM ATP and released Pi was detected using malachite green [68, 105]. For membrane ATPase SecYEG-proteoliposomes (0.2 µg membrane protein/ml) were added. For translocation ATPase, proOmpA (stored at 6M urea, 50mM TrisCl, pH 8.0) was freshly diluted (0.03 mg/ml) into the reaction. *In vitro* translocation of proOmpA labelled with [^{35}S]-methionine (1000 Ci/mmol; Amersham) into reconstituted SecYEG-proteoliposomes were carried out in buffer B as previously described [105]. Reactions were stopped by chilling on ice and untranslocated proOmpA was cleaved with proteinase K (1mg/ml; 15 min; 4 ^{o}C). Polypeptides were precipitated by TCA (15 % w/v; 4 ^{o}C) and analyzed by SDS-PAGE and phosphorimaging (Storm 840; Amersham).

VIII. Abbreviations

ADP: Adenosine Diphosphate

AMP-PNP: Adenosine 5'-(β, γ-imido)triphosphate (non hydrolysable analogue of ATP)

ASA: Accessible Surface Area

ATP: Adenosine Triphosphate

ATP-γ-S: Adenosine 5'-(γ-thio) triphosphate (non hydrolysable analogue of ATP)

B_0: Static magnetic field

cryo-EM: cryo-Electron Microscopy

CSA: Chemical Shift Anisotropy

CSI: Chemical Shift Index

CTD: C-Terminal Domain (also known as C-tail)

ΔC_p: Heat Capacity of binding

ΔG: Free Energy change

ΔH: enthalpy change

ΔS: Entropy change

DD: Dipole-Dipole

ER: Endoplasmic Reticulum

Ffh: 54 kDa Homologous to the subunit of eukaryotic SRP

FtsY: Signal Recognition Particle Receptor

GTP: Guanosine Triposphate

HetNOE: Heteronuclear ^{15}N-nuclear Overhouse effect

HSQC: Heteronuclear Single Quantum Coherence

IPTG: isopropyl β-D-1-thiogalactopyranoside

IRA1: Intramolecular Regulator of ATPase 2 (also known as HWD)

IRA2: Intramolecular Regulator of ATPase 2 (also known as NBF2)

ITC: Isothermal Titration Calorimetry

K_a : Association constant

K_d: Dissociation constant

LB: Luria Broth

NBD: Nucleotide Binding Domain (also known as NBF1)

NMR: Nuclear Magnetic Resonance

NS: Number of Scans

NTP: Nucleotide Triphospate

OD: Optical Density

PAGE: Polyacrylamide Gel Electrophoresis

PBD: Preprotein Binding Domain (also known as PPXD)

PDB: Protein Data Bank

P_i: Pyrophosphate

PMF: Proton Motive Force

R: the Universal gas constant

R_1: Longitudinal relaxation rate

R_2: Transverse relaxation rate

R_{ex}: Exchange Rate

RNC: Ribosome-Nascent Chain

SD: Scaffold Domain

SF2: Homologous to Superfamily 2

Sec: Secretory System/Protein

SecAΔC: C domain truncated SecA (residues 1-610 in *E. coli)*

SRP: Signal Recognition Particle

T: Absolute temperature

τ_c: Rotational correlation time

T_f: Temperature of folding transition

TAT: Twin Arginine Transport

TF: Trigger Factor

TMS: Transmembrane Segment

T_2: Transverse relaxation

TROSY: Transverse Relaxation Optimized Spectroscopy

WD: Wing Domain

IX. References

1. Schatz, G. and B. Dobberstein, *Common principles of protein translocation across membranes.* Science, 1996. **271**(5255): p. 1519-26.
2. Wickner, W. and R. Schekman, *Protein translocation across biological membranes.* Science, 2005. **310**(5753): p. 1452-6.
3. Driessen, A.J. and N. Nouwen, *Protein Translocation Across the Bacterial Cytoplasmic Membrane.* Annu Rev Biochem, 2007.
4. Papanikou, E., S. Karamanou, and A. Economou, *Bacterial protein secretion through the translocase nanomachine.* Nat Rev Microbiol, 2007. **5**(11): p. 839-51.
5. Alder, N.N. and S.M. Theg, *Energy use by biological protein transport pathways.* Trends Biochem Sci, 2003. **28**(8): p. 442-51.
6. Economou, A., et al., *Secretion by numbers: Protein traffic in prokaryotes.* Mol Microbiol, 2006. **62**(2): p. 308-19.
7. Sabatini, D.D., et al., *Ribosome-membrane interaction: Structural aspects and functional implications.* Adv Cytopharmacol, 1971. **1**: p. 119-29.
8. Blobel, G. and B. Dobberstein, *Transfer of proteins across membranes. I. Presence of proteolytically processed and unprocessed nascent immunoglobulin light chains on membrane-bound ribosomes of murine myeloma.* J Cell Biol, 1975. **67**(3): p. 835-51.
9. Brundage, L., et al., *The purified E. coli integral membrane protein SecY/E is sufficient for reconstitution of SecA-dependent precursor protein translocation.* Cell, 1990. **62**(4): p. 649-57.
10. Rapoport, T.A., *Protein translocation across the eukaryotic endoplasmic reticulum and bacterial plasma membranes.* Nature, 2007. **450**(7170): p. 663-9.
11. Wickner, W., A.J. Driessen, and F.U. Hartl, *The enzymology of protein translocation across the Escherichia coli plasma membrane.* Annu Rev Biochem, 1991. **60**: p. 101-24.
12. Hegde, R.S. and H.D. Bernstein, *The surprising complexity of signal sequences.* Trends Biochem Sci, 2006. **31**(10): p. 563-71.
13. von Heijne, G., *Signal sequences. The limits of variation.* J Mol Biol, 1985. **184**(1): p. 99-105.
14. Rapoport, T.A., *Transport of proteins across the endoplasmic reticulum membrane.* Science, 1992. **258**(5084): p. 931-6.
15. Gierasch, L.M., *Signal sequences.* Biochemistry, 1989. **28**(3): p. 923-30.
16. Randall, L.L. and S.J. Hardy, *SecB, one small chaperone in the complex milieu of the cell.* Cell Mol Life Sci, 2002. **59**(10): p. 1617-23.
17. Valent, Q.A., et al., *Early events in preprotein recognition in E. coli: interaction of SRP and trigger factor with nascent polypeptides.* Embo J, 1995. **14**(22): p. 5494-505.
18. Bruch, M.D., C.J. McKnight, and L.M. Gierasch, *Helix formation and stability in a signal sequence.* Biochemistry, 1989. **28**(21): p. 8554-61.
19. Plath, K., et al., *Signal sequence recognition in posttranslational protein transport across the yeast ER membrane.* Cell, 1998. **94**(6): p. 795-807.

20. Paetzel, M., et al., *Signal peptidases.* Chem Rev, 2002. **102**(12): p. 4549-80.
21. Mitra, K., J. Frank, and A. Driessen, *Co- and post-translational translocation through the protein-conducting channel: analogous mechanisms at work?* Nat Struct Mol Biol, 2006. **13**(11): p. 957-64.
22. Luirink, J. and I. Sinning, *SRP-mediated protein targeting: structure and function revisited.* Biochim Biophys Acta, 2004. **1694**(1-3): p. 17-35.
23. Osborne, A.R., T.A. Rapoport, and B. van den Berg, *Protein translocation by the Sec61/SecY channel.* Annu Rev Cell Dev Biol, 2005. **21**: p. 529-50.
24. Eisner, G., et al., *Ligand crowding at a nascent signal sequence.* J Cell Biol, 2003. **163**(1): p. 35-44.
25. Lee, H.C. and H.D. Bernstein, *The targeting pathway of Escherichia coli presecretory and integral membrane proteins is specified by the hydrophobicity of the targeting signal.* Proc Natl Acad Sci U S A, 2001. **98**(6): p. 3471-6.
26. Randall, L.L., et al., *Binding of SecB to ribosome-bound polypeptides has the same characteristics as binding to full-length, denatured proteins.* Proc Natl Acad Sci U S A, 1997. **94**(3): p. 802-7.
27. Randall, L.L., *Translocation of domains of nascent periplasmic proteins across the cytoplasmic membrane is independent of elongation.* Cell, 1983. **33**(1): p. 231-40.
28. Halic, M., et al., *Following the signal sequence from ribosomal tunnel exit to signal recognition particle.* Nature, 2006. **444**(7118): p. 507-11.
29. Rosendal, K.R., et al., *Crystal structure of the complete core of archaeal signal recognition particle and implications for interdomain communication.* Proc Natl Acad Sci U S A, 2003. **100**(25): p. 14701-6.
30. Schaffitzel, C., et al., *Structure of the E. coli signal recognition particle bound to a translating ribosome.* Nature, 2006. **444**(7118): p. 503-6.
31. Egea, P.F., et al., *Substrate twinning activates the signal recognition particle and its receptor.* Nature, 2004. **427**(6971): p. 215-21.
32. Poritz, M.A., et al., *An E. coli ribonucleoprotein containing 4.5S RNA resembles mammalian signal recognition particle.* Science, 1990. **250**(4984): p. 1111-7.
33. Bernstein, H.D., et al., *Functional substitution of the signal recognition particle 54-kDa subunit by its Escherichia coli homolog.* Proc Natl Acad Sci U S A, 1993. **90**(11): p. 5229-33.
34. Keenan, R.J., et al., *Crystal structure of the signal sequence binding subunit of the signal recognition particle.* Cell, 1998. **94**(2): p. 181-91.
35. Batey, R.T., et al., *Crystal structure of the ribonucleoprotein core of the signal recognition particle.* Science, 2000. **287**(5456): p. 1232-9.
36. Halic, M., et al., *Structure of the signal recognition particle interacting with the elongation-arrested ribosome.* Nature, 2004. **427**(6977): p. 808-14.
37. Ullers, R.S., et al., *SecB is a bona fide generalized chaperone in Escherichia coli.* Proc Natl Acad Sci U S A, 2004. **101**(20): p. 7583-8.
38. Bechtluft, P., et al., *Direct observation of chaperone-induced changes in a protein folding pathway.* Science, 2007. **318**(5855): p. 1458-61.
39. Zhou, J. and Z. Xu, *The structural view of bacterial translocation-specific chaperone SecB: implications for function.* Mol Microbiol, 2005. **58**(2): p. 349-57.

40. Dekker, C., B. de Kruijff, and P. Gros, *Crystal structure of SecB from Escherichia coli.* J Struct Biol, 2003. **144**(3): p. 313-9.
41. Xu, Z., J.D. Knafels, and K. Yoshino, *Crystal structure of the bacterial protein export chaperone secB.* Nat Struct Biol, 2000. **7**(12): p. 1172-7.
42. Knoblauch, N.T., et al., *Substrate specificity of the SecB chaperone.* J Biol Chem, 1999. **274**(48): p. 34219-25.
43. Randall, L.L., et al., *The interaction between the chaperone SecB and its ligands: evidence for multiple subsites for binding.* Protein Sci, 1998. **7**(11): p. 2384-90.
44. Randall, L.L., T.B. Topping, and S.J. Hardy, *No specific recognition of leader peptide by SecB, a chaperone involved in protein export.* Science, 1990. **248**(4957): p. 860-3.
45. Kimsey, H.H., M.D. Dagarag, and C.A. Kumamoto, *Diverse effects of mutation on the activity of the Escherichia coli export chaperone SecB.* J Biol Chem, 1995. **270**(39): p. 22831-5.
46. Flower, A.M., *The SecY translocation complex: convergence of genetics and structure.* Trends Microbiol, 2007. **15**(5): p. 203-10.
47. Pohlschroder, M., et al., *Protein translocation in the three domains of life: variations on a theme.* Cell, 1997. **91**(5): p. 563-6.
48. Mitra, K., et al., *Structure of the E. coli protein-conducting channel bound to a translating ribosome.* Nature, 2005. **438**(7066): p. 318-24.
49. Van den Berg, B., et al., *X-ray structure of a protein-conducting channel.* Nature, 2004. **427**(6969): p. 36-44.
50. Breyton, C., et al., *Three-dimensional structure of the bacterial protein-translocation complex SecYEG.* Nature, 2002. **418**(6898): p. 662-5.
51. Collinson, I., et al., *Projection structure and oligomeric properties of a bacterial core protein translocase.* Embo J, 2001. **20**(10): p. 2462-71.
52. Tam, P.C., et al., *Investigating the SecY plug movement at the SecYEG translocation channel.* Embo J, 2005. **24**(19): p. 3380-8.
53. Li, W., et al., *The plug domain of the SecY protein stabilizes the closed state of the translocation channel and maintains a membrane seal.* Mol Cell, 2007. **26**(4): p. 511-21.
54. Cheng, Z., et al., *Identification of cytoplasmic residues of Sec61p involved in ribosome binding and cotranslational translocation.* J Cell Biol, 2005. **168**(1): p. 67-77.
55. Raden, D., W. Song, and R. Gilmore, *Role of the cytoplasmic segments of Sec61alpha in the ribosome-binding and translocation-promoting activities of the Sec61 complex.* J Cell Biol, 2000. **150**(1): p. 53-64.
56. Menetret, J.F., et al., *Ribosome binding of a single copy of the SecY complex: implications for protein translocation.* Mol Cell, 2007. **28**(6): p. 1083-92.
57. Zimmer, J., Y. Nam, and T.A. Rapoport, *Structure of a complex of the ATPase SecA and the protein-translocation channel.* Nature, 2008. **455**(7215): p. 936-43.
58. Karamanou, S., et al., *Assembly of the translocase motor onto the preprotein-conducting channel.* Mol Microbiol, 2008. **70**(2): p. 311-22.
59. Tani, K., H. Tokuda, and S. Mizushima, *Translocation of ProOmpA possessing an intramolecular disulfide bridge into membrane vesicles of Escherichia coli. Effect of membrane energization.* J Biol Chem, 1990. **265**(28): p. 17341-7.

60. De Keyzer, J., C. Van Der Does, and A.J. Driessen, *Kinetic analysis of the translocation of fluorescent precursor proteins into Escherichia coli membrane vesicles.* J Biol Chem, 2002. **277**(48): p. 46059-65.
61. Duong, F. and W. Wickner, *Sec-dependent membrane protein biogenesis: SecYEG, preprotein hydrophobicity and translocation kinetics control the stop-transfer function.* Embo J, 1998. **17**(3): p. 696-705.
62. Cannon, K.S., et al., *Disulfide bridge formation between SecY and a translocating polypeptide localizes the translocation pore to the center of SecY.* J Cell Biol, 2005. **169**(2): p. 219-25.
63. Bessonneau, P., et al., *The SecYEG preprotein translocation channel is a conformationally dynamic and dimeric structure.* Embo J, 2002. **21**(5): p. 995-1003.
64. Scheuring, J., et al., *The oligomeric distribution of SecYEG is altered by SecA and translocation ligands.* J Mol Biol, 2005. **354**(2): p. 258-71.
65. Osborne, A.R. and T.A. Rapoport, *Protein translocation is mediated by oligomers of the SecY complex with one SecY copy forming the channel.* Cell, 2007. **129**(1): p. 97-110.
66. Tomkiewicz, D., N. Nouwen, and A.J. Driessen, *Pushing, pulling and trapping--modes of motor protein supported protein translocation.* FEBS Lett, 2007. **581**(15): p. 2820-8.
67. Driessen, A.J., E.H. Manting, and C. van der Does, *The structural basis of protein targeting and translocation in bacteria.* Nat Struct Biol, 2001. **8**(6): p. 492-8.
68. Lill, R., W. Dowhan, and W. Wickner, *The ATPase activity of SecA is regulated by acidic phospholipids, SecY, and the leader and mature domains of precursor proteins.* Cell, 1990. **60**(2): p. 271-80.
69. Miller, A., L. Wang, and D.A. Kendall, *SecB modulates the nucleotide-bound state of SecA and stimulates ATPase activity.* Biochemistry, 2002. **41**(16): p. 5325-32.
70. Schmidt, M.G. and D.B. Oliver, *SecA protein autogenously represses its own translation during normal protein secretion in Escherichia coli.* J Bacteriol, 1989. **171**(2): p. 643-9.
71. Rajapandi, T. and D. Oliver, *Integration of SecA protein into the Escherichia coli inner membrane is regulated by its amino-terminal ATP-binding domain.* Mol Microbiol, 1996. **20**(1): p. 43-51.
72. denBlaauwen, T., et al., *Domain interactions of the peripheral preprotein translocase subunit SecA.* Biochemistry, 1996. **35**(37): p. 11994-12004.
73. Hunt, J.F., et al., *Nucleotide control of interdomain interactions in the conformational reaction cycle of SecA.* Science, 2002. **297**(5589): p. 2018-26.
74. Osborne, A.R., W.M. Clemons, Jr., and T.A. Rapoport, *A large conformational change of the translocation ATPase SecA.* Proc Natl Acad Sci U S A, 2004. **101**(30): p. 10937-42.
75. Or, E., A. Navon, and T. Rapoport, *Dissociation of the dimeric SecA ATPase during protein translocation across the bacterial membrane.* Embo J, 2002. **21**(17): p. 4470-9.
76. Benach, J., et al., *Phospholipid-induced monomerization and signal-peptide-induced oligomerization of SecA.* J Biol Chem, 2003. **278**(6): p. 3628-38.

77. de Keyzer, J., et al., *Direct demonstration of ATP-dependent release of SecA from a translocating preprotein by surface plasmon resonance.* J Biol Chem, 2003. **278**(32): p. 29581-6.
78. Economou, A. and W. Wickner, *SecA promotes preprotein translocation by undergoing ATP-driven cycles of membrane insertion and deinsertion.* Cell, 1994. **78**(5): p. 835-43.
79. van der Wolk, J.P., J.G. de Wit, and A.J. Driessen, *The catalytic cycle of the escherichia coli SecA ATPase comprises two distinct preprotein translocation events.* Embo J, 1997. **16**(24): p. 7297-304.
80. Schiebel, E., et al., *Delta mu H+ and ATP function at different steps of the catalytic cycle of preprotein translocase.* Cell, 1991. **64**(5): p. 927-39.
81. Joly, J.C. and W. Wickner, *The SecA and SecY subunits of translocase are the nearest neighbors of a translocating preprotein, shielding it from phospholipids.* Embo J, 1993. **12**(1): p. 255-63.
82. Woodbury, R.L., S.J. Hardy, and L.L. Randall, *Complex behavior in solution of homodimeric SecA.* Protein Sci, 2002. **11**(4): p. 875-82.
83. Akita, M., et al., *SecA, an essential component of the secretory machinery of Escherichia coli, exists as homodimer.* Biochem Biophys Res Commun, 1991. **174**(1): p. 211-6.
84. Shinkai, A., et al., *Quantitative renaturation from a guanidine-denatured state of the SecA dimer, a 200 KDa protein involved in protein secretion in Escherichia coli.* Biochem Biophys Res Commun, 1990. **172**(3): p. 1217-23.
85. Jilaveanu, L.B., C.R. Zito, and D. Oliver, *Dimeric SecA is essential for protein translocation.* Proc Natl Acad Sci U S A, 2005. **102**(21): p. 7511-6.
86. de Keyzer, J., et al., *Covalently dimerized SecA is functional in protein translocation.* J Biol Chem, 2005. **280**(42): p. 35255-60.
87. Driessen, A.J., *SecA, the peripheral subunit of the Escherichia coli precursor protein translocase, is functional as a dimer.* Biochemistry, 1993. **32**(48): p. 13190-7.
88. Karamanou, S., et al., *Escherichia coli SecA truncated at its termini is functional and dimeric.* FEBS Lett, 2005. **579**(5): p. 1267-71.
89. Jilaveanu, L.B. and D. Oliver, *SecA dimer cross-linked at its subunit interface is functional for protein translocation.* J Bacteriol, 2006. **188**(1): p. 335-8.
90. Or, E., et al., *The bacterial ATPase SecA functions as a monomer in protein translocation.* J Biol Chem, 2005. **280**(10): p. 9097-105.
91. Tziatzios, C., et al., *The bacterial protein-translocation complex: SecYEG dimers associate with one or two SecA molecules.* J Mol Biol, 2004. **340**(3): p. 513-24.
92. Duong, F., *Binding, activation and dissociation of the dimeric SecA ATPase at the dimeric SecYEG translocase.* Embo J, 2003. **22**(17): p. 4375-84.
93. Tsukazaki, T., et al., *Conformational transition of Sec machinery inferred from bacterial SecYE structures.* Nature, 2008. **455**(7215): p. 988-91.
94. Shiozuka, K., et al., *The proton motive force lowers the level of ATP required for the in vitro translocation of a secretory protein in Escherichia coli.* J Biol Chem, 1990. **265**(31): p. 18843-7.

95. Nishiyama, K., et al., *Membrane deinsertion of SecA underlying proton motive force-dependent stimulation of protein translocation.* Embo J, 1999. **18**(4): p. 1049-58.
96. Koonin, E.V. and A.E. Gorbalenya, *Autogenous translation regulation by Escherichia coli ATPase SecA may be mediated by an intrinsic RNA helicase activity of this protein.* FEBS Lett, 1992. **298**(1): p. 6-8.
97. Sianidis, G., et al., *Cross-talk between catalytic and regulatory elements in a DEAD motor domain is essential for SecA function.* Embo J, 2001. **20**(5): p. 961-70.
98. Cordin, O., et al., *The DEAD-box protein family of RNA helicases.* Gene, 2006. **367**: p. 17-37.
99. Caruthers, J.M. and D.B. McKay, *Helicase structure and mechanism.* Curr Opin Struct Biol, 2002. **12**(1): p. 123-33.
100. Zimmer, J., W. Li, and T.A. Rapoport, *A novel dimer interface and conformational changes revealed by an X-ray structure of B. subtilis SecA.* J Mol Biol, 2006. **364**(3): p. 259-65.
101. Papanikolau, Y., et al., *Structure of dimeric SecA, the Escherichia coli preprotein translocase motor.* J Mol Biol, 2007. **366**(5): p. 1545-57.
102. Sharma, V., et al., *Crystal structure of Mycobacterium tuberculosis SecA, a preprotein translocating ATPase.* Proc Natl Acad Sci U S A, 2003. **100**(5): p. 2243-8.
103. Vassylyev, D.G., et al., *Crystal structure of the translocation ATPase SecA from Thermus thermophilus reveals a parallel, head-to-head dimer.* J Mol Biol, 2006. **364**(3): p. 248-58.
104. Baud, C., et al., *Allosteric communication between signal peptides and the SecA protein DEAD motor ATPase domain.* J Biol Chem, 2002. **277**(16): p. 13724-31.
105. Karamanou, S., et al., *A molecular switch in SecA protein couples ATP hydrolysis to protein translocation.* Mol Microbiol, 1999. **34**(5): p. 1133-45.
106. Papanikou, E., et al., *Identification of the preprotein binding domain of SecA.* J Biol Chem, 2005. **280**(52): p. 43209-17.
107. Price, A., et al., *Separable ATPase and membrane insertion domains of the SecA subunit of preprotein translocase.* J Biol Chem, 1996. **271**(49): p. 31580-4.
108. Tanner, N.K. and P. Linder, *DExD/H box RNA helicases: from generic motors to specific dissociation functions.* Mol Cell, 2001. **8**(2): p. 251-62.
109. Vrontou, E., et al., *Global co-ordination of protein translocation by the SecA IRA1 switch.* J Biol Chem, 2004. **279**(21): p. 22490-7.
110. Keramisanou, D., et al., *Disorder-order folding transitions underlie catalysis in the helicase motor of SecA.* Nat Struct Mol Biol, 2006. **13**(7): p. 594-602.
111. Mori, H. and K. Ito, *The long alpha-helix of SecA is important for the ATPase coupling of translocation.* J Biol Chem, 2006. **281**(47): p. 36249-56.
112. Breukink, E., et al., *The C terminus of SecA is involved in both lipid binding and SecB binding.* J Biol Chem, 1995. **270**(14): p. 7902-7.
113. Matousek, W.M. and A.T. Alexandrescu, *NMR structure of the C-terminal domain of SecA in the free state.* Biochim Biophys Acta, 2004. **1702**(2): p. 163-71.

114. Dempsey, B.R., et al., *Solution NMR structure and X-ray absorption analysis of the C-terminal zinc-binding domain of the SecA ATPase.* Biochemistry, 2004. **43**(29): p. 9361-71.
115. Fekkes, P., et al., *Zinc stabilizes the SecB binding site of SecA.* Biochemistry, 1999. **38**(16): p. 5111-6.
116. Zhou, J. and Z. Xu, *Structural determinants of SecB recognition by SecA in bacterial protein translocation.* Nat Struct Biol, 2003. **10**(11): p. 942-7.
117. Pyle, A.M., *Translocation and unwinding mechanisms of RNA and DNA helicases.* Annu Rev Biophys, 2008. **37**: p. 317-36.
118. Singleton, M.R., M.S. Dillingham, and D.B. Wigley, *Structure and mechanism of helicases and nucleic acid translocases.* Annu Rev Biochem, 2007. **76**: p. 23-50.
119. Story, R.M., I.T. Weber, and T.A. Steitz, *The structure of the E. coli recA protein monomer and polymer.* Nature, 1992. **355**(6358): p. 318-25.
120. Ye, J., et al., *RecA-like motor ATPases--lessons from structures.* Biochim Biophys Acta, 2004. **1659**(1): p. 1-18.
121. Gorbalenya, A.E. and E.V. Koonin, *Helicases - Amino-Acid-Sequence Comparisons and Structure-Function-Relationships.* Current Opinion in Structural Biology, 1993. **3**(3): p. 419-429.
122. Walker, J.E., et al., *Distantly related sequences in the alpha- and beta-subunits of ATP synthase, myosin, kinases and other ATP-requiring enzymes and a common nucleotide binding fold.* Embo J, 1982. **1**(8): p. 945-51.
123. Scheffzek, K. and M.R. Ahmadian, *GTPase activating proteins: structural and functional insights 18 years after discovery.* Cell Mol Life Sci, 2005. **62**(24): p. 3014-38.
124. Bourne, H.R., *G proteins - The arginine finger strikes again.* Nature, 1997. **389**(6652): p. 673-674.
125. Crampton, D.J., et al., *The arginine finger of bacteriophage T7 gene 4 helicase: Role in energy coupling.* Proceedings of the National Academy of Sciences of the United States of America, 2004. **101**(13): p. 4373-4378.
126. Woodbury, R.L., et al., *Complexes between protein export chaperone SecB and SecA. Evidence for separate sites on SecA providing binding energy and regulatory interactions.* J Biol Chem, 2000. **275**(31): p. 24191-8.
127. Fekkes, P., C. van der Does, and A.J. Driessen, *The molecular chaperone SecB is released from the carboxy-terminus of SecA during initiation of precursor protein translocation.* Embo J, 1997. **16**(20): p. 6105-13.
128. Crane, J.M., et al., *Mapping of the docking of SecA onto the chaperone SecB by site-directed spin labeling: insight into the mechanism of ligand transfer during protein export.* J Mol Biol, 2005. **353**(2): p. 295-307.
129. Gelis, I., et al., *Structural Basis for Signal-Sequence Recognition by the Translocase Motor SecA as Determined by NMR.* Cell, 2007. **131**(4): p. 756-69.
130. Chou, Y.T. and L.M. Gierasch, *The conformation of a signal peptide bound by Escherichia coli preprotein translocase SecA.* J Biol Chem, 2005. **280**(38): p. 32753-60.
131. Natale, P., et al., *Binding of SecA to the SecYEG complex accelerates the rate of nucleotide exchange on SecA.* J Biol Chem, 2004. **279**(14): p. 13769-77.

132. Hartl, F.U., et al., *The binding cascade of SecB to SecA to SecY/E mediates preprotein targeting to the E. coli plasma membrane.* Cell, 1990. **63**(2): p. 269-79.
133. Mori, H. and K. Ito, *Different modes of SecY-SecA interactions revealed by site-directed in vivo photo-cross-linking.* Proc Natl Acad Sci U S A, 2006. **103**(44): p. 16159-64.
134. van der Sluis, E.O., et al., *Identification of two interaction sites in SecY that are important for the functional interaction with SecA.* J Mol Biol, 2006. **361**(5): p. 839-49.
135. Matsumoto, G., et al., *Genetic dissection of SecA: suppressor mutations against the secY205 translocase defect.* Genes Cells, 2000. **5**(12): p. 991-9.
136. de Keyzer, J., A. Regeling, and A.J. Driessen, *Arginine 357 of SecY is needed for SecA-dependent initiation of preprotein translocation.* FEBS Lett, 2007. **581**(9): p. 1859-64.
137. Mori, H. and K. Ito, *An essential amino acid residue in the protein translocation channel revealed by targeted random mutagenesis of SecY.* Proc Natl Acad Sci U S A, 2001. **98**(9): p. 5128-33.
138. Alami, M., et al., *Nanodiscs unravel the interaction between the SecYEG channel and its cytosolic partner SecA.* Embo J, 2007. **26**(8): p. 1995-2004.
139. Jilaveanu, L.B. and D.B. Oliver, *In vivo membrane topology of Escherichia coli SecA ATPase reveals extensive periplasmic exposure of multiple functionally important domains clustering on one face of SecA.* J Biol Chem, 2007. **282**(7): p. 4661-8.
140. Chiba, K., H. Mori, and K. Ito, *Roles of the C-terminal end of SecY in protein translocation and viability of Escherichia coli.* J Bacteriol, 2002. **184**(8): p. 2243-50.
141. Mori, H., Y. Shimizu, and K. Ito, *Superactive SecY variants that fulfill the essential translocation function with a reduced cellular quantity.* J Biol Chem, 2002. **277**(50): p. 48550-7.
142. Ferentz, A.E. and G. Wagner, *NMR spectroscopy: a multifaceted approach to macromolecular structure.* Q Rev Biophys, 2000. **33**(1): p. 29-65.
143. Kay, L.E., *NMR studies of protein structure and dynamics.* J Magn Reson, 2005. **173**(2): p. 193-207.
144. Sattler, M., *Introduction to biomolecular NMR spectroscopy.* EMBL Heidelberg, 2004.
145. Yee, A.A., et al., *NMR and X-ray crystallography, complementary tools in structural proteomics of small proteins.* J Am Chem Soc, 2005. **127**(47): p. 16512-7.
146. Kumar, T.K. and C. Yu, *Monitoring protein folding at atomic resolution.* Acc Chem Res, 2004. **37**(12): p. 929-36.
147. Korzhnev, D.M. and L.E. Kay, *Probing invisible, low-populated States of protein molecules by relaxation dispersion NMR spectroscopy: an application to protein folding.* Acc Chem Res, 2008. **41**(3): p. 442-51.
148. Burz, D.S., et al., *Mapping structural interactions using in-cell NMR spectroscopy (STINT-NMR).* Nat Methods, 2006. **3**(2): p. 91-3.

149. Serber, Z., et al., *Investigating macromolecules inside cultured and injected cells by in-cell NMR spectroscopy.* Nat Protoc, 2006. **1**(6): p. 2701-9.
150. Goh, C.S., D. Milburn, and M. Gerstein, *Conformational changes associated with protein-protein interactions.* Curr Opin Struct Biol, 2004. **14**(1): p. 104-9.
151. Zuiderweg, E.R., *Mapping protein-protein interactions in solution by NMR spectroscopy.* Biochemistry, 2002. **41**(1): p. 1-7.
152. Takeuchi, K. and G. Wagner, *NMR studies of protein interactions.* Current Opinion in Structural Biology, 2006. **16**(1): p. 109-117.
153. Akke, M., *NMR methods for characterizing microsecond to millisecond dynamics in recognition and catalysis.* Current Opinion in Structural Biology, 2002. **12**(5): p. 642-647.
154. Pellecchia, M., *Solution nuclear magnetic resonance spectroscopy techniques for probing intermolecular interactions.* Chem Biol, 2005. **12**(9): p. 961-71.
155. Mittermaier, A. and L.E. Kay, *New tools provide new insights in NMR studies of protein dynamics.* Science, 2006. **312**(5771): p. 224-8.
156. Henzler-Wildman, K. and D. Kern, *Dynamic personalities of proteins.* Nature, 2007. **450**(7172): p. 964-72.
157. Ishima, R. and D.A. Torchia, *Protein dynamics from NMR.* Nat Struct Biol, 2000. **7**(9): p. 740-3.
158. Gordon S. Rule, T.K.H., *Fundamentals of Protein NMR Spectroscopy*. 1st ed, ed. R. Kaptein. Vol. 5. 2006, Dordrecht: Springer. 530.
159. Pellecchia, M., D.S. Sem, and K. Wuthrich, *NMR in drug discovery.* Nat Rev Drug Discov, 2002. **1**(3): p. 211-9.
160. Clore, G.M. and A.M. Gronenborn, *Structures of Larger Proteins in Solution - 3-Dimensional and 4-Dimensional Heteronuclear Nmr-Spectroscopy.* Science, 1991. **252**(5011): p. 1390-1399.
161. Sattler, M., J. Schleucher, and C. Griesinger, *Heteronuclear multidimensional NMR experiments for the structure determination of proteins in solution employing pulsed field gradients.* Progress in Nuclear Magnetic Resonance Spectroscopy, 1999. **34**(2): p. 93-158.
162. Foster, M.P., C.A. McElroy, and C.D. Amero, *Solution NMR of large molecules and assemblies.* Biochemistry, 2007. **46**(2): p. 331-40.
163. Fernandez, C. and G. Wider, *TROSY in NMR studies of the structure and function of large biological macromolecules.* Curr Opin Struct Biol, 2003. **13**(5): p. 570-80.
164. Wider, G. and K. Wuthrich, *NMR spectroscopy of large molecules and multimolecular assemblies in solution.* Curr Opin Struct Biol, 1999. **9**(5): p. 594-601.
165. Gardner, K.H. and L.E. Kay, *The use of 2H, 13C, 15N multidimensional NMR to study the structure and dynamics of proteins.* Annu Rev Biophys Biomol Struct, 1998. **27**: p. 357-406.
166. Sprangers, R., A. Velyvis, and L.E. Kay, *Solution NMR of supramolecular complexes: providing new insights into function.* Nat Methods, 2007. **4**(9): p. 697-703.

167. Isaacson, R.L., et al., *A new labeling method for methyl transverse relaxation-optimized spectroscopy NMR spectra of alanine residues.* J Am Chem Soc, 2007. **129**(50): p. 15428-9.
168. Tugarinov, V. and L.E. Kay, *Methyl groups as probes of structure and dynamics in NMR studies of high-molecular-weight proteins.* Chembiochem, 2005. **6**(9): p. 1567-77.
169. Sprangers, R. and L.E. Kay, *Quantitative dynamics and binding studies of the 20S proteasome by NMR.* Nature, 2007. **445**(7128): p. 618-22.
170. Bax, A. and D.A. Torchia, *Structural biology: molecular machinery in action.* Nature, 2007. **445**(7128): p. 609.
171. Pervushin, K., et al., *Attenuated T2 relaxation by mutual cancellation of dipole-dipole coupling and chemical shift anisotropy indicates an avenue to NMR structures of very large biological macromolecules in solution.* Proc Natl Acad Sci U S A, 1997. **94**(23): p. 12366-71.
172. Fiaux, J., et al., *NMR analysis of a 900K GroEL GroES complex.* Nature, 2002. **418**(6894): p. 207-11.
173. Pervushin, K., *Impact of transverse relaxation optimized spectroscopy (TROSY) on NMR as a technique in structural biology.* Q Rev Biophys, 2000. **33**(2): p. 161-97.
174. Tugarinov, V., et al., *Cross-correlated relaxation enhanced 1H[bond]13C NMR spectroscopy of methyl groups in very high molecular weight proteins and protein complexes.* J Am Chem Soc, 2003. **125**(34): p. 10420-8.
175. Marintchev, A., D. Frueh, and G. Wagner, *NMR methods for studying protein-protein interactions involved in translation initiation.* Methods Enzymol, 2007. **430**: p. 283-331.
176. Nakanishi, T., et al., *Determination of the interface of a large protein complex by transferred cross-saturation measurements.* J Mol Biol, 2002. **318**(2): p. 245-9.
177. Ikura, M., et al., *Solution structure of calmodulin and its complex with a myosin light chain kinase fragment.* Cell Calcium, 1992. **13**(6-7): p. 391-400.
178. Otting, G. and K. Wuthrich, *Heteronuclear filters in two-dimensional [1H,1H]-NMR spectroscopy: combined use with isotope labelling for studies of macromolecular conformation and intermolecular interactions.* Q Rev Biophys, 1990. **23**(1): p. 39-96.
179. Sarkar, P., et al., *Proline cis-trans isomerization controls autoinhibition of a signaling protein.* Mol Cell, 2007. **25**(3): p. 413-26.
180. Kern, D., E.Z. Eisenmesser, and M. Wolf-Watz, *Enzyme dynamics during catalysis measured by NMR spectroscopy.* Nuclear Magnetic Resonance of Biological Macromolecules, Part C, 2005. **394**: p. 507-524.
181. Boehr, D.D., et al., *The dynamic energy landscape of dihydrofolate reductase catalysis.* Science, 2006. **313**(5793): p. 1638-42.
182. Popovych, N., et al., *Dynamically driven protein allostery.* Nat Struct Mol Biol, 2006. **13**(9): p. 831-8.
183. Wand, A.J., *Dynamic activation of protein function: a view emerging from NMR spectroscopy.* Nat Struct Biol, 2001. **8**(11): p. 926-31.
184. Renner, C., et al., *Practical aspects of the 2D 15N-[1h]-NOE experiment.* J Biomol NMR, 2002. **23**(1): p. 23-33.

185. Palmer, A.G., 3rd, *Probing molecular motion by NMR.* Curr Opin Struct Biol, 1997. **7**(5): p. 732-7.
186. Hammes, G.G., *Multiple conformational changes in enzyme catalysis.* Biochemistry, 2002. **41**(26): p. 8221-8.
187. Haynie, D.T., *Biological Thermodynamics*. 2001: Cambridge University Press. 379.
188. Pierce, M.M., C.S. Raman, and B.T. Nall, *Isothermal titration calorimetry of protein-protein interactions.* Methods, 1999. **19**(2): p. 213-21.
189. Perozzo, R., G. Folkers, and L. Scapozza, *Thermodynamics of protein-ligand interactions: history, presence, and future aspects.* J Recept Signal Transduct Res, 2004. **24**(1-2): p. 1-52.
190. Liang, Y., *Applications of isothermal titration calorimetry in protein science.* Acta Biochim Biophys Sin (Shanghai), 2008. **40**(7): p. 565-76.
191. Jelesarov, I. and H.R. Bosshard, *Isothermal titration calorimetry and differential scanning calorimetry as complementary tools to investigate the energetics of biomolecular recognition.* Journal of Molecular Recognition, 1999. **12**(1): p. 3-18.
192. Velazquez-Campoy, A. and E. Freire, *ITC in the post-genomic era... ? Priceless.* Biophysical Chemistry, 2005. **115**(2-3): p. 115-124.
193. Cooper, A., et al., *Heat does not come in different colours: entropy-enthalpy compensation, free energy windows, quantum confinement, pressure perturbation calorimetry, solvation and the multiple causes of heat capacity effects in biomolecular interactions.* Biophys Chem, 2001. **93**(2-3): p. 215-30.
194. Eftink, M.R., A.C. Anusiem, and R.L. Biltonen, *Enthalpy-entropy compensation and heat capacity changes for protein-ligand interactions: general thermodynamic models and data for the binding of nucleotides to ribonuclease A.* Biochemistry, 1983. **22**(16): p. 3884-96.
195. Brady, G.P. and K.A. Sharp, *Entropy in protein folding and in protein-protein interactions.* Current Opinion in Structural Biology, 1997. **7**(2): p. 215-221.
196. Prabhu, N.V. and K.A. Sharp, *Heat capacity in proteins.* Annu Rev Phys Chem, 2005. **56**: p. 521-48.
197. Murphy, K.P. and E. Freire, *Thermodynamics of structural stability and cooperative folding behavior in proteins.* Adv Protein Chem, 1992. **43**: p. 313-61.
198. Xie, D. and E. Freire, *Molecular basis of cooperativity in protein folding. V. Thermodynamic and structural conditions for the stabilization of compact denatured states.* Proteins, 1994. **19**(4): p. 291-301.
199. Edgcomb, S.P. and K.P. Murphy, *Structural energetics of protein folding and binding.* Current Opinion in Biotechnology, 2000. **11**(1): p. 62-66.
200. Fak, J.J., et al., *Nucleotide exchange from the high-affinity ATP-binding site in SecA is the rate-limiting step in the ATPase cycle of the soluble enzyme and occurs through a specialized conformational state.* Biochemistry, 2004. **43**(23): p. 7307-7327.
201. Zito, C.R., et al., *Role of a conserved glutamate residue in the Escherichia coli SecA ATPase mechanism.* J Biol Chem, 2005. **280**(15): p. 14611-9.
202. Schliwa, M. and G. Woehlke, *Molecular motors.* Nature, 2003. **422**(6933): p. 759-65.

203. Velankar, S.S., et al., *Crystal structures of complexes of PcrA DNA helicase with a DNA substrate indicate an inchworm mechanism.* Cell, 1999. **97**(1): p. 75-84.
204. Korolev, S., et al., *Major domain swiveling revealed by the crystal structures of complexes of E. coli Rep helicase bound to single-stranded DNA and ADP.* Cell, 1997. **90**(4): p. 635-47.
205. Karpowich, N., et al., *Crystal structures of the MJ1267 ATP binding cassette reveal an induced-fit effect at the ATPase active site of an ABC transporter.* Structure, 2001. **9**(7): p. 571-86.
206. Wang, J., *Nucleotide-dependent domain motions within rings of the RecA/AAA(+) superfamily.* J Struct Biol, 2004. **148**(3): p. 259-67.
207. Savvides, S.N., et al., *VirB11 ATPases are dynamic hexameric assemblies: new insights into bacterial type IV secretion.* Embo J, 2003. **22**(9): p. 1969-80.
208. Gai, D., et al., *Mechanisms of conformational change for a replicative hexameric helicase of SV40 large tumor antigen.* Cell, 2004. **119**(1): p. 47-60.
209. Mancini, E.J., et al., *Atomic snapshots of an RNA packaging motor reveal conformational changes linking ATP hydrolysis to RNA translocation.* Cell, 2004. **118**(6): p. 743-55.
210. Moro, F., V. Fernandez-Saiz, and A. Muga, *The allosteric transition in DnaK probed by infrared difference spectroscopy. Concerted ATP-induced rearrangement of the substrate binding domain.* Protein Sci, 2006. **15**(2): p. 223-33.
211. Bernstein, D.A., M.C. Zittel, and J.L. Keck, *High-resolution structure of the E.coli RecQ helicase catalytic core.* Embo J, 2003. **22**(19): p. 4910-21.
212. Shi, H., et al., *Crystal structure of the human ATP-dependent splicing and export factor UAP56.* Proc Natl Acad Sci U S A, 2004. **101**(51): p. 17628-33.
213. Xing, X. and C.E. Bell, *Crystal structures of Escherichia coli RecA in complex with MgADP and MnAMP-PNP.* Biochemistry, 2004. **43**(51): p. 16142-52.
214. Hendrick, J.P. and W. Wickner, *SecA protein needs both acidic phospholipids and SecY/E protein for functional high-affinity binding to the Escherichia coli plasma membrane.* J Biol Chem, 1991. **266**(36): p. 24596-600.
215. Miller, A., L. Wang, and D.A. Kendall, *Synthetic signal peptides specifically recognize SecA and stimulate ATPase activity in the absence of preprotein.* J Biol Chem, 1998. **273**(19): p. 11409-12.
216. Triplett, T.L., et al., *Functional signal peptides bind a soluble N-terminal fragment of SecA and inhibit its ATPase activity.* J Biol Chem, 2001. **276**(22): p. 19648-55.
217. Whittaker, J.W., *Selective isotopic labeling of recombinant proteins using amino acid auxotroph strains.* Methods Mol Biol, 2007. **389**: p. 175-88.
218. Caruthers, J.M., E.R. Johnson, and D.B. McKay, *Crystal structure of yeast initiation factor 4A, a DEAD-box RNA helicase.* Proc Natl Acad Sci U S A, 2000. **97**(24): p. 13080-5.
219. Story, R.M., H. Li, and J.N. Abelson, *Crystal structure of a DEAD box protein from the hyperthermophile Methanococcus jannaschii.* Proc Natl Acad Sci U S A, 2001. **98**(4): p. 1465-70.
220. Zhao, R., et al., *Crystal structure of UAP56, a DExD/H-box protein involved in pre-mRNA splicing and mRNA export.* Structure, 2004. **12**(8): p. 1373-81.

221. Carey, J., et al., *Protein reconstitution and three-dimensional domain swapping: benefits and constraints of covalency.* Protein Sci, 2007. **16**(11): p. 2317-33.
222. Nooren, I.M.A. and J.M. Thornton, *Structural characterisation and functional significance of transient protein-protein interactions.* Journal of Molecular Biology, 2003. **325**(5): p. 991-1018.
223. Chou, Y.T., J.F. Swain, and L.M. Gierasch, *Functionally significant mobile regions of Escherichia coli SecA ATPase identified by NMR.* J Biol Chem, 2002. **277**(52): p. 50985-90.
224. Dyson, H.J. and P.E. Wright, *Intrinsically unstructured proteins and their functions.* Nature Reviews Molecular Cell Biology, 2005. **6**(3): p. 197-208.
225. Volkman, B.F., et al., *Two-state allosteric behavior in a single-domain signaling protein.* Science, 2001. **291**(5512): p. 2429-2433.
226. Kalodimos, C.G., et al., *Structure and flexibility adaptation in nonspecific and specific protein-DNA complexes.* Science, 2004. **305**(5682): p. 386-389.
227. Cliff, M.J., et al., *Molecular recognition via coupled folding and binding in a TPR domain.* Journal of Molecular Biology, 2005. **346**(3): p. 717-732.
228. Baker, B.M. and K.P. Murphy, *Evaluation of linked protonation effects in protein binding reactions using isothermal titration calorimetry.* Biophys J, 1996. **71**(4): p. 2049-55.
229. Spolar, R.S. and M.T. Record, *Coupling of Local Folding to Site-Specific Binding of Proteins to DNA.* Science, 1994. **263**(5148): p. 777-784.
230. Bruzzese, F.J. and P.R. Connelly, *Allosteric properties of inosine monophosphate dehydrogenase revealed through the thermodynamics of binding of inosine 5'-monophosphate and mycophenolic acid. Temperature dependent heat capacity of binding as a signature of ligand-coupled conformational equilibria.* Biochemistry, 1997. **36**(34): p. 10428-10438.
231. Grucza, R.A., et al., *Thermodynamic study of the binding of the tandem-SH2 domain of the Syk kinase to a dually phosphorylated ITAM peptide: Evidence for two conformers.* Biochemistry, 1999. **38**(16): p. 5024-5033.
232. Kumaran, S., R.A. Grucza, and G. Waksman, *The tandem Src homology 2 domain of the Syk kinase: A molecular device that adapts to interphosphotyrosine distances.* Proceedings of the National Academy of Sciences of the United States of America, 2003. **100**(25): p. 14828-14833.
233. Crampton, D.J., et al., *The arginine finger of bacteriophage T7 gene 4 helicase: Role in energy coupling.* Proc Natl Acad Sci U S A, 2004. **101**(13): p. 4373-4378.
234. Karamanou, S., et al., *Preprotein-controlled catalysis in the helicase motor of SecA.* Embo Journal, 2007. **26**(12): p. 2904-2914.
235. Schmidt, M., et al., *Nucleotide binding activity of SecA homodimer is conformationally regulated by temperature and altered by prlD and azi mutations.* Journal of Biological Chemistry, 2000. **275**(20): p. 15440-15448.
236. Ramamurthy, V., V. Dapic, and D. Oliver, *secG and temperature modulate expression of azide-resistant and signal sequence suppressor phenotypes of Escherichia coli secA mutants.* Journal of Bacteriology, 1998. **180**(23): p. 6419-6423.

237. Liu, D., W.T. Windsor, and D.F. Wyss, *Double-stranded DNA-induced localized unfolding of HCV NS3 helicase subdomain 2.* Protein Sci, 2003. **12**(12): p. 2757-67.
238. den Blaauwen, T., et al., *Thermodynamics of nucleotide binding to NBS-I of the Bacillus subtilis preprotein translocase subunit SecA.* FEBS Lett, 1999. **458**(2): p. 145-50.
239. Tugarinov, V. and L.E. Kay, *An isotope labeling strategy for methyl TROSY spectroscopy.* J Biomol NMR, 2004. **28**(2): p. 165-72.
240. Palmer, A.G., *NMR probes of molecular dynamics: Overview and comparison with other techniques.* Annual Review of Biophysics and Biomolecular Structure, 2001. **30**: p. 129-155.
241. Benkovic, S.J. and S. Hammes-Schiffer, *A perspective on enzyme catalysis.* Science, 2003. **301**(5637): p. 1196-202.
242. Hackney, D.D., *Evidence for alternating head catalysis by kinesin during microtubule-stimulated ATP hydrolysis.* Proc Natl Acad Sci U S A, 1994. **91**(15): p. 6865-9.
243. Wong, I. and T.M. Lohman, *Allosteric effects of nucleotide cofactors on Escherichia coli Rep helicase-DNA binding.* Science, 1992. **256**(5055): p. 350-5.
244. Kourtz, L. and D. Oliver, *Tyr-326 plays a critical role in controlling SecA-preprotein interaction.* Mol Microbiol, 2000. **37**(6): p. 1342-56.
245. Harris, C.R. and T.J. Silhavy, *Mapping an interface of SecY (PrlA) and SecE (PrlG) by using synthetic phenotypes and in vivo cross-linking.* J Bacteriol, 1999. **181**(11): p. 3438-44.
246. Matsumoto, G., T. Yoshihisa, and K. Ito, *SecY and SecA interact to allow SecA insertion and protein translocation across the Escherichia coli plasma membrane.* Embo J, 1997. **16**(21): p. 6384-93.
247. Lian, L.Y., et al., *Protein-ligand interactions: exchange processes and determination of ligand conformation and protein-ligand contacts.* Methods Enzymol, 1994. **239**: p. 657-700.
248. Shilton, B., et al., *Escherichia coli SecA shape and dimensions.* FEBS Lett, 1998. **436**(2): p. 277-82.
249. Hamel, D.J. and F.W. Dahlquist, *The contact interface of a 120 kD CheA-CheW complex by methyl TROSY interaction spectroscopy.* Journal of the American Chemical Society, 2005. **127**(27): p. 9676-9677.

Curriculum Vitae

Dimitra Keramisanou

1975	Born July 2nd in Katochi Mesologiou, Greece
1993	Graduated with honors from high school Katochi Mesologiou, Greece
1994-1999	B.Sc. in Chemistry, University of Ioannina (Greece)
1999-2001	M.Sc. in Biomolecular Chemistry and Biochemistry, University of Ioannina (Greece)
2001-2003	Research Fellow, School of Medicine, University of Ioannina (Greece)
2004-2008	Teaching Assistant / Graduate Assistant; Rutgers-Newark, The State University of New Jersey, Department of Chemistry
2009	Ph.D. in Chemistry, Rutgers-Newark, The State University of New Jersey

Publications

[1] I. Gelis, A. M. Bonvin, **D. Keramisanou,** M. Koukaki, D. Gouridis, S. Karamanou, A. Economou, C. G. Kalodimos, *Cell*, 2007, 131, 756.

[2] S. Karamanou, G. Gouridis, E. Papanikou, G. Sianidis, I. Gelis, **D. Keramisanou,** E. Vrontou, C. G. Kalodimos, A. Economou, *EMBO J.,* 2007, 26, 2904

[3] **D. Keramisanou,** N. Biris, I. Gelis, G. Sianidis, S. Karamanou, A. Economou, C. G.Kalodimos, *NSMB*, 2006, 13, 594

[4] E. Papanikou, S. Karamanou, C. Baud, M. Frank, G. Sianidis, **D. Keramisanou,** C G. Kalodimos, A. Kuhn, A. Economou, *JBC,* 2005, 280, 43209